ANALYTICAL AND NUMERICAL SIMULATION OF LASER PLASMA WAKEFIELD ACCELERATION

Thesis Submitted for the Award of the Degree of

Doctor of Philosophy

in

Physics

By

Jagnishan singh

Registration Number: 41900654

Supervised By	Co-Supervised by
Dr Jyoti Rajput (13751)	**Dr Sandeep Kumar**
Department of Physics, (Professor)	**Department of Sciences**
Lovely Professional University	**(Physics-Prog), (Professor)**
Phagwara, Punjab	**Manav Rachna University**
	Faridabad, Haryana

LOVELY PROFESSIONAL UNIVERSITY, PUNJAB

2025

This thesis is dedicated to

My father Sardar Sadhu Singh

My mother Sardarni Sukhjinder Kaur

My Aunt Miss Sukhpal Kaur

My wife Harmandeep Kaur

For their endless love…

DECLARATION

I hereby declare that the presented work in the thesis entitled "ANALYTICAL AND NUMERICAL SIMULATION OF LASER PLASMA WAKEFIELD ACCELERATION" in fulfilment of degree of **Doctor of Philosophy (Ph. D.)** is outcome of research work carried out by me under the supervision **Dr. Jyoti Rajput**, working as professor, in the department of physics of Lovely Professional University, Phagwara, Punjab, India. In keeping with the general practice of reporting scientific observations, due acknowledgments have been made whenever the work described here has been based on the findings of another investigator. This work has not been submitted in part or full to any other University or Institute for the award of any degree.

(Signature of Scholar)

Name of the scholar: **Jagnishan Singh**

Registration No.: 41900654

Department/School: Dept. of Physics

Lovely Professional University, Phagwara

Punjab, India

CERTIFICATE

This is to certify that the work reported in the Ph.D. thesis entitled "ANALYTICAL AND NUMERICAL SIMULATION OF LASER PLASMA WAKEFIELD ACCELERATION" submitted in fulfillment of the requirement for the reward of the degree of **Doctor of Philosophy (Ph.D.)** in the department of physics, is a research work carried out by Jagnishan singh, 41900654, is bonafide record of his original work carried out under my supervision and that no part of the thesis has been submitted for any other degree, diploma or equivalent course.

(Signature of Supervisor)

Dr. Jyoti Rajput

(Professor)

Department of Physics

Lovely professional university, Phagwara, Punjab, 144411

(Signature of Co-Supervisor)

Dr. Sandeep Kumar

(Professor)

Department of Sciences (Physics-Prog.)

Manav Rachna University, Faridabad, Haryana, 121004

Abstract

The cost of conventional accelerators employed for particle acceleration is high owing to their substantial size. The maximal electric field gradient is limited by 100 MV/m because of the electrical failures of the walls. In contrast, vacuum and plasma-based particle accelerators, which are propelled by a laser or particle beam, exhibit significant promise due to their substantial acceleration gradient, resulting in the formation of more compact structures.

This research focuses on vacuum-based inverse free electron laser (IFEL) and laser-plasma wakefield acceleration (LPWA) using simulations and analysis. IFEL, a potential technology for particle acceleration, uses an electron beam and a laser field interacting in a vacuum. The study uses advanced simulation techniques to understand electron acceleration in IFEL systems. Additionally, it explores LPWA, a rapidly evolving area that uses interactions between intense laser pulses and plasma to accelerate particles to high energies. The study uses analytical approaches and simulations to explain the fundamental principles behind LPWA. Plasma waves can be generated by a powerful laser pulse, which can have accelerating gradients of up to 100s GV/m.

In the context of vacuum-based particle acceleration Inverse free electron laser acceleration is studied using helical and planar undulator. We conducted a comparative investigation to examine the acceleration of single electrons in an inverse free-electron laser (IFEL) under the influence of a tightly concentrated Gaussian laser beam, considering the existence of helical and planar wiggler magnetic fields. This study examines the impact of laser and wiggler field characteristics on the dynamics and acceleration of single electrons. To improve the efficiency of electron acceleration, the diffraction angle in the laser field expressions considers corrections up to the fifth order. We have numerically analysed the Lorentz equation using the fourth-order Runge-Kutta method. The numerical findings of our study demonstrate that a significant amount of electron energy is achieved by both the helical and planar wigglers when the laser and wiggler field parameters are optimized. This study examines the impact of the laser field, specifically its waist size, as well as the influence of

the wiggler field and its tapering on the undulator length. The helical wiggler exhibits a total electron energy gain of 1.331 GeV, whereas the planar wiggler demonstrates an electron energy gain of 300 MeV. We compare two different wiggler field geometries, namely helical and planar configurations, and show how electrons move in each.

The wakefield acceleration of a two-color laser is examined using a two-dimensional particle-in-cell (2D-PIC) simulation. When compared to a single-colour scheme, our simulations demonstrate that a two-colour laser Wakefield scheme can produce energy spectra that are more capable of maintaining their stability. An energy increase of 500 MeV is reported in a plasma channel that is 3.4 millimeters in length when the simulation parameters are specified. We also present the influence that the relative time delays of the two-color lasers have on the acceleration of electron bunches, as well as the polarization effect that the second laser has on the particles. These electron bunches, which are of such high quality, qualify as potential candidates for future XFEL and betatron sources.

This study involves the examination of electron acceleration dynamics within plasma formations characterized by various density profiles. To achieve this, we employ comprehensive numerical simulations and theoretical investigations. We study the various plasma density profiles, including generated wake potential, wakefield, and energy gain. The results indicate that plasma density has a significant impact on the overall wakefield, wake potential, and final energy gain. By employing deliberate manipulation of plasma and laser characteristics, such as the plasma density profile and laser field parameter, it becomes feasible to exercise authority over the produced wakefield and wake potential. Consequently, this enables the optimization of energy gain to a maximum value of 393 MeV. The primary objective of this research is to establish precise correlations to enhance LWFA configurations, get a more comprehensive understanding of plasma-assisted particle acceleration, and unlock the unexplored capabilities of this captivating technology.

Acknowledgement

Table of Contents

List of tables

List of figures

List of symbols

- E - Electric field
- B - Magnetic field
- p - Momentum
- F - Force
- e - Electric charge
- m - Mass of electron
- c - Speed of light
- t - Time
- I - Intensity of laser
- λ_l - Wavelength of laser
- ω - Angular frequency of laser
- k - Wave vector
- ϕ - Phase
- μ_0 - Permeability of free space
- ϵ_0 - Permittivity of free space
- $\vec{\nabla}$ - Delta operator
- q - Charge
- W - Watt
- w_0 - Beam waist parameter
- Z_R - Rayleigh length
- F_P - Ponderomotive force
- λ_D - Debye length
- K_B - Boltzman constant
- T - Absolute temperature
- n_0 - Plasma electron density
- ω_0 - Frequency of em wave
- ω_p - Plasma frequency
- P_C - Critical power of plasma

- λ_P - Plasma wavelength
- C - Coulomb
- nC - Nano coulomb
- α - Linear chirp parameter
- a_0 - Normalized intensity parameter
- b_0 - Normalized magnetic field parameter
- b - Decentered parameter
- r_0 - Laser spot size

Chapter 1

Introduction

1.1 Study Rationale

In physics, the history of particle accelerators is an enthralling journey of has significantly influenced numerous core scientific discoveries and technological advancements. J.J. Thomson's ground breaking discovery of breakthroughs serves as the foundation for crucial technologies, like synchrotron and free electron lasers (FEL). Effectiveness of conventional schemes is restricted by the electron in the electrically broken limit of the late 1800s and early 1900s laid RF (radio frequencies) cavities employed to produce the groundwork for understanding subatomic particles. John Cockcroft and Ernest Walton designed the revolutionary Cockcroft-Walton particle accelerator, the world's first particle accelerator, in 1932. This accelerator accelerated protons to induce artificial nuclear reactions. Robert Jemison Van de Graff invented the Van de Graff generator around the same time, facilitating the acceleration of electric fields responsible for accelerating charged particles to greater energies. The invention of the cyclotron by Ernest O. Lawrence in 1931 revolutionized particle acceleration, allowing circular accelerators to achieve significantly higher energies. Cyclotrons were instrumental in the production. Indeed, within these cavities, the accelerating field is constrained to approximately 100 MV/m. Consequently, contemporary high-energy accelerators span several tens of kilo meters in length and entail costs amounting to billions of dollars. Utilizing high-energy particle and photon beams represents an unparalleled approach to investigating matter at the most intricate levels. Rutherford employed a beam of helium nuclei to find out the dimensions of medical isotopes and the advancement of nuclear physics research. Synchrotrons were invented in 1952, expanding on the cyclotron concept by allowing particles to be accelerated to even higher energies by varying magnetic fields. The Lawrence Berkeley National Laboratory's Bevatron was the first

significant synchrotron. Since their invention in 1935, linear accelerators (LINACs), which accelerate particles in a straight line, have found pervasive use in numerous applications, including medical treatments of the nucleus, additionally, through the utilization of X-ray diffraction, Crick, Watson, and fundamental research. The Stanford Linear Accelerator Centre (SLAC) began operations in 1966, featuring the world's longest linear accelerator for accelerating electrons and positrons in high-energy physics experiments. In 2008, the Large Hadron Collider (LHC) at CERN in Switzerland was turned on. Franklin elucidated the cellular structure of DNA. Furthermore, The Large Hadron Collider (LHC) is one of the largest man made machine in the world for accelerating particle. Its loop has a circumference of 16.6 miles (~27km.) and runs 175 meters deep in the earth located at the border between France and Switzerland. This machine is operated by "CERN" ("Conseil Européen pour la Recherche Nucléaire"). This particle accelerator generates 13 TeV photon energy which is the highest one to date and ready to achieve new milestones. The Higgs boson[1], commonly known as the GOD particle, is one of the most recent historical discoveries in the field of particle acceleration. The particle accelerator has played a crucial role in enabling significant advancements in fundamental physics, as evidenced by the numerous Nobel prizes awarded in this field. The extensive period dedicated to the development of particle accelerators has been instrumental in facilitating these ground breaking discoveries. This was a huge step forward. By accelerating protons and heavy ions to extreme energies, this colossal machine continues particle accelerators have exhibited an increase in both energy levels and productivity as time has progressed. They are utilized within medical facilities to diagnose and provide medical care to patients, within semiconductor plants for the construction of microchips, and at synchrotron light sources to the particle accelerators, these particle accelerators are helps in investigating the fundamental building blocks of matter generate x-ray beams and recreating conditions like the early universe—high-intensity laser beams. Current accelerator technologies at the energy frontier necessitate the utilization of increasingly expansive facilities to

propel particles to greater energies. This progression culminates in the Large Hadron Collider, operating at 14TeV, boasting a diameter of 8.6km, and requiring a substantial capital investment of £3 billion. Consequently, it stands as one of the most immense and financially expensive technologies ever fabricated.

The proposed Future Circular Collider (FCC) from CERN promises to surpass the capabilities of the Large Hadron Collider (LHC), offering a circular conduit with a circumference of approximately 100 kilometers, opening new frontiers in particle physics and advancing human knowledge. Human ingenuity is exemplified by the lengthy history of particle accelerators, which has led to the exploration of the universe's greatest mysteries and applications in medicine and materials science. With ever-improving technology, the potential for even more potent and inventive accelerators offers unprecedented opportunities for scientific progress on a massive scale.

The advancement of efficient and cost-effective techniques for accelerating charged particles would result in a reduction in both financial expenses and physical dimensions. In recent years, there has been a resurgence of interest among researchers and scientists in vacuum and plasma due to its potential for achieving ultra-high energy gains in short distances. The availability of ultrahigh-power (more than tens of terawatt) and short-pulse table-top lasers equipped with the chirped pulse amplification (CPA) technique[2] has been attributed to advancements in technology. In recent decades, there has been a significant development towards the advancement of highly-intense and short-pulsed lasers, with a particular emphasis on the Chirped Pulse Amplification (CPA) method. As a result, numerous novel domains of application and development have arisen, with the laser-based acceleration of particles in vacuum and plasmas being particularly significant.

Electron accelerators are gaining significant attention within the realm of particle accelerators due to their status as elementary particles and their relatively lighter mass in comparison to other, more massive particles. Consequently, electron based particle accelerators are considered a more

effective substitute when compared to their heavier counterparts. Presently, two primary areas of focus have driven advancements in the field of electron accelerators: medical applications[3] and the generation of X-rays for research purposes in various disciplines, commonly referred to as synchrotron light sources[4]. In addition, electron accelerators play a significant part in a wide variety of other applications within the industrial sector, and they are becoming an increasingly common sight in the scientific, medical, and commercial spheres. The increasing necessity to enhance the properties of electron beams has resulted in a heightened requirement for improved control and efficiency of electron accelerators. Consequently, significant advancements have been made in accelerator technologies.

In this context, lasers were suggested as a viable option and powerful acceleration techniques utilizing high electric fields generated by intense laser pulses were proposed and investigated[5], [6], [7], [8], [9]. Concurrently, the utilization of plasma as an accelerating structure was also suggested due to its ability to maintain fields that surpass the l0pimits of material breakdown. Following this, several modern acceleration techniques based on plasma have been introduced [5], [6], [10], [11], which depend on the creation of plasma waves or wakes through space charge forces. In the year 1979, Tajima and Dawson introduced a method to generate wakefields by utilizing laser pulses with high intensity. This approach, known as the Laser Plasma Accelerator (LPA) and this phenomena follow on the interaction between laser and plasma [12]. The research yielded promising results, as it was observed that the wakes had the potential to generate high acceleration gradients exceeding 100 GV/m [5], [6], [9], [11]. Plasma Wakefield Acceleration (PWFA), as described in the literature[13], involves the stimulation of wakes through the utilization of charged particle beams consisting of electrons, positrons, or protons.

1.2 Vacuum particle acceleration
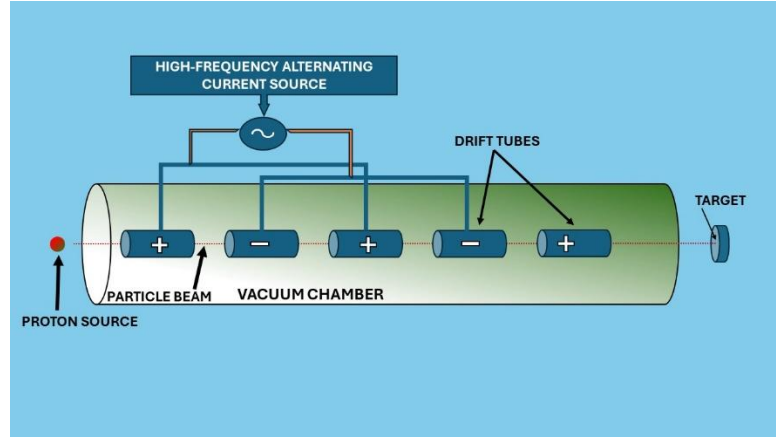
Figure 1.1 Schematic of linear particle accelerator using a vacuum chamber.

The acquisition of net energy and subsequent acceleration of charged particles in an electromagnetic field necessitates the violation of the Lawson-Woodward concept, according to this, that in a vacuum, highly relativistic electrons cannot gain or lose energy when interacting with an electromagnetic field[14]. Various approaches to contravening the Lawson-Woodward theorem have been investigated, including restricting the size of the interaction region. By employing the technique of concentrating the laser beam into a limited spatial extent and considering the ponder motive force.

The Electron's acceleration and the attainment of net energy gain can be accomplished using laser-electron interaction within a vacuum. This interaction can be confined to a specific region of the Rayleigh length by employing tightly focused high-intensity lasers that are limited to a finite-sized spot. In this instance, the utilization of high-intensity focused laser fields in a vacuum was employed to facilitate the acceleration of electrons within the focal region. This phenomenon was subsequently verified through experimental demonstration [15]. It is worth noting that the acquisition of finite energy in a vacuum can occur via ponderomotive acceleration, wherein the energy gain arises from the non-linear force exerted by a highly intense laser[10]. The utilization of this acceleration technique accelerates electrons up to several million electron volts

(MeV), accompanied by a broad distribution of laser energy and significant scattering.

1.3 Inverse free electron laser acceleration (IFELA)
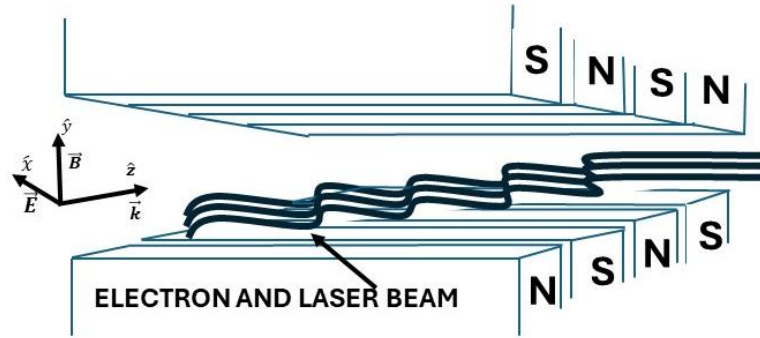
Figure 1.2 Schematic of motion of electrons under the influence of undulator in IFELAs

In recent years, significant advancements have been seen in plasma-based acceleration phenomena as well as vacuum based particle acceleration science. Plasma-based particle accelerators rely on the production of plasma waves with significant amplitudes, enabling them to achieve extremely high acceleration gradients. Additionally, these accelerators have the potential to guide laser pulses, thereby mitigating pulse diffraction. However, these systems experience challenges such as plasma instabilities, reduced group velocity, and electron scattering with residual ions. Laser vacuum acceleration offers several advantages[16], [17], [18], [19], [20], over laser-plasma acceleration because it doesn't have the inherent issues of plasma-assisted acceleration[12], [21], [22].

The utilization of an IFEL is considered a potential method. The initial experiment was conducted at Columbia University served as a pioneering demonstration of IFEL acceleration[23]. Subsequently, further experiments were conducted at Brookhaven National Laboratory (BNL)[25]. In an experiment, two different laser accelerators were utilized to act on an electron beam coherently and cumulatively. The study presents the initial findings of the

energy variation with the relative injection phase of electron bunches, as observed through the of a microwave based ifela (MIFELA)[26]. Subsequent investigations were conducted in the realm of IFEL research[27], [28], [29], [30]. IFEL acceleration was proposed by Palmer in the year 1972[7]. In IFEL, electrons exhibiting relativistic velocities propagate in parallel to the laser pulse within an arrangement of magnetic elements known as an undulator. These so called undulator magnets induces a minor transverse momentum, resulting in a wiggling motion that aligns with the transverse component of the laser's magnetic field. This setup enables the interchange of net energy between the electron and the laser beam. There exist certain practical constraints associated with IFEL accelerators. the major limitation in IFELA is the narrow interaction bandwidth that is observed as we use low-intensity laser pulses. Path of the electrons is significantly influenced by the diffraction edge field of a highly concentrated and long-pulse laser pulse during the initial stages of interaction. Diffraction of extended driving laser pulses is yet another restriction on IFEL interaction.

To achieve optimal energy conditions in the FEL, it is necessary to satisfy the resonance condition known as the wiggler. This condition can be expressed as

$$\gamma^2 = \frac{(1 + K^2)\lambda_w}{2\lambda_l}$$

where, λ_w is wiggler wavelength, K is wiggler strength, λ_l is laser wavelength.

The equations that govern the movement of electrons in an accelerator can be obtained by incorporating the force of radiation reaction into the Lorentz equation.

$$m\frac{d(\gamma v)}{dt} = e\left[E_L + \frac{v}{c} \times (B_L + B_w)\right]$$

variables E_L and B_L represent the electric field and magnetic field, respectively, of the laser radiation. B_w denotes the wiggler magnetic field.

1.4 Wakefield acceleration

Based on our comprehensive understanding of the behaviour of free electrons, we shall now direct our attention toward the examination of robust laser beam as it traverses through a plasma medium. Initially, the ponderomotive force exerts a propulsive effect on the electrons, propelling them forward. However, as the laser pulse progresses, it eventually surpasses the electrons, inducing a reverse motion in them. Due to the comparatively greater mass of ions, their inert nature leads to the emergence of a longitudinal fluctuation in the density of electric charges. This fluctuation can be resonantly stimulated when the duration of laser pulse precisely corresponds to half of the period of the plasma oscillation at the specific density of the plasma under consideration. A longitudinal plasma wave is generated, with its phase advancing alongside the group velocity of trailing laser pulse. In the context of plasma physics, it is possible to observe the acceleration of electrons within the density wave phenomenon. Given the analogous nature of the scenario to the hydrodynamic phenomenon observed in the wake generated by a boat traversing a body of water, it is aptly referred to as wakefield acceleration. In an ideal scenario, electrons are introduced into the leading edge of the wave with significant forward momentum and subsequently depart before the wave's overtaking. When the laser-induced resonant plasma wave is strongly excited, the energy dispersion of the accelerated electrons can show remarkable confinement, like how water waves behave. For example, in a low-amplitude water wave, only the phase of the wave moves forward, while the water molecules just move back and forth in their positions. Nevertheless, if the contrast of the wave exhibits a significant magnitude and subsequently undergoes a breaking phenomenon, a portion of the aqueous molecules become entrained by the propagating wave front and are subsequently transported until they ultimately reach a state of phase exhaustion, resulting in their cessation. In a similar vein, when the plasma wave experiences robust excitation, an electron deficit emerges on the leading edge. A cohort of electrons traverses into this 'plasma cavity' from the posterior region and undergoes uniform acceleration,

thereby attaining an equivalent level of kinetic energy. The phenomenon under consideration, commonly referred to as bubble acceleration, was initially postulated through numerical simulations in 2002[31]. Subsequently, experimental validation of this concept was achieved by three independent research groups hailing from the United Kingdom, France, and the United States in 2004[32], [33].

1.4.1 Laser Wakefield Acceleration (LWFA)

A potential method for accelerating electrons involves the utilization of a highly-intense laser beam that is directed into plasma medium. This phenomenon generates a region of high density, resulting in acceleration of charged particles, such as electrons, through the influence of its electric field. The acceleration gradient observed in a plasma wakefield surpasses the levels attained through conventional RF technology.
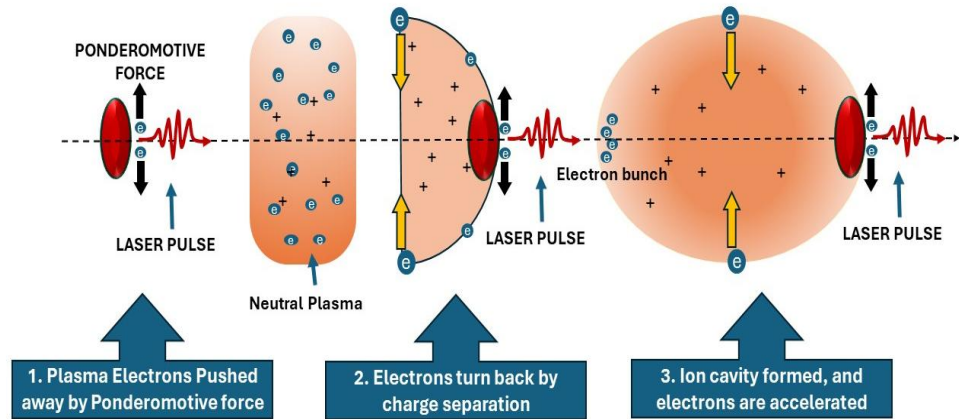
Figure 1.3 Schematic for laser wakefield acceleration

The concept of collective acceleration in the plasma medium was introduced by Veksler in 1956[34]. By utilizing plasma as the medium for acceleration, the researcher effectively resolved the issue of medium-induced limitations on the upper threshold of the accelerating gradient, thereby liberating accelerator researchers from this constraint. The individual's strategy involved inducing a plasma wave characterized by a substantial amplitude through the introduction

of an electron beam. This beam was intended to facilitate the acceleration of ions with greater mass. The desired outcome was for the ions' energy to augment by a factor of M/m about the energy of driving electron bunch. Here, M represents the mass of ions, while 'm' represents the mass of the electrons. The term "collective acceleration" pertains to the generation of plasma fields resulting from collective oscillations, which have the potential to surpass the acceleration levels observed in individual particles. The size of these collective fields is contingent upon the number of particles, denoted as N, and is of significant magnitude. The effects of clouds may be influenced by their inherent randomness.

Laser Wakefield Acceleration (LWFA) was conceptualized by Tajima and Dawson in year of 1979 [12]. In LWFA, a brief yet intense laser is employed to stimulate the formation of a wake in the plasma medium, thereby facilitating the acceleration of particles. When an highly-intense and short laser beam is directed towards plasma, the pressure exerted by the laser pulses causes the displacement of plasma electrons, while the ions remain stationary due to their greater mass. The phenomenon of electron movement in a leather pulse, resulting in a snap-back effect, can be attributed to the attractive forces generated between ions and electrons, commonly referred to as the Ponderomotive force. The phenomenon of electron snapback is observed, wherein electrons experience a rapid reversal in their direction. Simultaneously, these electrons become confined within the region of disturbed flow, commonly referred to as the wake, and undergo an acceleration process. The phenomenon referred to as "laser Wakefield acceleration" is widely recognized in scientific literature. The idea of employing a clustered electron beam to produce plasma wakes with, once more, GV/m accelerating gradients was first proposed in 1985 by Chen and Dawson[13]. In the immediate aftermath, the initial research into Particle Wakefield Acceleration (PWFA) was successfully executed utilizing electron beam drivers operating at low energy levels. In the year 1996, Katsouleas and Joshi put forth a proposition wherein they suggested the utilization of an ultra-relativistic electron beam, which would be supplied by the

SLAC (Stanford Linear Accelerator Centre) LINAC(stands for linear accelerator), to induce GV/m accelerating fields. It was postulated in 2009 that a proton bunch might be used to drive the acceleration of a plasma wakefield[35], and the researchers presented through computer simulations that TeV levels of energy could be obtained in a single accelerating stage if it was driven by a TeV proton bunch.

When the duration of the laser pulse is equivalent to the plasma wavelength [36], it is considered the most efficient approach for guiding the wakefield and delivering quasi-monoenergetic electron beams using lasers. The relationship can be expressed as, $\omega_p = e\sqrt{\dfrac{n_e}{m_e\epsilon_o}}$

In this context, n_e represents the plasma density measured in cubic centimetres ϵ_0 denotes the free space permittivity, while $'m_e'$ is the mass and $'e'$ is the charge on the electron, respectively. This is known as bubble regime, and most of the Wakefield studies have been conducted within this regime [37]. Within the bubble regime, the net energy of the laser pulses are focused into a region with a radius smaller than that of the plasma wakefield. Within this domain, the Pondermotive force exerts a radial impact on the electrons, resulting in their outward displacement and the subsequent generation of a wake. The provided equation represents the electric field E that can be sustained by a plasma.

$$E = \frac{cm_e\omega_p}{e}$$

Upon solving the equations for the variables ω_p, it is determined that the electric field sustained by plasma exhibits a proportionality to the square root of plasma density $(\sqrt{n})$. Tajima and Dowson posit that the utilization of a laser with a wavelength of 1μm to induce a wake in a plasma characterized by a density of $10^{-18}cm^{-3}$ has the potential to generate an electron exhibiting a 10 GeV/m accelerating gradient [14]. It is worth noting that the accelerating gradient observed in contemporary linear particle accelerators is merely one-third of the magnitude of the value. With advancements in laser technology and related

fields, the LWFA scheme has emerged as a highly notable method for particle acceleration. Before the invention of lasers, the utilization of short laser pulses was not feasible in LWFA. In response, Tajima and Dowson introduced an alternative approach known as Plasma Beat Wave Acceleration (PBWA). In the subject of Plasma-Based Wave Acceleration (PBWA), the generation of a plasma wave is achieved through the utilization of two elongated laser beams characterized by distinct frequencies, denoted as ω_1 and ω_2. This process is generally achieved by the resonance condition, which is expressed as:

$$\Delta\omega = \omega_1 - \omega_2 \approx \omega_p$$

As the resonance condition is matched, it is possible to generate a plasma wave of significant magnitude. Rosenbluth and Liu (1972) also researched the excitation of this wave for plasma heating[24].

Following the seminal work of Tajima *et. al.* in 1979 [12], the concept of Laser Wakefield Acceleration (LWFA) was subsequently rediscovered through independent investigations conducted by Gorbunov and Kirsanov [38]. The pioneering work of Bulanov *et al.*[39] and Sprangle *et al.*[40] development of one-dimensional (1-D) and two-dimensional (2-D) nonlinear theories of laser wakefield acceleration (LWFA), respectively. The seminal experimental manifestation of plasma wave generation through the LWFA was effectively demonstrated by Hamster *et al.* [41]. H. Dewa *et al.* have successfully demonstrated the acceleration up to 100 MeV via laser wakefield acceleration (LWFA) experiments employing a powerful 2-terawatt (TW) laser system [42]. These experimental operations have effectively demonstrated the fundamental principles underlying the concept of laser wakefield acceleration. Multiple studies[43][44] have reported the creation of narrow-energy-spread, quasi-monoenergetic beams. Leemans *et al.* generated monoenergetic electron beams with 1 GeV bunch energy and a 2.5% energy spread utilizing a plasma channel and a 40 TW laser system [45]. Wang *et al.* have successfully demonstrated, both experimentally and via simulation studies, the generation of accelerated electron bunches possessing a remarkable energy of 2 GeV and 10% energy

spread[46]. In a study conducted by Kim *et al.*, outstanding improvements in electron energy enhancement have been demonstrated, reaching up to 3 GeV. This significant progress was achieved through the utilization of a dual-stage laser-wakefield accelerator, which was effectively stimulated by a powerful 1-petawatt (PW) laser system [47].

A novel laser-plasma accelerator system has been successfully showcased, operating at exceedingly high intensity approximately $10^{19} \, watt/cm^2$. The ponderous, stationary ions give rise to an ionized column or cavity enveloped by a tenuous sheath of expelled electrons. This state is commonly denoted as the 'blowout', or 'bubble', regime within the context of plasma physics. In conjunction with the phenomenon of electron cavitation, it is worth noting that a certain proportion of the plasma's electrons undergo self-confinement within the ion cavity, subsequently experiencing a substantial acceleration towards elevated energy levels[32], [33], [48].

1.4.2 Plasma Wakefield Acceleration

Approximately four decades ago, Toshiki Tajima and John Dawson[12] formulated the notion of plasma-based acceleration, a concept that has since gained significant prominence in the realm of theoretical physics. The fundamental concept of acceleration of the particles revolves around the utilization of the electric field that arises from periodic perturbations in the charge density within the plasma medium. Wakefields are accelerating structures that can be induced by driving beams such as laser beam or moveable particles. Given the inherent nature of the accelerated structure as a plasma wave within an ionized gas medium, the absence of any fabrication prerequisites, and its imperviousness to damage, it possesses the remarkable capability to sustain accelerating fields of magnitudes surpassing those achievable by conventional technologies by several orders of magnitude. Also, to speed up charged particles to high energies, you need a shorter length of plasma for a big accelerating field or gradient. In the 90s, the first experimental test was conducted to explain the theory of plasma wakefield acceleration[9] by using a long laser pulse to drive

wakefields. Due to the remarkable advent of chirped pulse amplification, the ground breaking achievement was duly recognized and bestowed with the prestigious Nobel Prize in Physics in 2018. Consequently, the investigations about laser-plasma wakefield experiments have experienced a notable surge in intensity.
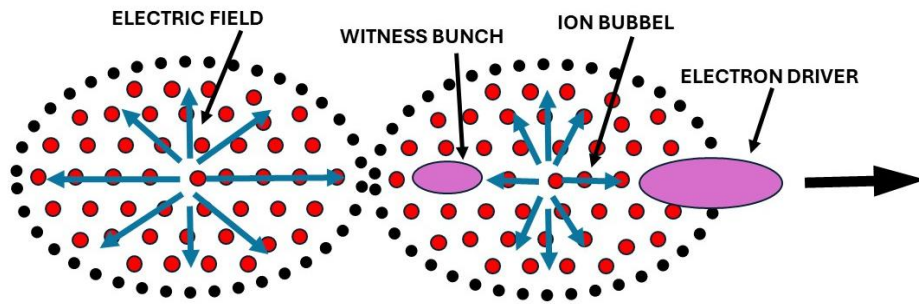
Figure1.4 Schematic layout of plasma wakefield acceleration

In the year 2006, three distinct research groups successfully showcased the phenomenon of electron acceleration to energies reaching the Gigaelectron Volt (GeV) scale. This achievement was accomplished through the utilization of short-duration, high-intensity laser pulses within plasmas spanning a length of approximately one millimetre. In the year 2014, a laser system acknowledged as a PW-laser was employed to achieve ten's of GeV energy within a plasma medium spanning several centimetres. This process yielded the acceleration gradient of approximately $46 GeV m^{-1}$.

In the year 2007, a series of experiments conducted at SLAC (Stanford Linear Accelerator Centre) demonstrated that within an 85cm plasma column, the energy of accelerated electrons experienced an increase of twice from 42GeV to 85GeV. This increase in energy corresponds to a gradient of $52 GeV m^{-1}$. In 2014, notable advancements were made in achieving enhanced precision in energy distribution as well as maximizing energy transfer efficiency. Nevertheless, the electron beams that were accelerated exhibited a continuous spectrum of energy. Additional experiments on PWFA were conducted at the Facilities for Accelerator Science and Experimental Test

(FACET) located at SLAC in the United States. The objective of these experiments was to attain an enhanced acceleration gradient, less energy spread and reduced transverse emittance[49]. In addition to the FACET beamline, a newly developed beamline known as FLASH Forward (Future-oriented wakefield accelerator research and development at FLASH) has been established at DESY(Deutsches Elektronen-Synchrotron) in Germany [50]. Furthermore, another beamline called FACET-II has been constructed at SLAC for the production of highly-energetic electron beams through wakefield-induced ionization-induced injection. These beamlines have been implemented to facilitate further investigation into this scheme.

Currently, most beam experiments involving laser drivers and particle drivers are conducted within the bubble regime. This regime is characterized by laser pulses or particle bunches that possess a length comparable to the wavelength of the wakefields. However, the driver beam's energy is often less than 100 J, limiting electron energy growth in the single stage. To reach TeV energies, numerous phases are needed. Current proton-driven beams can theoretically accelerate electrons to TeV energy in a single step. This is because proton-driver beams possess significantly higher energy compared to laser pulses or electron beams, generally ranging from tens to hundreds of kilojoules. Nevertheless, the generation of substantial wakefields is observed when short bunches are employed, resulting in large amplitudes. In the case of proton bunches, which typically span a length of 6-12 cm, those bunches are limited to drive the high acceleration gradients. The Advanced Wakefield Experiment (AWAKE) conducted at CERN demonstrated that when plasma is utilized, a bunch of protons undergo self-modulation, resulting in the formation of a series of micro-bunches that are only a few millimeters in length. These micro-bunches then efficiently generate wakefields through resonance, In the year 2018, the AWAKE experiment successfully showcased the remarkable phenomenon of accelerating electrons to multiple Gigaelectron volts (GeV) within a plasma medium spanning a length of 10 meters [51].

1.5 Literature Review

Tajima and Dawson [52] first demonstrate the idea of using the plasma medium to accelerate electrons at a short range. They achieved a GeV energy gradient in a few centimetres of the plasma chamber.

Musumeci *et al.* [53] proposed Inverse Free Electron Laser (IFEL) accelerator that is intended to be constructed at the ATF beamline in BNL. The accelerator is designed to accelerate an existing ATF electron beam up to 120 MeV in a 60-cm-long and tapered permanent magnetic helical undulator that has been designed at UCLA(University of California, Los Angeles).

Strickland and Morou [54] first investigated the phenomena of the chirp pulse amplification (CPA) technique in 1985. In this phenomenon, the duration of the pulse is in time before amplification and then compressed it back to a short pulse to generate a highly-powerful laser pulse. The fundamental principle of CPA is to extend the pulse in time using a pair of gratings which reduces the peak power of the pulse but increases its energy. A second set of gratings is used to compress the stretched pulse back to its original length after it has been amplified in a laser amplifier. The advantage of CPA is that it allows for the generation of extremely high-intensity laser pulses.

Cline *et al.* [55] experimented with BNL. A Co_2 laser is focused and encounters an electron beam that has been accelerated to 20 MeV using a high-quality laser photo cathode-originated beam with low emittance. An electron beam is produced, which is then passed through a magnet spectrometer and recorded with a fast image-capturing device.

Gadjev *et al.* [56] use a small, less expensive single-colour X-ray generators. An experimental examination demonstrated that a TW-class Co_2 laser pulse may be divided in two to generate a strong electron bunch and create up to 13 KeV X-rays using inverse Compton scattering.

Parsa *et al.* [57] demonstrated a different method of IFELA using a square wave wiggler magnetic field and produced approximately double as compared to a simple IFELA scheme using a sinusoidal wiggler field.

Sandeep Kumar *et al.* [58] investigated chirp based IFELA phenomena using a Gaussian laser pulse that is tightly focused. A helical magnetic wiggler is used to confine the electron in a vacuum. For the optimized values of field and laser parameters, they extracted an electron of GeV energy from a 10 MeV electron.

Salamin *et al.* [65] accelerates electrons from the rest to GeV of energies by interacting with the axial electric field element of a petawatt-power laser's lowest-order axicon fields. For practical applications, electron bunch simulations are needed, and electron axial injection should be investigated. The research also indicates the requirement for higher-order components in the diffraction angle ϵ to adequately simulate the tightly concentrated beam.

Duris *et al.* [59] provide the first observation of a helical IFEL accelerator that is capable to generates an electron heaving 54 MeV energy gain with 100 MeV/m accelerating gradient. The IFEL undulator used to be the world's first-ever strongly tapered and 54 cm in length. Approximately 30% of the electron beam is captured with 1.8% of final energy spreading.

Roserwieg *et al.* [60] Demonstrated the experimental method to avoid the defocusing and misalignment of the laser beam. They used a waveguide to accelerate the laser beam. A special kind of undulator design is investigated to enhance the final energy.

Dunning *et al.* [61] Present a novel phenomenon that demonstrates precise control over electron beam acceleration or deceleration using injectable optical microbubbles and relative laser pulse phases. Experimental results verify theoretical predictions, suggesting significant potential for improving IFEL beam quality and impacting future laser-driven accelerators.

Mussumeci *et al.* [62] used an IFEL accelerator to gain over 20 MeV trapped electrons. In this experiment, they used a 14.5 MeV energetic electron beam and a 400 GW Co_2 laser beam both were propagated through an undulator of 50 cm in length, with the period and field amplitude considerably tapered towards the

end. The experiment revealed that most energy gains occurred in the first half at 70 MeV/m.

Duris *et al.* [63] demonstrated that an IFEL accelerator driven by a 20 TW laser system can accelerate an electron beam to 1 GeV beam with a normalized emittance of 0:5 mm mrad, and a more then 1 kA in over the distance of 1 meter. One challenge with the IFEL scheme is the requirement of high initial electron energy. Advancement in the field of undulators technology, such as development of mm- period undulators or the utilization of IFEL harmonic interactions, could potentially overcome this limitation.

Salamin *et al.* [64] mathematically investigate the motion for a single electron in Gaussian-beam-modelled laser fields, including terms for diffraction angles up to the fifth order. During reflection and transmission, they saw energy gains of up to a few GeV. Sometimes, they saw energy losses. The study suggests that a static magnetic field in a lab can be used to eject an electron that has been captured, giving it extra energy. In this case a magnetic field with a uniform strength of 2.5 T can expel an electron with a 3.633 MeV energy level if it is injected at an angle of 6 degrees to the axis of a linearly polarised beam. This beam has generates the power output of 10 PW and is directed to a location of focus. The electron gains 1128 MeV just from the laser field, but because of the small magnetic field, it gains a total of 1230 MeV.

Moody *et al.*[66] Experimentally investigate IFELA. In this experiment produced gradients greater than 200 MV/m utilizing a 4 TW 100 fs long 800 nm TiSa laser pulse. With the short durations of both the laser and electron pulses, synchronization was one of the significant difficulties in this experiment. This experiment helps to buit a single-shot, non-destructive, electro-optic sampling-based diagnostics system. Each laser accelerator shot could be time-stamped with an accuracy of less than 100 fs. The results of this experiment are expected to help build GeV-class IFEL accelerators in the future.

N Sudar *et al.*[67] show how they extracted almost 30% of the initial electron energy as coherent radiation by decelerating a 65 MeV electron beam to 35 MeV, sharply tapered helical magnetic undulator using a 200 GW CO_2 laser

source. These results, validated by radiation field evolution models, show essential step towards the high peak and average powerful coherent radiation sources.

Duris *et al.* [68] demonstrated an experiment at UCLA and BNL at ATF. They used a helical magnetic wiggler to capture a highly energetic e-beam. A 0.5-meter-long undulator is used for passing powerful lasers. A 52 MeV high-quality electron beam with an acceleration gradient of more than 100MV/m is produced.

Khullar *et al.* [69] presented the IFEL theory. The significant impact of synchrotron radiation loss on IFEL is accounted for in an analytical solution. Based on the findings of the research, it appears that for a given pole-to-pole gap, the undulator with a shorter period delivers a stronger acceleration gradient and a reduced saturation length.

Palmer *et al.* [70] showed that a particle moving along the axis of a helical magnet can be constantly sped up by its interaction with circularly polarised radiation moving in the same direction. An electron is accelerated to 10 GeV using a $10^{14} Watt$ laser as an illustration. A second illustration demonstrates how pions and kaons may be separated at energies greater than 1 GeV. Also, it is demonstrated that clustered charged particles travelling through a helical magnet would emit coherent circularly polarised electromagnetic radiation, and it is hypothesized that the needed clustering may in certain cases be self-generating. A 10 Ampere current of 15-MeV electrons generates a 75-MW beam of 10μ radiation.

Mirzanejhad *et al.* [71] numerically analysed electron bunch acceleration using a laser under the influence of static helical magnetic wiggler in a vacuum. For simulations, they used a beam with 10MeV initial energy. In comparison to the plane-wave approximation. An external axial magnetic field helps to focus the electron bunch and mitigate the decrease in the acceleration gradient. Finally, a virtually monoenergetic femtosecond (fs) micro bunch with an optimal beginning phase is accelerated, 0.2 GeV/m acceleration gradient is achieved in this process.

Agarwal *et al.*[72] investigated electron acceleration in the presence of a static magnetic field using an inverse free electron laser (IFEL) pulse. Plasma wakefield accelerate injected particles using high-intensity lasers and plasma interactions. Static magnetic fields increase the resonance to trapped electrons, transferring laser energy to them and creating highly energetic electrons with better energy gain.

Singh *et al.*[73] has been investigate the acceleration of electrons using a laser beam that has a circularly polarised light beam in the presence of a strong axial magnetic field. They showed that electrons and the laser field can resonate with one another, allowing for efficient energy transmission. Optimal magnetic field depends upon the initial energy of electron and is independent of laser intensity.

Khazaeinezhad [74] investigated the acceleration of electrons in IFEL utilizing the helical wiggler in under the influence of ion-channel guidance and magnetic fields. The Fourth-order Runge-Kutta method is used for numerical investigation. different keynotes that are noticed by authors are: (I) axial magnetic field is much beneficial and superior to the ion-channel guidence because it produces more energy. (II) Progressively decreasing the field's strength, electron acceleration is enhanced. (III) When the consequences of tapering are considered, a greater increase is realized than when one is tapered.

Amiranoff *et al.* [75] examine the production of robust electric fields within plasma through the utilization of high-power laser beams. This phenomenon facilitates the acceleration of charged particles with relativistic properties to exceedingly elevated energy levels. The research investigates various approaches employed to accomplish the aim, including the beat wave technique and the self-modulated wakefield method. The researchers discovered that the beat wave technique can generate electric fields within the range of $1\text{-}10 Gvm^{-1}$, facilitating the acceleration of electrons to energy levels ranging from 1 MeV to over 30 MeV. Additionally, the self-modulated wakefield method has the potential to generate electric fields surpassing 100 Gvm^{-1}, thereby enabling electron acceleration up to 100 MeV.

Jung *et al.* [76] focused on examining the impact of the ponderomotive force on magnetization in cold plasmas, specifically in relation to quantum effects. It has been demonstrated that induction of a magnetic field is impossible without the presence of quantum effects in plasmas. Additionally, it has been observed that the presence of quantum effects leads to an augmentation of the cyclotron frequency. This augmentation can be attributed to the ponderomotive force, which arises from the temporal fluctuations in the intensity of the electromagnetic field.

Plastro *et al.*[77] propose a new approach to laser wakefield accelerator (LWFA) design restrictions. In this approach they produces an ultrashort, highlly-intense laser pulse. Spatial-temporal pulses may reduce wakefield dephasing. Trapped electrons beyond the acceleration phase cause this. Spatiotemporally formed pulses can travel any distance and speed. This dephasing-less laser wakefield acceleration (LWFA) technique can accelerate electrons in shortest distance rather than conventional LWFA methods. This method achieves TeV energies in a single 4.5-meter stage without guiding structures. This research introduces a new technique for laser wakefield accelerator (LWFA) design limitations. A spatiotemporally structured pulse may reduce wakefield dephasing, where trapped electrons exceed the accelerating phase. They demonstrate the pulse's ability to travel long distances at different speeds, according to linear regime simulations and bubble regime scaling laws. This method achieves Teravolt (TeV) energy in a single 4.5-meter stage without guiding structures.

Andreev *et al.*[78] present a study demonstrating the feasibility of producing quasi-monoenergetic electron beams in the plasma based LWFA method. This is achieved by ensuring that the injected electrons constitutes only a minor portion of the plasma wavelength in both longitudinal and transverse directions. The researchers conduct a simulation of a hypothetical two-stage 1 GeV Laser Wakefield Acceleration (LWFA) experiment. The input parameters are representative of the practical approach at of the BNL Accelerator Test Facility,

which includes a CO_2 laser with a picosecond-terawatt power output and an electron gun with high brightness characteristics.

Clayton [43] provides a detailed account of ionization-induced injection phenomena in order to attain electron acceleration with energies reaching up to GeV in the presence of laser wakefield accelerator. Through the examination of the spatial and spectral attributes of the laser light emanating from the plasma, the researchers deduce that a laser pulse with a duration of 60 femtoseconds and a power of 110 terawatts is effectively directed and produces a wake across the entire length of the gas cell, which measures 1.3 centimetres. This phenomenon occurs specifically when the densities of the gas cell are below 1.5 times 10 to the power of 18 per cubic centimetre. The observation of high-energy electron generation is limited to instances where a minor quantity (3%) of CO2 gas is introduced into the He gas. Computer simulations have been employed to confirm that the oxygen's K-shell electrons of undergo ionization and are subsequently introduced into the wake, where they are subsequently accelerated to energies exceeding 1 GeV.

Amiranoff *et al.* [79] aimed to examine the process of electron acceleration in a plasma wave created using a laser wakefield mechanism. The research revealed that the maximum energy gain measured was 1.6 MeV, with an anticipated strength of the electric field at 1.5 GV/M. These experimental results align, with theoretical predictions that consider three-dimensional effects. Moreover, the estimated duration of the plasma wave is 1 picosecond.

Essarey *et al.* [36], present a detailed examination of plasma-based accelerator concepts is presented. The article delves into the characteristics of nonlinear plasma waves, providing a thorough analysis of how electron trapping, and acceleration take place within these waves. Additionally, it explores the propagation characteristics of electron's motion or laser beams, focusing on the challenges posed by instabilities and discussing methods employed to guide laser pulses. To wrap up, the paper provides an overview of experimental findings in this specific field of study.

Faure *et al.* [32], present a significant advancement in the laser-plasma accelerators. They emphasize the successful mitigation of electron beam randomization by employing a novel technique, thereby improving the overall quality of the generated electron beams. The researchers employ laser-induced plasma dynamics to propel a plasma bubble across a limited span of 3 mm, thereby facilitating the confinement and propulsion of plasma electrons. The procedure yields a tightly focused and nearly monochromatic stream of electrons, possessing a notable charge of 0.5 nano coulombs, while operating at an energy level of 170 million electron volts. This achievement represents a noteworthy progression in the field of compact particle acceleration technology.

Maier *et al.* [80] establish a correlation between drive laser pulse and electron-beam variables using a large sample size. The primary objective of this research is to identify and figure out the various sources of the electron's energy drift and jitter. Based on their findings, they present a parametrization that predicts energy drift with sub-percent accuracy over many hours based on recorded laser parameters, paving the way for performance enhancements through active stabilization. The attainment of results is facilitated by the initial establishment of a laser-plasma accelerator that operates consistently for 24 hours. Additionally, the analysis of data obtained from 100,000 successive electron beams represents a significant achievement.

Mehrling *et al.* [81] conducted a study that examines the evolution of emittance in electron. Researchers utilized the 3-D PIC code OSIRIS for their investigation. It has been determined that the refocusing of electron beams is an essential measure to effectively mitigate the degradation of beam quality. It can be deduced that this decay is pertinent to electron energies extending to the TeV-energy. Furthermore, the authors engage in a quantitative analysis of the fundamental consequences associated with the deterioration of beam quality resulting from inadequate control over electron-beam matching in staged plasma accelerators.

Osterhoff *et al.* [82] Investigated the observation of laser-driven, quasi-mono-energetic e-beams with energies up to 200 Mev emitted from steady-state-flow

gas cells. The laser-wakefield acceleration method utilizing gas cells presents a straightforward and reliable approach to producing relativistic electrons, rendering it well-suited for various applications, including the generation of extreme ultraviolet undulator radiation.

Mangles *et al.* [48] examine the phenomenon of intense laser-plasma interactions. The researchers focus on the utilization of high-power lasers within university-scale laboratories to generate relativistic electron beams. These beams exhibit characteristics such as low divergence and minimal energy spread, which are observed under specific plasma conditions. This research holds significant promise for the advancement of ultrashort monoenergetic electron bunches in the future.

Kim *et al.* [47] generates GeV electron beam employing a laser-wakefield accelerator with two stages that were controlled by a petawatt (PW) femtosecond laser. Compared to previous studies on laser-driven electron acceleration, this one found that the electron's energy in the second medium (10-mm gas jet) increased significantly, to 3 GeV. The findings were validated through the utilization of 3-D PIC. According to the authors, the utilization of a picosecond (PW) laser system presents novel opportunities for investigating laser-wakefield acceleration in research.

Malik *et al.* [83] analyze laser-produced wakefield electron acceleration, focusing on pulse shape. The research investigated that a) Mathematical analysis of longitudinal field, plasma density perturbations, and potential are derived back to the laser pulse passing in the plasma heaving a pulse length of the plasma period. b) Three laser pulse shapes—Gaussian-like (GL), rectangular-triangular (RT), and rectangular-Gaussian (RG)—are tested for practicality, and c) The RT pulse has the highest electron energy gain. The same-duration GL and RG pulses have gains of 28.6 and 28.8 MeV, respectively. For all pulse forms, increasing laser frequency, pulse duration, and intensity increases the wakefield and energy gain. The study shows that the RT pulse shape is best for laser-produced wakefield electron acceleration.

Nakajima *et al.* [84] observed high-energy electrons accelerated upto hundred's of MeV across a few centimeters of underdense plasma. They showed that pulse self-modulation due to laser pulse ionization and self-channelling in plasma can explain acceleration augmentation at greater pressures than the resonant pressure. These effects must aid electron acceleration above 1 GeV. The wakefield excitation matches acceleration experiments after frequency domain interferometry directly measured electron density oscillation.

Luttikhof [85] presents a theoretical examination of external injection systems for laser wakefield acceleration (LWFA) and proposes strategies for increasing the control, scalability, and quality of the accelerating particle bunches. In addition to this, the research emphasizes the possibility of producing ultrafast electron bunches using wakefield acceleration.

Matsuoka *et al.* [86] provide an experimental explanation of the laser wakefield acceleration (LFA) technique, showcasing its remarkable capability to generate high-energy electron beams within a compact configuration. Additionally, the research underscores the inherent constraints of conventional accelerators and emphasizes the imperative of exploring alternative approaches to attain particles with increased energies. The investigation focuses on the Laser Wakefield Acceleration (LWFA) experiments carried out at the esteemed University of Michigan, wherein a self-propagating laser pulse is employed within a supersonic gas-jet environment. The HERCULES laser facility, boasting the capability of wavefront correction, successfully achieved the delivery of an impressive peak intensity square $8 \times 10^{19} W/cm^2$ by harnessing a laser power of 100 TW. This remarkable feat was accomplished through the utilization of f/10 focusing optics, which enabled precise concentration of the laser beam onto the gas jet.

Downer *et al.* [87] present an in-depth analysis of different diagnostic methodologies employed in plasma-based electron accelerators. The primary emphasis is placed on the development of single-shot diagnostic techniques capable of accurately measuring modest normalized transverse emittance and

lower duration in a non-invasive manner, while also achieving high resolution. The present discourse explores the challenges associated with the previously mentioned imaging methodologies, while also providing an elucidation of the plasma-based acceleration physics insights that have been derived from the analysis of these images and their subsequent comparison with simulated plasma structures.

Tozufras *et al.* [88] propose an approach that outlines the process of introducing negative charges into a nonlinear, 3-D plasma wakefield. One way to achieve this goal is by using either a laser or an electron beam, both of which displace plasma electrons and form a near-spherical ion channel that is affected by the beam load. The study presents analytical solutions for the shape of the ion channel and the corresponding fields. The research findings indicate the possibility of achieving a high level of beam-loading efficiency while still preserving the energy spread of the bunch. The theoretical findings presented in this study have been verified through the utilization of the Osiris particle-in-cell code.

Gorbunov *et al.* [38] investigated laser wakefield acceleration using 30-femtosecond petawatt laser beams. These lasers focus on a 100-micron plasma area. The nonlinear plasma wakefield accelerates electrons to Giga-electron volt energies without pulse channelling. Accelerating electrons across eight centimetres yielded 1 GeV energy in simulations. For 330 femtoseconds, non-resonant electron beam lets containing 1 MeV particle can create low-emitting bunches with energies of approximately 900 MeV and an energy spread of 10%. WAKE simulated two-dimensional circular geometry.

Rowlands-Rees *et al.* [89] investigate how to make quasi-monoenergetic high energetic electron beams. They do this by using laser-plasma acceleration phenomena inside a hydrogen-filled capillary discharge waveguide. The investigation reveals that the injection and electrons motion are significantly impacted by the temporal interval between the initiation of discharging of current and ejection of the laser beam.

Silva *et al.* [90] investigate the most appropriate setups for an individual Laser Wakefield Accelerator (LWFA) stage utilizing theoretic scaling for the duration of the pulse and the energy. The results suggest that self-injected electron bunches can be accelerated to energies above 10 GeV and externally injected bunches above 50 GeV. The assumptions for the greatest energy gain and injection of charge agree with the simulation results, proving that a 10 PW laser can self-guide over distances more than 10 cm and that a 12 Gega-electron volt self-injected electron beam can achieve the same results.

Zhang *et al.* [91] examined the utilization of mid-infrared (mid-IR) laser pulses in the context of laser wakefield acceleration. This technique can produce quasi-monoenergetic electron beams characterized by a limited energy spread. The research demonstrates that the utilization of mid-infrared (mid-IR) laser pulses can yield a greater ponderomotive force. This, in turn, leads to an earlier occurrence of electron self-injection into the wake wave, a lower threshold of plasma density required for injection, and a significant enhancement in the charge. The paper suggests that the implementation of mid-IR terawatt laser systems has the potential to significantly advance studies in laser wakefield acceleration.

Muggli *et al.* [92] provide a detailed account of an experiment on plasma wakefield acceleration that took place at the Stanford Linear Accelerator Centre. The main aim of this experiment was to study the difficulties encountered and the corresponding resolutions in implementing a one-meter-long plasma accelerator module inside the framework of a high-energy accelerator. The conducted experiment provides evidence of the effective utilization of plasma wakefield acceleration across a considerable spatial extent.

Kozawa *et al.* [93] report an experiment on plasma wakefield acceleration produced by narrow bunches in the over-dense regime at the University of Tokyo. The driven bunches induced energy and beam size changes in the test bunches and an acceleration gradient of roughly 1 MeV/m. Plasma wakefield acceleration is promising for next-generation linear colliders' high acceleration gradients. The paper compares experimental data to linear theory predictions.

Hafaz *et al.* [94] simulate a two-color laser wakefield acceleration (LWFA) technique in which fundamental ('red') and second harmonic ('blue') 30 fs laser pulses are used to speed up electron beams in an under-dense plasma. The approach exploits the inverse quadratic dependence of depletion length on laser wavelength. Experimental results reveal that using a single red laser pulse, electron beams were accelerated up to 400 MeV, while utilizing both 'blue' and red laser pulses, maximum final energy reaches up to 700–800 MeV.

Lotov *et al.* [95] introduced a proton-driven plasma wakefield acceleration domain. Plasma nonlinearity causes the excited wave's phase velocity to be higher than the protons' in this domain. By using a beam charge that surpasses the lowest threshold for creating a nonlinear wave and carefully setting the longitudinal plasma density profile, wave velocities can approach the speed of light. This technology uses a 400 GeV proton driver to boost electron or positron velocity to 200 GeV.

Cianchi *et al.* [96] discussed plasma-based acceleration in particle beam accelerators, which use plasma's strong electric fields to create higher accelerating gradients than previous technology. A particle beam is created by accelerating an existing particle beam in a plasma channel or by directly interacting a high-power laser with a gas jet. Correctly measuring emerging beam characteristics, especially emittance, is essential for device optimization. Due to plasma channels' wide energy spread, tight focusing, and background noise, beam parameter diagnostics are difficult. The study highlights diagnostic difficulties and proposes and implements solutions.

Pousa *et al.* [97] proposed a novel methodology to address the issue of energy spreading in plasma-based particle accelerators. Their approach involves dividing the acceleration method in two distinct plasma stages, both are magnetically connected. A 5.5 GeV beam is generated with relative energy spreads of 1.2×10^{-3} (total) and 2.8×10^{-4} (slice), and submicron emittance is preserved in this case, is demonstrated by simulations conducted on a specific setup of 1.5 meters in length. This technological advancement represents a

notable enhancement compared to existing techniques and holds the capacity to facilitate the compact FEL's and other related applications.

Hogan *et al.* [98] present a plasma-wave accelerator experiment that compresses a 28.5 GeV electron pulse heaving 1.8×10^{10} electrons to 20 mm and focuses it to a 10 mm spot size at the beginning of a 10 cm long lithium vapour column with 2.8×10^{17} $atom/cm^3$. A plasma is created and expelled by the electron bunch fully ionizing lithium vapour. Expelled electrons produce a high-amplitude plasma wake that accelerates back-bunch particles by over 2.7 GeV.

Joshi *et al.* [99] have made significant advances PWFA concept, including high-gradient electron acceleration, powerful acceleration of narrow energy spread electron bunches, positron acceleration, and emittance preservation. Future studies will demonstrate plasma wake creation, high-efficiency acceleration, energy doubles of trailing bunches, and process parameter quantification.

1.6 Objectives of the proposed research work:

Prob. 1 To study Laser Wakefield acceleration (LWFA) with single- and two-colour Gaussian laser pulses.

Prob. 2 To study the tapering effect of wiggler magnetic field in Inverse free electron laser for efficient electron acceleration.

Prob. 3 To improve the emittance property of accelerated electron bunch in Electron beam driven plasma Wakefield acceleration (PWFA).

Prob. 4 To study the effect of density modulated plasma medium on electron acceleration in LWFA.

1.7 Thesis Outline

This dissertation aims to elaborate the concept of particle acceleration interaction of laser pulse with either vacuum or in plasma. The whole research

work is based on the analytical, numerical and simulation analysis of laser-plasma interactions. The dissertation is organized as follows: -

Chapter 2 this chapter introduces the theoretical framework necessary for examining the events outlined in this thesis. This offers a concise summary of the pertinent plasma physics, including the interaction between lasers and plasmas. Apart from this, in this chapter, we try to understand the basic methodology of Inverse free electron laser acceleration (IFELA).

Chapter 3 presents the comparison investigation conducted to examine the acceleration of single electrons utilising a Gaussian laser beam that is precisely concentrated in conjunction with helical and planar wiggler fields. In the case of helical wiggler net 1.3 GeV electron energy is achieved, because of the longer interacting length, but for the planar magnetic wiggler, the electron energy gain is restricted to 300 MeV, due to its lower interacting length. Work related to this, was published in the Optik journal in 2022. Crossing of two lasers and chirp effect on the particle acceleration in IFELA also investigate in this chapter.

Chapter 4 Two-color laser Wakefield acceleration is investigated through 2D-PIC simulation. Our calculations indicate that a two-color laser Wakefield system generates more stable energy spectra than a single-color scheme. A 500 MeV energy gain is reported in a 3.4 mm long plasma channel under specified simulation settings. The author has also presented work related to this study at the international conference, AMRP-2020. The author has also given a poster presentation on this work in AMRP-2020.

Chapter 5 Study how frequency-chirp in ionisation laser affects witness bunch features in TH injection scheme. Electron injection and trapping in plasma bubbles are studied under plasma Wakefield and ionisation laser fields. Simulation results are presented in the results and discussion part.

Chapter 6 investigate the novel approach of LWFA using different values of plasma density profiles. In this chapter we systematically investigates the impact of various density profiles on energy gain, generated wakefield, and wake potential.

Chapter 2

Research Methodology

2.1 Introduction

The investigation of the interaction between intense laser radiation and both vacuum and plasmas provides a valuable initiation into the realm of particle acceleration physics. In this dissertation, we investigate both vacuum and plasma-based acceleration schemes. In the context of vacuum acceleration, we studied the inverse free electron laser acceleration in the presence of different kinds of magnetic fields i.e., planar magnetic wiggler field and helical wiggler magnetic field. While we were discussing about plasma-based particle acceleration, we focused on laser and plasma wakefield acceleration, *i.e.* LWFA and PWFA. For this simulation study we use different simulation codes and high power computer setups for run these codes.

2.2 Inverse Free Electron Laser Acceleration (IFELA).

Efficient particle acceleration in IFEL acceleration relies on a well-concentrated laser field. The initial stage of this technique is creating an electron bunch using an electron gun and injecting it into an area where it interacts with a closely focused laser field. This generates intense electric fields that propel electrons to high energy across short distances. Effective IFEL acceleration requires exact synchronization b/w the electron bunch and laser achieve maximum acceleration efficiency. Scientists can modify eyesight to optimize energy gain and achieve specific beam characteristics. Specifically, by regulating characteristics like laser strength, polarization, and focusing. This compact and efficient technology for accelerating particles offers new opportunities for future particle accelerators and high-energy physics research, with possible applications ranging from medical imaging to fundamental particle physics studies

2.2.1 Tightly focused laser pulse

This method utilizes tightly focused laser pulses for inverse free electron (IFEL) acceleration, incorporating the fifth-order term in the diffraction angle. By employing numerical modelling, this technique aims to achieve precise control over electron beam dynamics and maximize acceleration efficiency. Laser pulse focusing techniques are used to enhance spatial and temporal resolution by optimizing parameters for optimal performance. Simulation results Analysis is conducted via MATLAB. Simulation is essential for creating a detailed framework to enhance the knowledge and practical use of IFEL acceleration, offering insights into beam quality and efficiency in small accelerator systems.

For numerical simulation, a strongly concentrated laser beam with the following field parameters is used:

$$E_x = E_0 \left\{ \begin{array}{c} S_0 + \epsilon^2 [\, \xi^2 S_2 - \rho^4 s_3/4] \\ + \epsilon^4 [s_2/8 - \rho^2 s_3/4 - \rho^2(\rho^2 - 16\xi^2)s_4/16 - \rho^4(\rho^2 + 2\xi^2)S_5/8 + \rho^8 S_6/32] \end{array} \right\}$$

$$E_y = E_0 \xi v \{ \epsilon^2 S_2 + \epsilon^4 [\rho^2 S_4 - \rho^4 S_5/4\,] \}$$

$$E_z = E_0 \xi \left\{ \begin{array}{c} \epsilon C_1 + \epsilon^3 [-C_2/2 + \rho^2 C_3 - \rho^4 C_4/4] \\ + \epsilon^5 [-3C_3/8 - 3\rho^2 C_4/8 + 17\rho^4 C_5/16 - 3\rho^6 C_6/8 + \rho^8 C_7/32] \end{array} \right\}$$

The corresponding magnetic fields are given by,

$$\Rightarrow \ \nabla \times \vec{\mathbf{E}} = -\partial \vec{\mathbf{B}}/\partial t$$

More detailed description of given fields is provided in chapter 3

To determine the energy change experienced by an electron moving in the same direction as the wiggler magnet, one must solve the equation of motion. We utilize the usual Lorentz equation, which is given as follows.

$$\frac{d\mathbf{p}_i}{dt} = -e[\mathbf{E}_i + (\boldsymbol{\beta}_i \times \mathbf{B}_i)];$$

$$\frac{d(\gamma mc^2)}{dt} = -ec\boldsymbol{\beta}_i \cdot \mathbf{E}_i$$

where $i = x, y, z$.

Here, $\boldsymbol{p_i} = \gamma mc\boldsymbol{\beta_i}$ and Lorentz factor $\gamma = \sqrt{1 - \boldsymbol{\beta_i^2}}$, $\boldsymbol{\beta_i} = \boldsymbol{v_i}/c$ is normalized electron velocity and c is the speed of light. We decompose eq. (8) into x, y, z coordinates and normalize the variables throughout the equations in terms of normalized constant defined as $\tau \to \omega\tau$, $a_i \to eE_i/m_0\omega_0$, and $b_i \to eB_i/m_0\omega_0$, where $i = x, y, z$, respectively.

2.2.2 Undulators

2.2.2.1 Wiggler magnetic field

This section focuses on characterizing and applying helical and planar wiggler magnetic fields in the field of particle accelerator technology. Helical wiggler configurations involve magnets placed in a helical pattern to create a magnetic field that oscillates along the path of charged particles. The oscillating field generates synchrotron radiation, which is essential for scientific and industrial purposes including producing X-rays for medical imaging and materials analysis. Planar wiggler configurations consist of magnets placed in a planar pattern, generating a transverse magnetic field that results in lateral oscillation of charged particles. The oscillations lead to increased energy spread and reduced emittance, which are crucial for improving particle beam quality in accelerators. This chapter offers valuable insights into the design principles, operational parameters, and performance characteristics of helical and planar wiggler magnetic fields. It discusses how these fields can be used to advance accelerator technology and support cutting-edge research in various scientific disciplines. Profiles that are used to describe the wiggler magnetic field.

2.2.2.2 For helical wiggler magnetic field

First, we consider the helical wiggler field given as

$$\vec{B} = B_0 \cos(k_w z)\hat{e}_x + B_0 \sin(k_w z)\hat{e}_y \qquad \text{for } z \leq z_t$$

Here B_0 is maximum value of the wiggler magnetic field, k_w is the wiggler wave vector. After certain length of the wiggler, constant tapering is applied along the wiggler length.

$\vec{B} = B_0 \hat{e}_y$ for $z > z_t$.

2.2.2.3 Planar wiggler magnetic field

In addition, we study IFEL interaction using a planar wiggler magnetic field described as,

$\vec{B} = B_0 \sin(k_w z) \hat{e}_y$ for $z \le z_t$

with constant tapering after a certain length, and the profile is given as

$\vec{B} = B_0 \hat{e}_y$ for $z > z_t$

2.3 Laser wakefield acceleration

Here, we first introduce the basic principles of laser wakefield acceleration (LWFA). The initial discussion covers the fundamental characteristics of plasma and laser physics. LWFA is then introduced by combining these.

2.3.1 Plasma

Plasma is composed of charged particles. For instance, plasma is formed when a gas is heated to the point where electrons can escape their nucleus. Plasmas exhibit the characteristic attribute of particle interaction at a distance. Atoms and molecules in a gas or liquid are generally electrically neutral and mostly interact through collisions at proximity. Interactions in solids can be explained using models in which a vibrating atom transfers energy to its closest neighbouring atoms. In a plasma, charged particles interact across greater distances through electromagnetic interaction and collisions. This leads to physics that is not observed in the other three states.

This thesis only deals with quasi-neutral plasmas, when the total charge in the plasma is balanced to zero.

2.3.2 Plasma frequency

When a neutral plasma experiences a localized displacement of charge, it will generate an electric field to rectify the situation. The result will be plasma particles moving in an oscillatory pattern. The following assumptions can be used to directly derive the oscillation's frequency, ω_p. We think about a plasma that has no magnetic fields and is at 0 Kelvin in one-dimensional, endless space. In this case, it is assumed that ions will stay still, while electrons are thought to be moving about thousand times faster. Because ions are much heavier than electrons so they can't move. This implies that in this straightforward plasma model, ions remain stationary even though strong forces may speed up electrons.

So, the plasma frequency is given by the relation:

$$\omega_p = e\sqrt{\frac{n_o}{\epsilon_0 m_e}}$$

Where the $'e'$ is charge of electron, m_e is the mass of an electron.

The plasma frequency can be expressed using this non-relativistic formula. The fact that the frequency ω_p doesn't depend on the wave vector k is an intriguing observation. This rules out the possibility of defining a wavelength using plasma oscillations alone. Therefore, the speed of the displacement source is used to determine the wavelength of a plasma wave.

2.3.3 Electromagnetic pulses in vacuum

We analyse the transmission of electromagnetic waves in a uniform plasma with an external magnetic field $(B = B_0\hat{j})$ under weakly nonlinear conditions.

Profile of field distribution of Gaussian laser pulse

$$E^2 = E_0{}^2 \exp\left[-\frac{2\left(\xi - \frac{L}{2}\right)^2}{r_0{}^2}\right] \qquad 0 \le \xi \le L$$

Where E_0 is the maximum amplitude of Gaussian laser.

The value of a_0 is given by.

$$a_0 = 0.85\lambda_0^2[\mu m]\sqrt{I_0(10^{18}W/cm^2)}$$

a_0 Is a relation between the electric field's driving strength and the $'m'$ electron's relativistic mass. An $a_0 = 1$, laser pulse, for instance, causes electrons to tremble with kinetic energy mc^2 equivalent to their mass.

2.3.4 Ponderomotive force

The pondermotive force is a key concept in laser wakefield theory, responsible for displacing electrons as the laser pulse propagates in an LWFA. The force is highly relativistic due to typical laser pulse intensities exceeding $10^{18}W/cm^2$ with $a_0 > 1$.

For plasma density n_0 the ponderomotive force is given by.

$$F_{PM} = -\frac{\epsilon_0 \omega_p^2}{4\omega^2}\nabla\langle E\rangle$$

2.4 Simulation study of two-color laser wakefield acceleration

2.4.1 Simulation Codes

In this study, we utilised two robust simulation tools, namely EPOCH and cpl PIC code, to examine the acceleration of single and two-color laser wakefields. The utilisation of these codes is of great significance within our technique, as they provide advanced functionalities for the modelling and analysis of intricate physical phenomena at the nanoscale scale. The EPOCH software, known for its adaptability and durability, allows us to accurately simulate plasma-related phenomena, offering in-depth understanding of the dynamics of particle acceleration in laser-plasma interactions. Furthermore, the cpl PIC code, renowned for its high efficiency and precision, enhances our simulations by providing sophisticated particle-in-cell (PIC) techniques. This enables us to effectively simulate the complex interplay between electromagnetic fields and charged particles within the plasma milieu. By using the synergistic capabilities of these two codes, we can do detailed and

trustworthy simulations of single and two-color laser wakefield acceleration, thus enhancing our comprehension of this state-of-the-art area of study.

2.4.2 Simulation Setup

Key parameters of the single and two-colour laser wakefield acceleration.

For single-colour laser wakefield acceleration

1.	Laser's energy	2.1J
2.	Normalised vector potential (a_0)	1.83
3.	Pulse duration	$30fs$
4.	Laser intensity (I_{L1})	$7.2 \times 10^{18} W/cm^2$
5.	Laser wavelength	800nm
6.	Beam waist size $(2w_{L1})$	$50\mu m$

Table 2.1 field parameters for single-color laser wakefield acceleration

- key parameters of the two-colour laser

parameters	For driving laser pulse	For the second laser pulse
Laser energy	1.9J	82.8mJ
Normalised vector potential	a_{L1}=1.74	$a_{L2} = 1.8$
Pulse duration	τ_{L1}=30fs	τ_{L2}=30fs
Laser intensity	I_{L1}=6.5 $\times 10^{18} W/cm^2$	I_{L2}=2.8 $\times 10^{19} W/cm^2$
Laser wavelength	λ_1=800 nm	λ_2= 400 nm

Beam waist size	$2w_{L1}=50\mu m$	$2w_{L2}=5\mu m$

Table 2.2 field parameters for two-color laser wakefield acceleration

- Explain the characteristics of the plasma medium (e.g., density, temperature).

1	Plasma density	$8 \times 10^{18}\text{cm}^{-3}$

Table 2.3 field parameters for plasma

- the simulation domain size and boundary conditions.

1	Simulation box size	$250c/\omega_p \times 450c/\omega_p$
2	Simulation box divided	2000×5000 cells
3	No. of particles in a cell	16
4	Velocity of light	c

Table 2.4 field parameters for simulation setup.

Sources of data: Experimental results from numerous research papers will be compared to theoretical results.

Research Design: the whole analysis is based on numerical, simulation and analytical modelling.

Research Tools: MATHEMATICA, and ORIGIN for programming and curve designs. Python for for simulation study.

Chapter 3 (3.1)

Comparative study of inverse free-electron acceleration based on helical and planar wiggler field

3.1.1 Introduction

Laser-induced particle acceleration in a vacuum remains an active area of research for the last few decades because conventional particle accelerators are highly expensive and huge. The vacuum particle acceleration scheme provides the base to accelerate electrons within a few mm length range as compared to the conventional one. In 2004 Neptune laboratory at UCLA conducted an experiment and an electron with 70 MeV/m accelerating gradients and 20 MeV(150%) energy gain in 54cm long tapered undulator is achieved[62], this is the first experimental demonstration to achieve high-level energy gain till the date. In 2010 another experimental setup was designed at ATF in BNL to accelerate electron beam with more than 70 MeV energy gain and 120 MV/m acceleration gradient with the help of 0.5 TW CO_2 laser system and 60cm long tapered and helical magnetic undulator[53]. Chirped-pulse amplification [100] and tightly focused laser-beam phenomena's promises to produce ultra-high and ultra-intense laser beams. The development of these schemes can reveal the new horizons to accelerate electrons in the tens of the GeV regime and produce up to 100Mv/m gradient beam by using Inverse Free Electron Laser phenomena in helical undulator[28]. The phenomena of IFEL is similar to Free Electron Laser (FEL), besides in IFEL, net energy is transferred from laser radiation to electron. A magnetic undulator generates a transverse motion of the wave in the direction of its electric field, resulting in the transfer of net energy from the laser to the electron, therefore accelerating the electron. In a study, Gashti and Jafri present the importance of an external wiggler magnetic field to produce table top particle accelerators[101]. Numerical and analytical analysis of electro-magnetic fields under the influence of tightly focused laser beams is investigated in a vacuum [64], [65], [102]. The

phenomenon of the tightly focused and chirped laser pulse in a vacuum has been examined by Li. The significance of laser focussing and the optimisation of various pulse parameters for achieving maximum electron energy gain has been demonstrated.[103]. Moody *et al.* demonstrated a laser technology that accelerates a 75 MeV electron beam to 125 MeV using a 0.8 μm wavelength, 100fs, and 500 mJ commercial Ti: Sa laser beam in a strong, tapered planar undulator.[66]. Singh and Tripathi[104] studied the IFELA of electrons in vacuum and plasma under the influence of a tapered magnetic wiggler undulator. Sudar *et al.* evaluated experimental data and successfully extracted approximately 30% of coherent radiation by deaccelerating a 65MeV e-beam up to 35MeV [67]. A simulation study presented by Duris *et al.* accelerates more than 70% of the particle beam within 2% energy spread and 97 MeV final energy by using a half of milimeter-long and strongly tapered helical undulator[68]. Gupta *et al.* have presented a scheme to accelerate electrons up to the tens of GeV by circularly polarized laser beam in the pulsed magnetic field. The radial field is diminished but the longitudinal field remains for trapping the particle and the external magnetic field enhances the energy of an electron[105]. Khullar *et al.* investigated the effect of a staggered undulator on IFELA and showed that the periodic length and gap between two poles of a staggered undulator affect the electron acceleration in IFEL[69]. Gupta *et al.* have investigated the role of a tightly focused laser beam and chirped pulse for more energy gain and increasing eelectron acceleration[106]. Khazaeinezhad *et.al.* found that a tapered wiggler magnetic field of a proper tapering point increased electron acceleration.[74]. Azimuthal magnetic field and circularly polarised chirped laser in electron acceleration is investigated by Ghotra *et al.*[107]. An electron with a gain of GeV in energy was accelerated from a few MeV of beginning energy by Kant *et al.* using a linearly polarised chirped laser pulse influenced by a magnetic field.[108]. Duris *et al.* get the attention of researchers in the field of particle acceleration by producing an electron with ~50 MeV energy gain in a powerful undulator[59]. A design of helical undulator to minimize the diffraction and maximize the electron energy gain is preferred

by Rosenzweig *et al.*[60] and A novel type of undulator, termed as a laser-driven bifilar capacitor coil, is introduced[109]. The impact of chirping in laser and tapering in the planar magnetic field were numerically examined by Kumar *et al.* The results indicate that the optimisation of laser and magnetic field parameters leads to an increase in electron energy gain.[110]. By optimising the injection parameters, Salamin and Keitel have investigated the impact of a highly concentrated laser beam and achieved an electron energy gain in the GeV range.[18]. Mirzanejhad *et al.* have investigated dynamics of an electron bunch (10^5 e^- of 10 MeV and 0.1% energy spread) in the influence of helical magnetic wiggler field and analyzed that electron–pulse interaction is becoming less in the case of radial Gaussian profile scheme rather than a temporal profile, and for batter energy gain, a scheme of the micro bunching of electrons is also proposed and show the results by proper numerical analysis[71]. For the increment in the electron's energy, a collective behavior of laser and plasma interaction and IFEL electron acceleration is studied in the presence of a static wiggler magnetic field by Agarwal *et al.*[72]. Singh *et al.* have studied the electron's motion in radially polarised laser pulse for different and optimized laser field and magnetic parameters and show that the value of energy gain is enhanced with increasing both laser and magnetic field parameters[111]. Kumar *et al.* numerically achieved an electron with GeV energy by injecting an electron of MeV energy, and optimization of field parameters was also done for high energy gain[58]. A comparative numerical analysis of IFEL interaction with a misaligned electron beam under the influence of an electromagnetic wiggler and helical electrostatic wiggler is investigated by Khullar *et al.* in which they have shown that the presence of electromagnetic wiggler provides better results over the magnetostatic wiggler[112]. Nikhrah and Jafri have employed the novel scheme of electrostatic wiggler known as Poul wiggler to confine the electron and numerically analysed the trajectory of the electron and found that the electron can attain maximum gain in the small region of high amplitude magnetic wiggler and effect of the initial velocity of e-beam also investigated[113]. Experimental study of splitting a laser pulse into two parts in

which one part is used for accelerating the electron and another is used to generating an electromagnetic undulator and produced a MeV energy beam by introducing a KeV power laser beam is presenting by Gadjev *et al.*[56].

In this chapter, single-electron dynamics and its acceleration is investigated in a tightly focussed Gaussian laser and a planar as well as in a helical wiggler magnet. Typical geometry of tightly focused laser beam including the fifth-order term in the diffraction angle ϵ is presented in section 3.1.2. Numerical analysis of helical and planar wiggler fields for different field parameters is presented in section 3.1.3. Finally, the conclusion and results are discussed in section 3.1.4

3.1.2 Electron acceleration in inverse free-electron laser
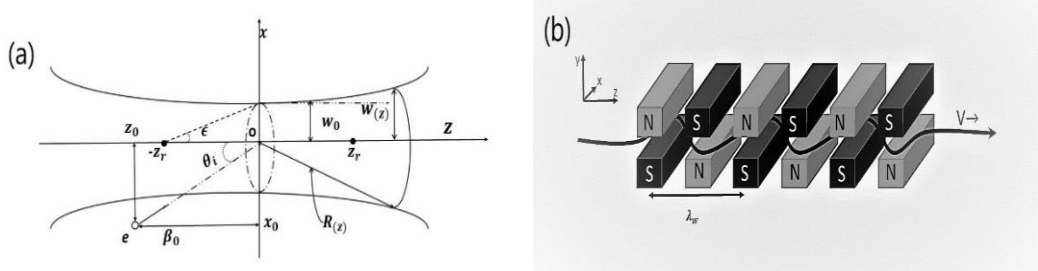
Figure 3.1 (a) Schematic layout of tightly focused laser beam and (b) planer wiggler geometry and associated magnetic field.

3.1.2.1 Tightly focused laser field

For numerical simulation, a tightly focused laser beam is taken whose different field parameters are given as [24],

$$E_x = E_0 \left\{ \begin{array}{c} S_0 + \epsilon^2 [\, \xi^2 S_2 - \rho^4 s_3/4\,] \\ +\epsilon^4 [s_2/8 - \rho^2 s_3/4 - \rho^2(\rho^2 - 16\xi^2)s_4/16 - \rho^4(\rho^2 + 2\xi^2)S_5/8 + \rho^8 S_6/32] \end{array} \right\}$$

(3.1)

$$E_y = E_0 \xi v \{\epsilon^2 S_2 + \epsilon^4 [\rho^2 S_4 - \rho^4 S_5/4\,]\}$$

(3.2)

$$E_z = E_0 \xi \left\{ \begin{array}{c} \epsilon C_1 + \epsilon^3 [-C_2/2 + \rho^2 C_3 - \rho^4 C_4/4] \\ +\epsilon^5 [-3C_3/8 - 3\rho^2 C_4/8 + 17\rho^4 C_5/16 - 3\rho^6 C_6/8 + \rho^8 C_7/32] \end{array} \right\}$$

(3.3)

And the components of corresponding magnetic fields are given by,

$$\nabla \times \vec{\mathbf{E}} = - \partial \vec{\mathbf{B}}/\partial t \qquad (3.4)$$

In figure (1) $w(z)$ Represent the beam waist size at any point z on the axis and $w(z)$ is given as $w(z) = w_0\sqrt{1 + (z/z_r)^2}$, where w_0 is the radius of laser beam focus. Here z_r represent the Rayleigh length which is given by $z_r = kw_0^2/2$. Other parameters are $\epsilon = w_0/z_r$, $\xi = x/w_0$, $v = y/w_0$ and

$$E = E_0(w_0/w)exp\,[-r^2/w^2]; \quad E_0 = kA_0 \qquad (3.5)$$

$$S_n = (w_0/w)^n sin\,(\psi + n\psi_G)\,; \quad n = 1,2,3, \qquad (3.6)$$

$$C_n = (w_0/w)^n cos\,(\psi + n\psi_G) \qquad (3.7)$$

Further, $k = \omega/c$, $r^2 = x^2 + y^2$ and $\rho = r/w_0$. Above equations are calculated using a vector potential A_0, and frequency ω. The ψ is read as $\psi = \psi_p - \psi_R + \psi_G + \psi_0$, where ψ_0 is known as the initial constant phase. ; $\psi_p = \eta = \omega t - kz$ is plane wave phase and $\psi_G = (z/z_r)$ is the Guoy phase. z varies from $-\infty\ to\ \infty$; the value of $\psi_R = kr^2/2R$, where $R_z = z + z_r^2/z$ is the radius of curvature of the wavefront.

3.1.2.2 Helical wiggler field

Here, the helical wiggler field given as, $\vec{B} = B_0 \cos(k_w z)\hat{e}_x + B_0 \sin(k_w z)\hat{e}_y$ for $z \leq z_t$ Here B_0 is the maximum value of the wiggler magnetic field ampliude, k_w is the wiggler wave vector. After certain length of the wiggler, constant tapering is applied along the wiggler length.

3.1.2.3 Planar wiggler field

In addition, we study IFEL interaction using a planar wiggler magnetic field described as, $\vec{B} = B_0\,sin(k_w z)\,\hat{e}_y$ for $z \leq z_t$ with constant tapering after a certain length, and the profile is given as $\vec{B} = B_0\hat{e}_y$ for $z > z_t$.

3.1.3 Electron acceleration in IFEL

Net energy gain or loss obtained by an electron in its interaction with a laser field co-propagating along the wiggler magnet calculated by using following equations. We use the standard Lorentz equation which is described as follows,

$$\frac{d\boldsymbol{p_i}}{dt} = -e[\boldsymbol{E_i} + (\boldsymbol{\beta_i} \times \boldsymbol{B_i})]; \qquad (3.8)$$

$$\frac{d(\gamma mc^2)}{dt} = -ec\boldsymbol{\beta_i} \cdot \boldsymbol{E_i} \qquad (3.9)$$

Here, $\boldsymbol{p_i} = \gamma mc\boldsymbol{\beta_i}$ and Lorentz factor $\gamma = \sqrt{1 - \boldsymbol{\beta_i^2}}$, $\boldsymbol{\beta_i} = \boldsymbol{v_i}/c$ is normalized velocity of electron and c is speed of light. We decompose eq. (8) into x, y, z coordinates and normalize the variables throughout the equations in terms of normalized constant defined as $\tau \to \omega\tau$, $a_i \to eE_i/m_0\omega_0$, and $b_i \to eB_i/m_0\omega_0$, where $i = x, y, z$, respectively.
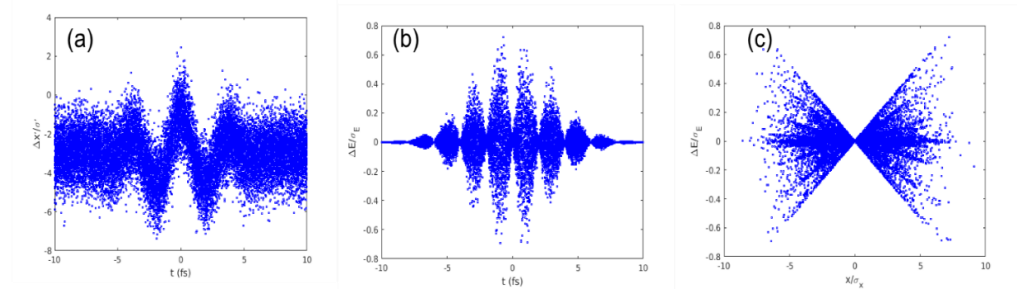
Figure 3.2 (a) shows angular modulation of electrons inside the wiggler. (b) shows the energy modulation of electrons, and (c) shows correlation of the horizontal coordinate and energy generated due to interaction with the laser.

3.1.4 Numerical results and discussion

For an illustration of the above IFEL technique, we present calculations for a single electron dynamic and its acceleration under the influence of a tightly focused laser. Two different geometries of the wiggler magnet are considered; one helical and another one is a planar wiggler. In laser parameters, laser field

parameter a_0 is derived from the expression, $a_0 = 0.85 \times 10^{-9}\lambda_0(\mu m)\sqrt{I_0\,(W/cm^2)}$. Here laser's wave-length $\lambda_0 = 800$ nm and I_0 is laser intensity in W/cm^2. We choose electron's initial position at $(kx_0, ky_0, kz_0 \equiv 0, 0, 0.01)$ and the laser is focused at (0,0,0) position. It is customary to use dimensionless constants; normalized laser field amplitude $a_0 = eE_0\,/m\omega_0 c$, normalized wiggler field amplitude $b_0 = eB_0/m\omega_0$. For maximum energy gain in IFEL acceleration, FEL resonance condition $\gamma^2 = (1 + K^2)\lambda_w/2\lambda_0$ is maintained along the undulator. Here $c\;\lambda_0$ is the laser wavelength, and $K = eB_0 k_w/2\pi mc$ is a normalized wiggler parameter, k_w is the wiggler wave vector and B_0 is the maximum wiggler field amplitude and m is the electron mass. The tapering of wiggler field is introduced along the undulator length for maintain the resonance [114] .

3.1.4.1 Electron acceleration in helical wiggler field

In the following discussion, electron dynamics and acceleration is studied in tightly focused laser field and helical wiggler geometry. The wiggler fields are given by eqations (8) and (9).

46
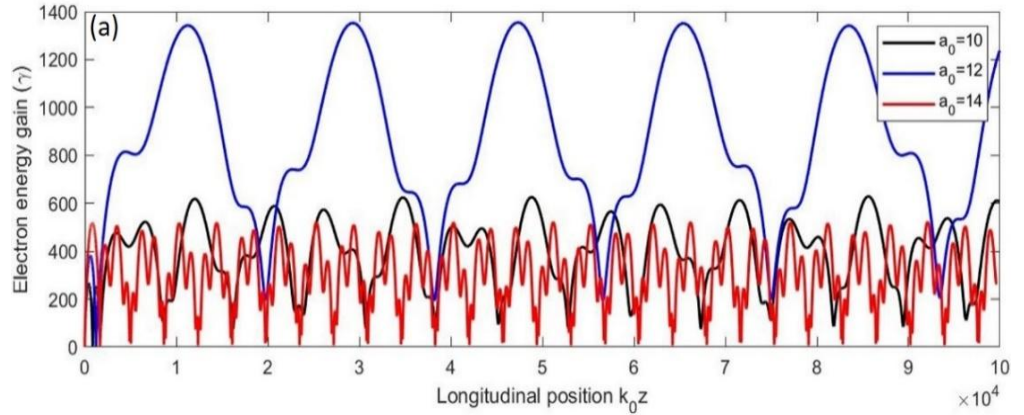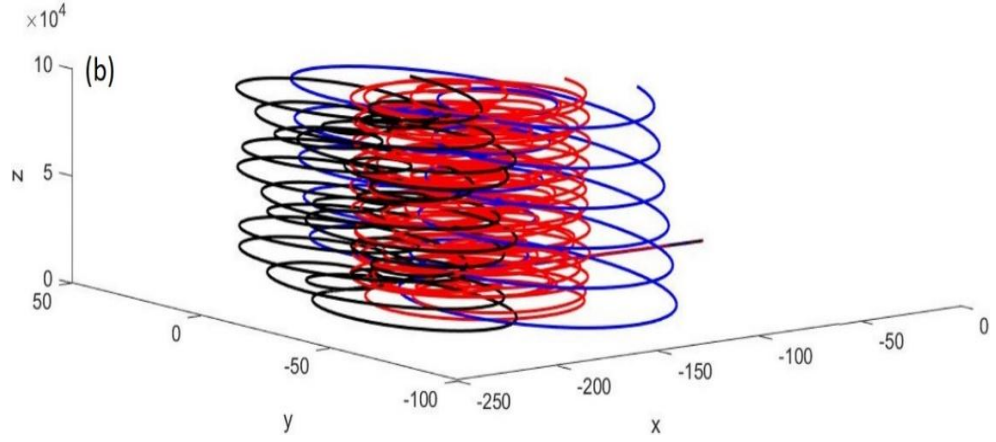
Figure 3.3 (a) Evolution of the electron energy gain (γ) with longitudinal position $(k_0 z)$. Different laser field parameter $a_0 = 10$ $(I_0 = 2.16 \times 10^{20} \, W/cm^2)$, $a_0 = 12$ $(I_0 = 3.11 \times 10^{20} \, W/cm^2)$, $a_0 = 14$ $(I_0 = 4.23 \times 10^{20} \, W/cm^2)$ respectively. Other laser parameters are as: beam-waist $w_0 = 300$, initial-laser phase $\psi_0 = 0$, pulse duration $\tau = 100$, normalized wiggler field $b_0 = 0.5$, tapering point $k_0 z_t = 2000$, respectively. Figure 4.3 (b) shows 3-D trajectory of the electron.

Figure 3.3 shows electron acceleration and its dynamics using a tightly focused laser and helical magnetic wiggler field. The electron energy gain (γ) is shown with the longitudinal position $(k_0 z)$ in figure 3.3(a). The outcomes show that energy gain is sensitive to the normalized laser field amplitude a_0. An energy gain of 677 MeV $(\gamma = 1355)$ is observed for $a_0 = 12$, which is higher than the energy gain achieved 314.65 MeV $(\gamma = 629.3)$ for $a_0 = 10$ and the energy gain 261.4MeV $(\gamma = 522.8)$ for $a_0 = 14$, respectively. Other laser and wiggler normalized parameters in the calculation are as follows: $w_0 = 300$, $\tau = 100$, $b_0 = 0.5$, $kz_t = 2000$, and $\psi_0 = 0$. Thus, for a higher laser field, the electron energy gain continuously increases if the electron remains in the accelerating phase of the laser fields and losses energy quickly in the decelerating phase. An increase in its electric field that causes a sharp increase in the electron energy gain. Similar investigations are reported in the past in[59],[115], [125] that show similar enhancement. In IFEL interaction, tapering of wiggler field plays crucial role in maintaining the FEL resonance condition discussed earlier. We have

used tapering of magnetic field B_0 after $kz_t = 2000$ to maximize the energy gain. In Figure 3(b), the dependency of laser field parameter a_0 is shown on electron trajectory. One can notice that electron follows a circular trajectory in the presence of laser fields and wiggler fields.
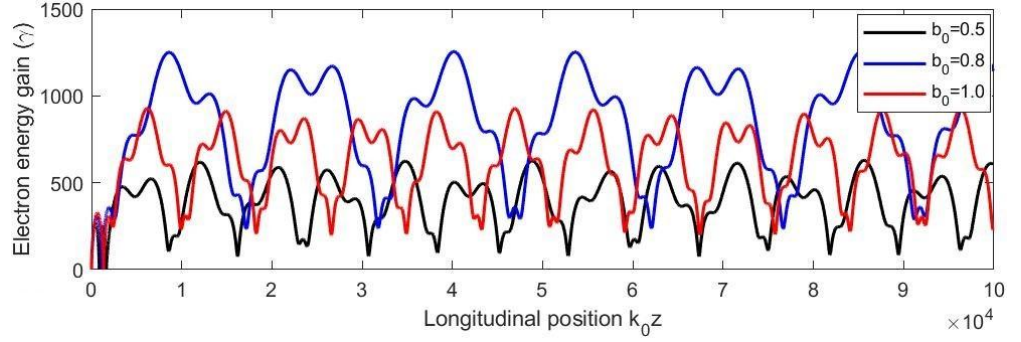
Figure 3.4 Variation in the electron energy gain (γ) vs longitudinal position ($k_0 z$) for different normalized wiggler field amplitudes b_0=0.5 , 0.8 , and 1.0, respectively. Other parameters are as: $a_0 = 10$, $w_0 = 300$, $\psi_0 = 0$, $\tau = 100$, and $k_0 z_t = 2000$, respectively.

In figure 3.4, the effect of helical field amplitude (b_0) is shown on the electron's energy gain. Enhanced energy gain is observed with increasing helical wiggler field. However, necessary optimization is required to find the optimal value of b_0. The maximum electron energy gain of 629 MeV is spoted for the value of $b_0 = 0.8$ (corresponding magnetic field ~ 53.6 MG). With further increasing the magnetic field, the electron gain decreases. The peak gain is 314.65 MeV and 464.6 MeV for $b_0 = 0.5$ (magnetic field ~33.5 MG) and for $b_0 = 1.0$ (corresponding magnetic field ~67MG) respectively. This work demonstrates that the optimised magnetic field is essential for sustaining the IFEL resonance condition and maximising electron energy gain.
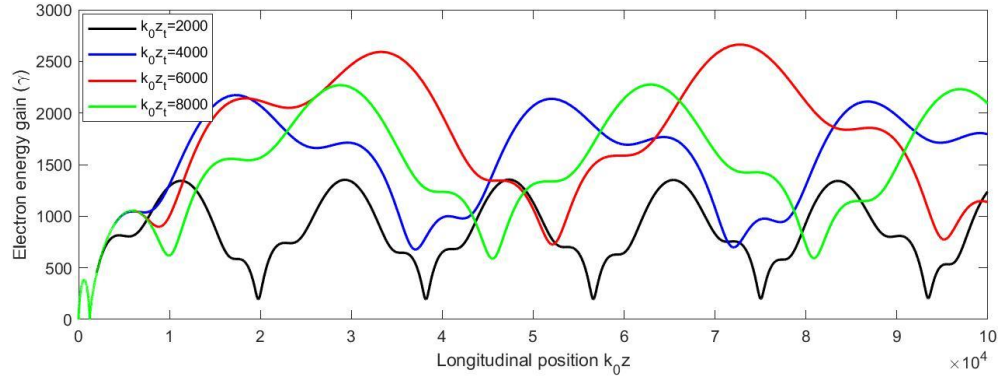
Figure 3.5 Evolution of γ versus longitudinal position $k_0 z$ for different tapering points of helical wiggler field b_0 as: $k_0 z_t = 2000, 4000, 6000$ and 8000, respectively. Other parameters are as: $a_0 = 12$, $\psi_0 = 0$, $b_0 = 0.5$, and $w_0 = 300$, respectively.

Figure 3.5 shows electron energy gain (γ) v/s $k_0 z$ for different tapering point along the helical wiggler magnet. Results show that the constant tapering effect is impressive in achieving higher electron energy gain in IFEL interaction. If we change the tapering point $k_0 z_t$ along the wiggler magnet, the electron energy gain highest value of energy 1.331 GeV ($\gamma \sim 2662$) for optimal value $k_0 z_t = 6000$. Strong tapering in helical wiggler provides more resonant energy to achieve a high acceleration gradient, that's why the electron acquires more energy gain. If we further increase the value of the tapering, the electron-laser interaction dephased and the electron loses its energy. Strong tapering effect in helical undulator is experimentally studied at ATF (Accelerator Test Facility) at brookhaven national laboratory[74].

3.1.4.2 Electron acceleration in planar wiggler field

In the following discussion, electron dynamics and acceleration is studied in tightly focused laser and planar wiggler interaction. The planar wiggler field is described by eqs. (8) and eqs. (9).
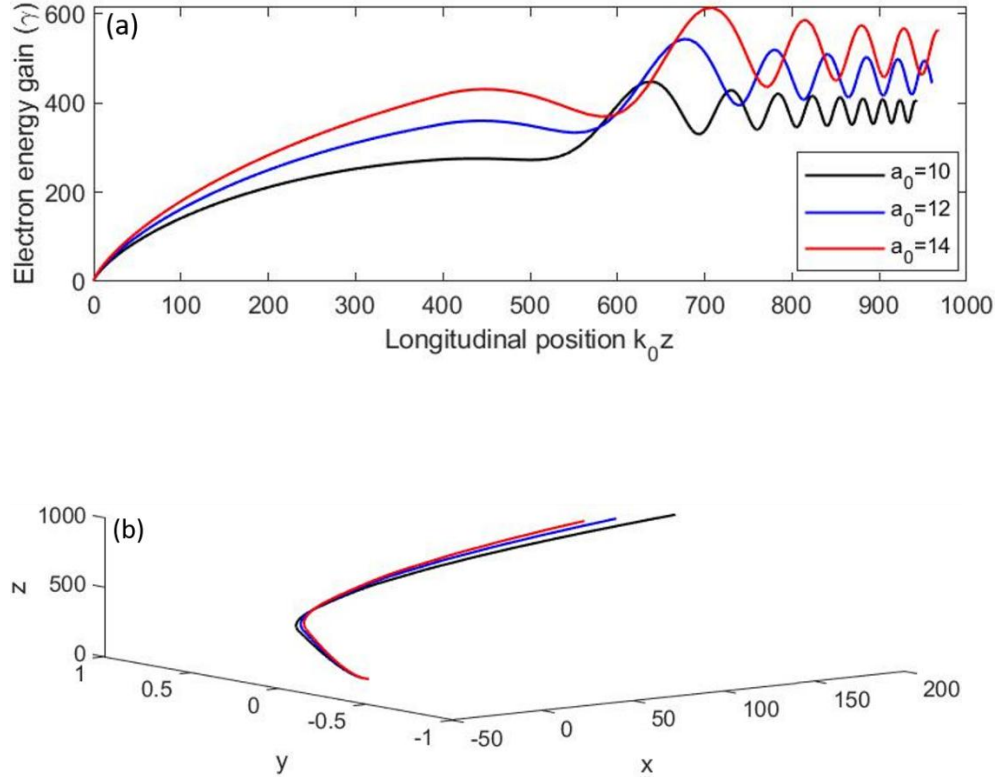
Figure 3.6 (a) Illustrate the electron energy gain(γ) versus longitudinal position $(k_0 z)$ for different laser field parameters $a_0 = 10, 12$, and 14, respectively. The tapering point is chosen at $k_0 z_t = 400$ for planer wiggler. Figure 3.6(b) shows a 3D electron trajectory.

Figure 3.6 (a) shows that maximum energy gained is enhanced as we increasing the value of the laser field parameter a_0. An increment in laser field parameter enhances the electric field by the factor $a_0 = eE_0/m\omega_0 c$ and higher electric field increases the resonance condition duration and interaction time. The maximum energy gain is 306.75 MeV for $a_0 = 14$ $(I_0 = 4.23 \times 10^{20}\ W/cm^2)$ and this energy gain is higher than 223.95 MeV for $a_0 = 10$ $(I_0 = 2.16 \times 10^{20}\ W/cm^2)$, and 271.5MeV for $a_0 = 12$ $(I_0 = 3.11 \times 10^{20}\ W/cm^2)$. Figure 6(b) shows corresponding trajectory for planar wiggler case.
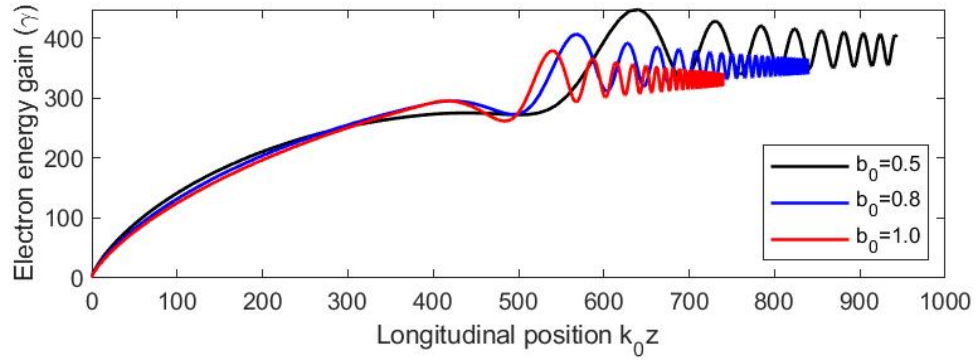
Figure 3.7 shows variation of energy gain v/s longitudinal position $k_0 z$ for different magnetic field parameters $b_0 = 0.5$, $b_0 = 0.8$, and $b_0 = 1.0$, respectively. Other parameters are $a_0 = 10$, $w_0 = 300$, $\beta = 0.5$, $k_0 z_t = 400$, $\psi_0 = 0$, respectively.

Figure 3.7 explain the how wiggler field affects energy gains decreases with increasing the value of planer wiggler field parameters. We figured out from figure 4.7 that decreasing the value of b_0 causes the short of the interaction length and the electron is no longer in the phase with laser field and slow down the motion of the electron. The peak value of energy gain is 223.9 MeV for an optimal value of $b_0 = 0.5$ in the case of the planer wiggler. Electron's energy of 203.7 MeV and 189.6 MeV corresponding to $b_0 = 0.8$ and $b_0 = 1.0$ respectively.
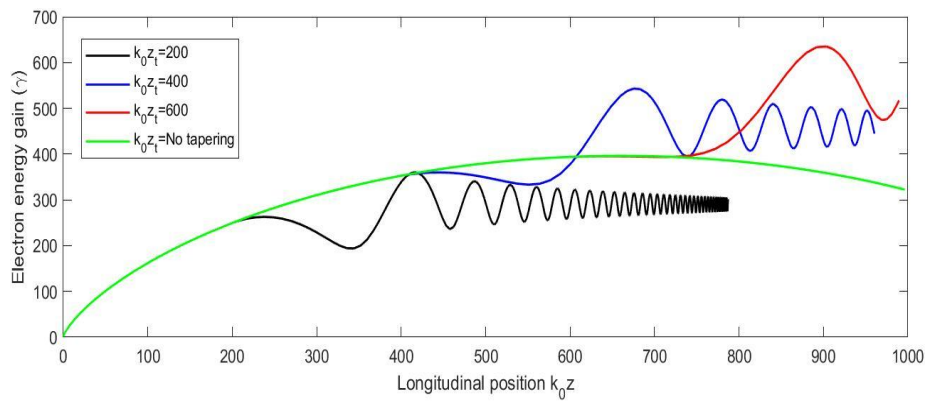
Figure 3.8 Variation of γ versus longitudinal position $(k_0 z)$ with different tapering points $k_0 z_t = 200, 400, 600$, zero tapering along the undulator length, respectively (check figure) is presented for the planar wiggler.

51

The effect of the tapering point is tested on electron energy gain in the planar wiggler geometry as shown in figure 4.7. There is an optimum value of tapering point for which electron achieves the maximum energy gain γ in the planer undulator in IFEL. The maximum electron energy is 180 MeV, 271 MeV, 317 MeV, and 198 MeV, respectively for $kz_t = 200, 400, 600,$ and 1000 (without tapering) respectively.
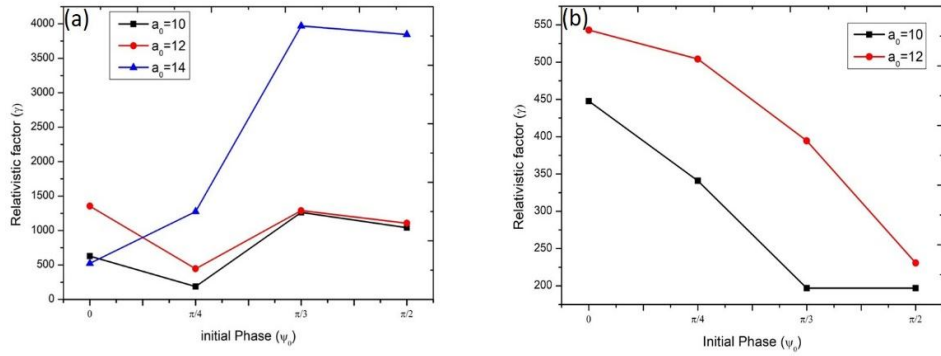
Figure 3.9 Shows change in the maximum energy gain (γ) versus initial phase of the laser pulse (ψ_0), **(a)** for chosen helical geometry for three different a_0=10, 12 and 14 with kz_t=2000, **(b)** for planar geometry with a_0=10 and 12 with k_0z_t=400. Other laser parameters are $b_0 = 0.5$, and $w_0 = 300$, respectively.

Figure 3.9 (a) shows the change in the maximum energy gain (γ) with initial laser phase ψ_0 for various laser field parameters. The initial phase ψ_0 affects electron energy gain. in helical and attains the maximum energy gain γ=3971(~1.95 MeV) at $\psi_0 = \pi/3$, which shows that a legitimate condition of synchronization is required to achieved better electron acceleration. In Figure 3.9 (b), electron energy gain γ vs initial phase ψ_0 for planar wiggler is shown. Here, energy gain is smoothly decreasing in range $\psi_0 \in [0, \pi/2]$. Maximum energy gain $\gamma = 543$ (~271MeV) is achieved in planar wiggler. Comparative study shows that helical wiggler geometry with proper field parameters is superior for IFEL acceleration compared to planar wiggler geometry.

3.1.5 Conclusion

A comparative analysis of single-electron motion with a tightly focused laser beam by using a planer and helical undulator is investigated numerically. Effect of different laser parameters is investigated to maximize the electron acceleration in the IFEL accelerator. For laser field descriptions, a more accurate fifth-order correction in the diffraction angle is considered. Helical wigglers gain more electron energy than planar ones. while we choose helical wiggler, the highest value of maximum energy is 1.331GeV obtained for optimized values of laser field intensity with proper tapering parameters. However, in the planar wiggler, the maximum energy is 300 MeV is received. In planar wiggler, our study shows that electron achieves the highest energy gain earlier but can't maintain it for a longer time. It is observed that the highest gain in the case of helical wiggler is greater than that of planar wiggler under identical laser and wiggler conditions.

Chapter 3.2

Electron acceleration in an inverse free electron laser with a tapered wiggler field

3.2.1 Introduction

Free electron lasers (FELs) are the devices that is use to generate a coherent, ultra-short duration (up to a few femtoseconds) radiation pulse, combining unprecedented power density up to 10^2 W/cm^2 [126]. These fourth-generation light sources are huge in size, very expensive high energy particle accelerators[63], [116], [117].

Direct laser electron acceleration is a favourite topic on the table for researchers from last few decades. The IFEL scheme was first investigated by Palmer in 1972[70], and then courant *et al.* Presented a scheme to achieve high energy particle beam in 1985[118], an experimental demonstration was presented by Columbia University[23] and Brookhaven National Laboratory (BNL) experiments using a nano-second duration 1-5 GW CO$_2$ laser[24], [25], [119].

In IFEL mechanism, a relativistic electron beam is boosted by the power of laser pulse which co-propagates with electron beam[66]. Due to the absence of any propagation medium (plasma or dielectric), the IFEL scheme accelerates electrons by using energy from laser directly instead of dissipating in a medium, additionally, it removes the different plasma potential problems like plasma-instabilities, non-linear propagation of laser, etc.[120], [121], [122]. The coupling of electromagnetic radiation in the magnetic undulator is provided by the ponderomotive force along the beam propagation axis. The undulator magnet transfers energy from wave to electron by oscillating transversely parallel to the electric field in the electromagnetic wave[123], [124]. In resonating condition required energy exchange takes place, the condition for maximum energy transfer from a laser beam to particle in IFEL is as $\lambda_r \approx \lambda_w(1 + b_w^2)/2\gamma^2)$, where λ_r is the wavelength of the laser pulse, λ_w is wiggler

field wavelength, b_w is wiggler field amplitude, and γ is Lorentz factor[118]. Several experiments are carried out on coupling of the laser beam and electron in the IFEL scheme[125], [126], [127], [128], [129], [130]. In an experiment high energy (20MeV) and peak gradient (70 MV/m) with high intense, Co_2 laser beam and tapered magnetic field undulator were achieved at UCLA. In another experiment, a 100 MV/m gradient and highly intense and the focused beam is demonstrated by using helical undulator in the IFEL scheme[59]. Later, the interaction of tightly focused chirped laser pulse is discussed [103]. Dependence of acceleration and retardation of the beam on the phase difference of two laser pulses is investigated in[61]. Later, it was observed that electron motion is highly influenced by longitudinal electric field near by tightly focused laser in ultra-relativistic medium[131]. A new concept of the IFEL acceleration scheme with chirped pulse amplification is demonstrated in[132], where both tapering, and CPA techniques are introduced for improvement in the IFEL gradient and interacting bandwidth also increases. In addition, the influence of chirped laser magnetic field interaction in the IFEL acceleration scheme was investigated and they showed how tightly focused chirped pulse enhances the energy from MeV to GeV[108]. In other work, how magnetic wiggler perpetuates the resonance of betatron and enhances the energy gain (up to 4 times more) is shown[133]. Mirzanejhad *et al.* examined an electron bunch interacting with a helical magnetic wiggler field to achieve greater gain[134]. Kumar at el. investigated electron dynamics by a radially polarised chirped laser, and studied the effect of wiggler magnetic field[135]. Kumar *et al.* studied an IFEL scheme, in this scheme they investigated a chirped Gaussian laser beam in IFEL by considering more accurate (*i.e.,* the seventh order spatial term and first order temporal term in the laser) field expressions. Optimum values are selected for achieving a better resonance condition to enhance the net energy gain, As a result they show that the combination of tightly focused laser beam and short pulse length interaction is much dominate then the combination of narrow beam with larger pulse and wide beam waist with longer pulse, and extract GeV energy gain from 10 MeV electron by using optimised laser parameters and considering tapering

and chirp phenomena[58]. Salamin *et al.* demonstrate that electron acceleration in GeV reign is feasible if we inject the electron at a small angle towards the beam axis, and present mathematically result of dynamics of electron for the optimized values of injected laser parameters, and numerically shows the importance of introduction of the 5th order corrections in diffraction angle of the auxiliary field[125].

In this paper, we investigate the IFEL scheme in using tightly focused laser beam. The effect of planer wiggler field with tapering effect is modelled on electron dynamics in sections 3.2.2. The electron acceleration is studied for different laser intensities, for frequency-chirped parameters. Here we introduce up to the fifth-order term of diffraction angle ϵ in the field to focusing the laser beam at a few micron spot sizes. In section3.2.3, numerical results are presented. Finally, in section 3.2.4, a conclusion is given.

3.2.2 Electron acceleration by a tightly focused laser beam in a wiggler field

The schematic layout of IFEL interaction is presenteed in Figure 5.1. The laser beam shown is described by a vector potential linearly polarized along $+y$ direction and followed by a planar wiggler magnet.
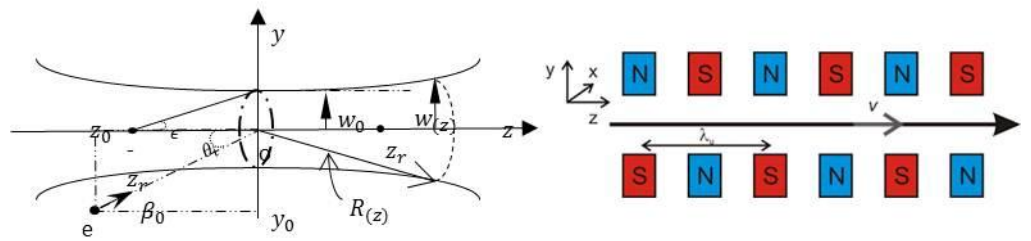
Figure 3.10 schematic layout of the tightly focused laser and planar wiggler.

3.2.2.1 Tightly focused laser field

Here we consider the tightly focused laser whose field components are given as [35],

$$E_x = E\left\{S_0 + \epsilon^2\left[\xi^2 S_2 - \frac{\rho^4 S_3}{4}\right] + \epsilon^4\left[\frac{S_2}{8} - \frac{\rho^2 S_3}{4} - \frac{\rho^2(\rho^2 - 16\xi^2)S_4}{16} - \frac{\rho^4(\rho^2 + 2\xi^2)S_5}{8} + \frac{\rho^8 S_6}{32}\right]\right\}$$

(3.2.1)

$$E_y = E\xi v\left\{\epsilon^2 S_2 + \epsilon^4\left[\rho^2 S_4 - \frac{\rho^4 S_5}{4}\right]\right\}$$

(3.2.2)

$$E_z = E\xi\left\{\epsilon C_1 + \epsilon^3\left[-\frac{C_2}{2} + \rho^2 C_3 - \frac{\rho^4 C_4}{4}\right] + \epsilon^5\left[-\frac{3C_3}{8} - \frac{3\rho^2 C_4}{8} + \frac{17\rho^4 C_5}{16} - \frac{3\rho^6 C_6}{8} + \frac{\rho^8 C_7}{32}\right]\right\}$$

(3.2.3)

And the components of corresponding magnetic fields are given by,

$$B_x = 0 \tag{3.2.4}$$

$$B_y = E\left\{S_0 + \epsilon^2\left[\frac{\rho^2 S_2}{2} - \frac{\rho^4 S_3}{4}\right] + \epsilon^4\left[-\frac{S_2}{8} + \frac{\rho^2 S_3}{4} + \frac{5\rho^4 S_4}{16} - \frac{\rho^6 S_5}{4} + \frac{\rho^8 S_6}{32}\right]\right\}$$

(3.2.5)

$$B_z = Ev\left\{\epsilon C_1 + \epsilon^3\left[\frac{C_2}{2} + \frac{\rho^2 C_3}{2} - \frac{\rho^4 C_4}{4}\right] + \epsilon^5\left[\frac{3C_3}{8} + \frac{3\rho^2 C_4}{8} + \frac{3\rho^4 C_5}{16} - \frac{\rho^6 C_6}{4} + \frac{\rho^8 C_7}{32}\right]\right\}$$

(3.2.6)

Here, the laser beam waist size $w(z)$ at any point z on the axis is given by $w(z) = w_0\sqrt{1 + \left(\frac{z}{z_r}\right)^2}$ where w_0 is circular radius of laser beam focus. Here z_r represent the Rayleigh length and given by $z_r = \frac{kw_0^2}{2}$. Other parameters are $\epsilon = \frac{w_0}{z_r}$ and $\xi = \frac{x}{w_0}$, $v = \frac{y}{w_0}$ and

$$E = E_0\frac{w_0}{w}\exp\left[-\frac{r^2}{w^2}\right], \quad E_0 = kA_0,$$

(3.2.7)

57

$$S_n = \left(\frac{w_0}{w}\right)^n \sin\left(\psi + n\psi_G\right); \quad n = 1,2,3,.$$ (3.2.8)

$$C_n = \left(\frac{w_0}{w}\right)^n \cos\left(\psi + n\psi_G\right)$$ (3.2.9)

Further $k = \frac{\omega}{c}$, $\quad r^2 = x^2 + y^2$, and $\rho = \frac{r}{w_0}$. For numerical analysis we choose a vector potential heaving amplitude A_0 and frequency ω. The value of ψ is read as: $\psi = \psi_0 + \psi_p - \psi_R + \psi_G$,; $\psi_p = \eta = \omega t - kz$ is plane wave phase and $\psi_G = \left(\frac{z}{z_r}\right)$ is the Guoy phase. ψ_0 is constant phase.

3.2.2.2 Planar wiggler field with tapering

In addition, we consider planar wiggler magnetic field with constant tapering and the profile is given as,

$$\vec{B} = B_0 \sin(kz)\,\hat{e}_y \quad \text{For} \quad z \le z_0$$ (3.2.10)

$$\vec{B} = B_0\hat{e}_y \quad \text{For} \quad z > z_0$$ (3.2.11)

3.2.2.3 Electron acceleration in IFEL

For electron dynamics of the electron inside wiggler, we use standard Lorentz equation, which is described as follows,

$$\frac{dp}{dp} = -e[E + \beta \times B];$$ (3.2.12)

$$\frac{d(\gamma mc^2)}{dt} = -ec\beta \cdot E$$ (3.2.13)

In equation (12) and (13), are solved using Runge-kutta method. Here, $p = \gamma mc\beta$ and Lorentz factor is given by $\gamma = (1 - \beta^2)^{-\left(\frac{1}{2}\right)}$, c is speed of light, β is normalized electron velocity. We decompose eq. (12) into x, y, z coordinates, normalization constant defined as $\tau = \omega t$, $\beta_i = v_i/c$, $e_i = eE_i/m_0\omega c$, and $b_i = eB_i/m_0\omega$, where $i = x, y, z$ and $b_0 = eB_0/m_0\omega$, respectively.

3.2.3 Numerical results

In this part, we analyse the data for a single particle (electron) dynamics. For the analysis, we consider a laser pulse with the normalized laser field parameter calculated by, $a_0 = 0.85 \times 10^{-9} \lambda_0 (\mu m) \sqrt{I_0 (W/cm^2)}$, and corresponding laser field can be calculated by $a_0 = eE_0/m\omega_0 c$, with wavelength of 0.8 μm. We choose initial position of the electron at $(kx_0, ky_0, kz_0 \equiv 0,0,0.001)$ slightly ahead from the beam focus point (0,0,0). laser's initial phase ψ_0, different values of tapering point kz_t.
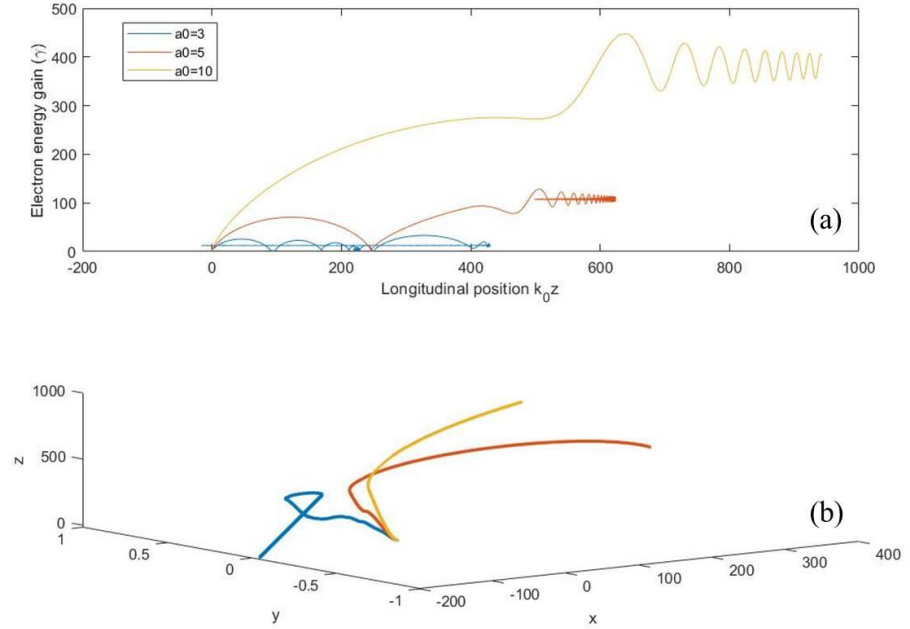
Figure 3.11 (a) shows the electron energy gain γ along kz_0 for laser parameters $a_0 = 3$ (blue curve), $a_0 = 5$ (orange curve), and $a_0 = 10$ (yellow curve) respectively. Other laser parameters are beam waist size, $kw_0 = 300$, $\tau = 100, \psi_0 = 0$, respectively. Maximum value of normalized wiggler field is $b_0 = 0.5$. (b) Corresponding electron trajectory of electron is shown.

Figure 3.11 (a) present the analysis of energy gain of an electron with respect to longitudinal position $k_0 z$ and shows that electron gain maximum energy for laser intensity parameter $a_0 = 10$ (yellow line) compare with $a_0 = 3$ (blue

line), and $a_0 = 5$ (orange line). Higher value of laser vector potential is entitled to maximum energy gain. Figure 3.11 (b) shows corresponding electron trajectories.
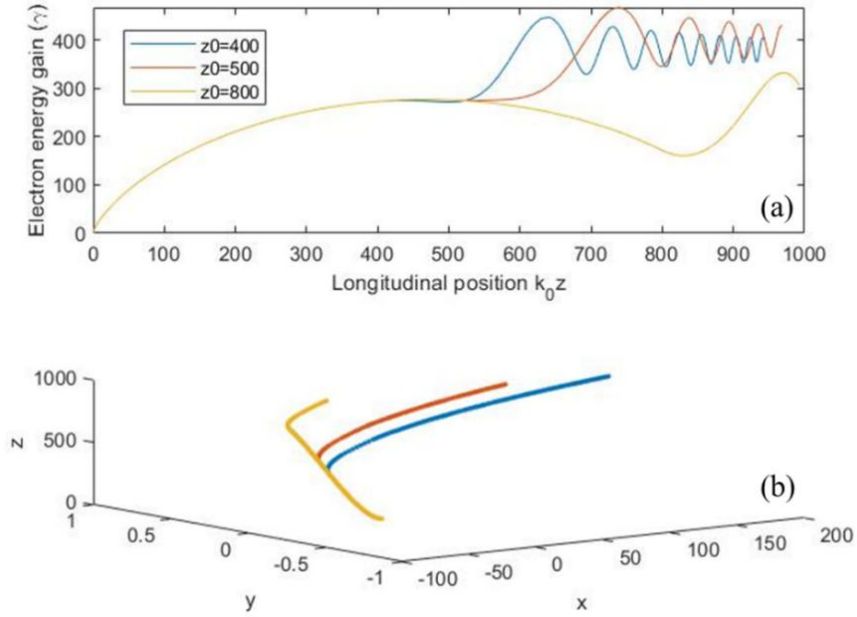
Figure 3.12 (a) Shows the electron energy gain γ along kz_0 for various tapering point of wiggler field b_0; $kz_t = 400$ (blue curve), $kz_t = 500$ (orange curve) and $kz_t = 800$ (yellow curve), respectively. Other laser parameters are $a_0 = 10$, $k w_0 = 300$, $\tau = 100$, $\psi_0 = 0$ respectively. Maximum value of normalized wiggler field is $b_0 = 0.5$. (b) Corresponding electron trajectory of electron is shown.

In Figure 3.12 (a), the tapering is applied along the wiggler length. Tapering is used to perpetuate the FEL resonance condition $\lambda_r(z) \approx \lambda_w (1 + b_0^2)/2\gamma^2(z)$ to maximize the energy gain, where $\lambda(z)$ is the laser wavelength, λ_w is the wiggler period, $b_0 = eB_0\lambda_w/2\pi m_0 c$ is the normalized wiggler amplitude, and $\gamma(z)$ is electron's energy. Figure 3.12 (a) shows the changes in electron's energy gain for different kz_t i.e. $kz_t = 400$ (blue), 500 (orange) and $kz_t = 800$ (yellow) while other parameters are fix as: $a_0 = 10$, $kw_0 = 300$, $\tau = 100$ and

$b_0 = 0.5$. The results show that electron obtains maximum energy for $kz_t = 500$ as compared to $kz_t = 400$ and 800 respectively.
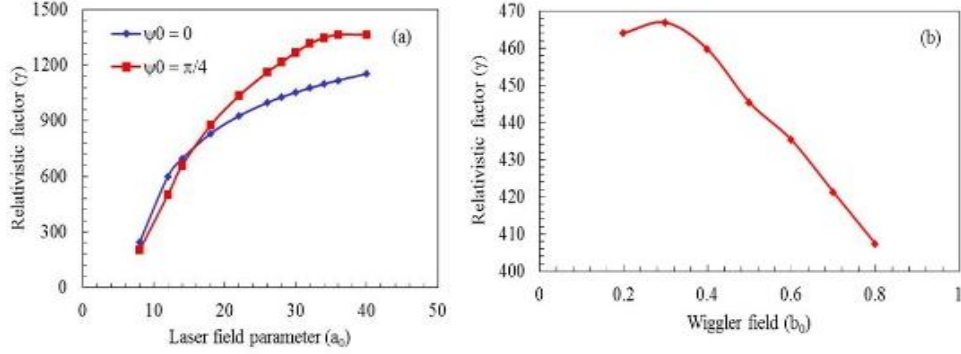
Figure 3.13 (a). The maximum energy gain versus normalized laser field a_0. (b) shows the effect of normalized wiggler field b_0 on maximum energy gain. Other parameters are similar to given in Figure 3.12.

Figure 3.13 (a) shows the maximum energy gain γ for normalized laser field a_0 of more accurate laser fields. It shows that energy gain increases linearly. The electron attains maximum acceleration, $\gamma = 1363$ (~700 MeV) at $\psi_0 = \pi/4$ for $a_0 = 40$. Similarly, for $\psi_0 = 0$, electron attains maximum acceleration, $\gamma = 1153$ (~590 MeV) for $a_0 = 40$. Figure 3.13(b) explained how wiggler magnetic field affects. For $b_0 = 0.3$, the gain is extreme.

3.2.4 Conclusion

In this work, we theoretically investigates the single electron dynamics in IFEL geometry. A more realistic laser field expression is considered, and a planer magnetic wiggler field is used. The results are analysed for maximum energy gain by optimizing different parameters. Electron energy gain is sensible to the initial laser field. By increasing laser field electron's energy increases. More intense laser beam generates high electric field and high electric field provides more energy gain. Energy gain can be maximized by optimizing the tapering point. Finally, it is shows that precise selection of wiggler field is essential to keep the resonance and in maximizing the energy gain. This study

will be useful in optimizing a set of laser and wiggler parameters for experiment purpose. Comparison with tapered helical wiggler and more realistic simulation of an electron bunch is considered as future work.

Chapter 3.3

Synergistic enhancement of electron acceleration by chirp laser modulation and wiggler magnetic field

3.3.1 Introduction

Within the context of particle acceleration, the search for higher and higher energies has led scientists to delve into a plethora of naval techniques. Historically, plasma-based acceleration [136], [137], [138], [139], [140] schemes have been at the forefront, utilizing the dynamic nature of ions to shoot particles with the speed of light. In a turbulent medium like plasma, electric fields and electromagnetic waves are intense enough to push electrons until they move with the speed of light. However our understanding of particle physics has advanced enormously, and we have begun to investigate other methods of acceleration as well. Of these alternative methods, vacuum-based particle acceleration [141], [142], [143], [144], [145], [146], [147] has emerged as an attractive way to accelerate particles. Unlike their plasma-based counterparts[148] dependent on intricate motion in ionised matter, the vacuum-based particle acceleration approach is based on manipulating the electromagnetic fields in a vacuum. These vacuum-based approaches encompass a wide variety of methods, each with unique benefits and challenges. From laser-driven accelerators to radio-frequency cavities and wakefield accelerators, researchers have come up with innovative ways to exploit the vacuum for particle acceleration. These possibilities pave the way to the next level of energy gain, as well as new realms for scientific exploration. Highly energetic particles are opening up possibilities for various applications, such as advanced particle accelerators, radars, plasma fusion and heating, medical science, material property exploration, and directed energy applications.

Recent advances in laser technology, such as chirped pulse amplification[100], have made it possible to carry out experimental and theoretical investigations on electron acceleration schemes using lasers in a vacuum. Chirped pulse

amplification is a technique that stretched, amplifies, and then compresses ultra-short laser pulse is generated to high peak power without damaging the amplifying medium. The Inverse Free Electron Laser (inverse-FEL) acceleration method, proposed by Palmer in the 1970s, is highly suitable for transferring energy from a strong laser pulse to electron beams in a vacuum[149], and the first experiment was conducted at BNL(Brookhaven National Laboratory)[150] in which an undulator magnet is used to couple the cross-sectional electromagnetic waves to accelerate the electrons in inverse-FEL phenomena.

Inverse-FEL accelerators have practical problems, such as limited interaction bandwidth in moderate-intensity laser beams. Confined electrons in the inverse-FEL method experience phase slippage issues due to the electron no longer meeting the resonance requirement of the FEL as it gains energy[151]. Diffraction of laser beams is also an issue in Inverse-FEL interaction, and these effects might be diminished by using an ultra-intense pulse or tapered magnetic undulator[152]. Troha *et al.* [153] conducted theoretical and computational studies on the inverse-FEL accelerator and demonstrated how this pulse enhances the interaction bandwidth and accelerating gradient, resulting in higher energy gain. The effect of radially polarised cosh Gaussian laser for optimum electron acceleration has been studied. To accelerate picosecond electron bunches with a high gradient (GeV/m) with extremely less energy spreading, Hartemann *et al.*[132] developed a small vacuum particle accelerator. Galow *et al.* [154] suggested a method for vacuum auto-resonance laser acceleration (ALA) using a circularly polarised laser and demonstrated a simulation study for multi-GeV final energy. It is even possible to generate high energy electron by applying an externally magnetic field of a few KG [139], [155]. IFELA in a vacuum is studied for electron dynamics in a planar wiggler field. It shows the role of undulator tapering is crucial for IFEL resonance and energy gain [156].

Gupta *et al.* [157] demonstrated an electron acceleration scheme utilising a chirped-laser under the influence of an axial magnetic field for injection of an electron. The constructive interface of two chirped laser pulses incident on an obelic angle is investigated by Gupta *et al.* [158] examine more increased energy gain while using frequency chirp rather than without chirp, it is also shown the frequency chirp helps to maintain the energy gain for long-distance. Numerical investigation of different laser and magnetic field parameters circularly polarised and chirped laser pulse is studied by Kumar *et al.* [110]. Li *et al.* have investigated proton dynamics by radially polarised 1-PW chirped laser pulse for proton acceleration up to hundreds of MeV from rest [159]. In a study, Salamin, *et al.*[160] received multi GeV energy using quadratic chirped laser pulse which is approximately doubled as compared to linear chirp. Sohbatzadeh *et al.* [161] studied different field parameters and introduced linear and negative chirp characteristics in Gaussian laser beams. The influence of two different types of frequency profiles in chirp laser pulses was explored in a comparative study. Song *et al.*[162] discussed the unusual behaviour of the laser phase related to the dynamics of an electron in a chirped laser beam. Rajablou *et al.* [163] studied a two-colour, two-pumping system, where the non-collinear and phase matching orientations are separately investigated for the interactions of pump-signal. Middha *et al.* [164] numerically investigate the beat wave acceleration using a Gaussian laser pulse and examine the effect of linear chirp, quadratic chirp and without chirp on the final energy and found that the energy gain is higher in the case of chirping rather than without chirping, it is also founding that the small value of quadratic chirp is more effective than the high value of linear chirp.

3.3.2 Analytical demonstration of electron's motion using chirped laser pulse

Here, we studied qualitative equations for the mean energy of an electron in a chirped electromagnetic (EM) plane wave. The schematic of the chirp laser pulse under the helical wiggler, is presented in figure 3.14.
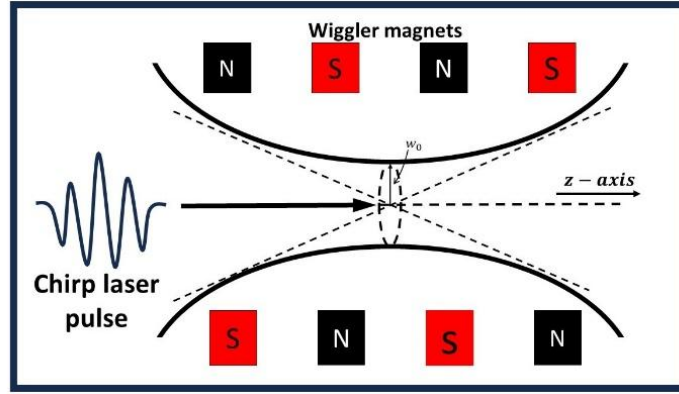
Figure 3.14 Shown schematic of a focused chirp laser affected by a helical wiggler field.

The EM profile for chirped laser pulse is: -

$$\vec{E}(z,t) = \hat{x}E_0\cos{[kz - \omega(t)t + \phi_0]} \tag{3.3.1}$$

$$\overrightarrow{B_l}(z,t) = \frac{\vec{E}(z,t)}{c}\hat{y}, \tag{3.3.2}$$

The linear chirped laser profile yields[164]: $\omega(t) = \omega_0(1 - \beta t)$

Here, ω_0 represents laser frequency at $z = 0, t = 0$. The chirping parameter in the z- direction is defined by β, and $\omega(t) = kc$.

Motion of electron is controlled by:

$$\frac{d\vec{p}}{dt} = -e\vec{E} - e(\vec{v} \times \overrightarrow{B_l}); \text{ and } \gamma = \left(1 - \frac{v^2}{c^2}\right)^{-1} \tag{3.3.3}$$

We use approximations to analyse field expression interpretations. For that the value of kz is assumed very small, Here, γ (relativistic factor) is represented as$= \sqrt{[1 + (p_x^2 + p_y^2 + p_z^2)/m_e c^2]}$, $-e \: and \: m_e$ are charge and the mass of electrons.

Numerical analysis is done by using Rung-Kutta method to determine the electron energy, and the graphical representation of numerical analysis is

66

described between the longitudinal position ($k_0 z$) v/s normalised factor of energy gain (γ).

The electron's initial location (kx_0, ky_0, kz_0) and momentum parameters (p_x, p_y, p_z) are considered as $(0, 0, 0.9)$ and $(0, 0, 1)$ respectively, the inceptive velocity in the z direction with the optimized values of initial electron's velocity and energy as $v_{z0} = 0.99c$ with $\gamma = 0$

The following are the governing plane-polarised and normalised electric and magnetic field profiles for a plane-polarised chirped laser pulse:

$$E_x = \frac{E_0 w_0}{w(z)} \exp\left[-\frac{r^2}{w(z)^2} + i\left\{kz - \omega(t)t + \phi + \frac{kr^2}{2R(z)} + \phi_0\right\}\right] f(z, t) \qquad (3.3.4)$$

The corresponding magnetic field of the laser pulse is given by.

$$\vec{B_l} = -\frac{i}{\omega}\vec{\nabla} \times \vec{E} \qquad (3.3.5)$$

E_0 is a reference to an electric field, $w(z) = w_0\sqrt{1 + \alpha^2}$ is beam's width and w_0 laser beam spot size, $R(z) = z(1 + 1/\alpha^2)$, $\phi = \tan^-(1/\alpha)$, $\alpha = \frac{z}{z_R}$, here $R(z)$ is Rayleigh's length and $Z_R = kw_0^2/2$, and $r = \sqrt{(x^2 + y^2)}$, the initial phase of the laser is ϕ_0, , $f(z, t) = \exp\{-(z - ct)^2/c^2\tau^2\}$ is added Gaussian laser beam, where τ is laser pulse duration.

The profile for the helical wiggler magnetic field is as follows:

For $z < z_0$

$$B_{wx} = b_0 \cos(z)$$

$$B_{wy} = b_0 \sin(z)$$

$$Bw_z = 0$$

For $z > z_0$

$$B_{wx} = 0$$

$$B_{wy} = 0$$

$$Bw_z = b_0 \qquad (3.3.6)$$

The electron's motion is given by:

$$\frac{d\vec{p}}{dt} = -e\vec{E} - e\vec{v} \times (B_l + \overrightarrow{B_w}) \qquad (3.3.7)$$

and the energy is determined by the equation.

$$\frac{d\gamma}{dt} = -\left(\frac{e\vec{E}}{m_e c^2}\right).\vec{v} \qquad (3.3.8)$$

3.3.3 Numerical analysis

To illustrate the given chirped pulse phenomena, we are showing the motion of an electron using a chirp laser pulse and helical wiggler magnetic undulator. Based on the experimental feasibility and needs, the optimum values of laser pulse duration, external magnetic field, and laser intensity are selected. For numerical representation, the laser field parameters are followed as: $a_0 = eE_0/m\omega_0 c$ (corresponding laser intensity $I_{cp} = (1.36 \times 10^{18} a_0^2/\lambda_0^2)$, the wavelength of a given laser is $\lambda_0 = 0.8\mu m$. The expression for the normalized magnetic wiggler undulator parameter and laser magnetic field parameter is given as:- $b_0 = eB_w/m\omega_0$, and $b_{0l} = eB_l/m\omega_0$, and the normalised laser pulse duration is 100. The normalised beam waist size for this analysis is taken as $w_0 = 300$, initial normalised coordinates of momentum are set as (0, 0, 1) and the starting coordinates of electrons are as (0, 0, 0.9) which is a bit ahead from the pulse in the z-direction, the initial electron moving with velocity $v_{z0} = 0.99c$.
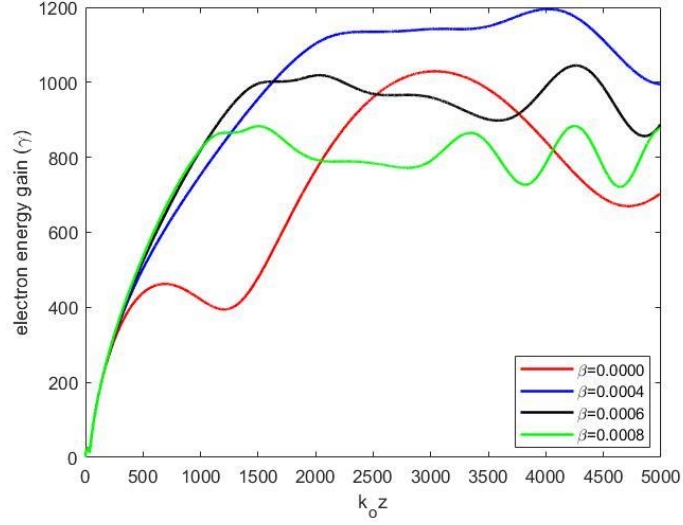
Figure 3.15 Plot between electron energy gain (γ) and longitudinal position ($k_0 z$) for the different values of the chirp parameter β as $\beta = 0.000$, 0.0004, 0.0006, 0.0008. Other parameters are laser field parameter $a_0 = 15, \tau = 100, b_0 = 0.7, and\ b_{0l} = 0.5$,

The numerical analysis illustrates curves plotted using different chirping parameters, including the case without chirp. The graph demonstrates that without chirp, the electron energy gain is approximately 514.5 MeV, corresponding to a relativistic factor γ =1028 (represented by the red curve). However, introducing various chirping parameters initially increases the electron energy gain. As the chirping parameter β is further increased, the energy gain eventually decreases.

Notably, incorporating chirp in the laser pulse causes an abrupt rise in electron energy, which then remains relatively constant, with minor fluctuations, until the electron reaches its energy state. In contrast, the absence of chirp leads to an anomalous shift in electron energy, as depicted by the red curve in the figure. The transverse momentum of the electron is amplified by the combined effects of chirp and the helical wiggler. Consequently, the longitudinal momentum is enhanced due to the force $(\vec{v} \times \vec{B_l})$ applied in the longitudinal direction, this would be enhances the overall gain.

69

The peak value of relativistic factor, $\gamma = 1200$, is achieved with the parameters $\beta = 0.0004$, $a_0 = 15$, $b_0 = 07$, and $b_{0l} = 0.5$ (blue curve), which are optimized for maximum gain. This observation aligns with the findings of references[107], [157], [165] reported an increase in energy with higher chirp parameters. Which shows that the chirping of pulse helps to enhance the final energy gain. The normalized energy gain for other chirp parameters includes $\gamma = 1045$ (black curve) at β=0.0006, $a_0 = 15$, and a net energy gain of γ=883.5 (green curve).

The overall pattern of energy gain with a chirped laser within a magnetic wiggler or undulator is particularly intriguing. Initially, the resonant matching between the chirped pulse and electron motion optimizes interaction periods, thereby enhancing energy gain and accelerating the electrons. However, surpassing the optimal range of the chirping parameter introduces phase mismatch and nonlinear effects, leading to deceleration and reduced efficiency in energy transfer. This results in energy gain curves that peak and subsequently decline, reflecting the delicate balance between resonant enhancement and diminishing returns in chirped laser-assisted electron acceleration within wiggler fields.
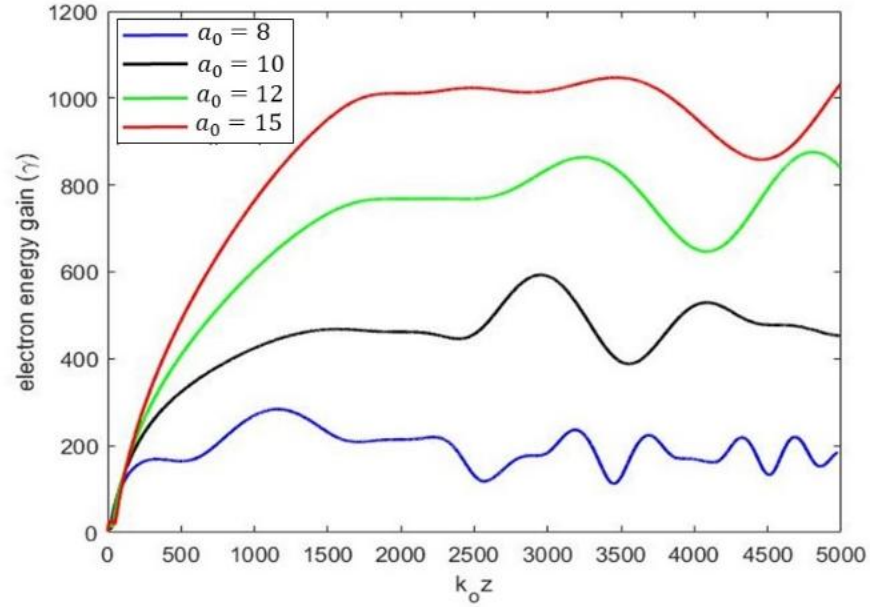
Figure 3.16 Variation between energy gain (γ) and longitudinal position ($k_0 z$) for different laser field parameters i.e., $a_0 = 5, 8, 10, 12, 15$. While $b_0 = 0.5, b_{0l} = 0.5$.

Figure 3.16 illustrates graph between energy gain (γ) and longitudinal position ($k_0 z$). The laser field parameters and the pulse strength influence the fundamental principles of electron acceleration within the laser field, allowing us to examine the consistent rise in the final energy. Increasing the laser field improves the interaction between electrons, leading to a more effective transfer of energy and acceleration, the energy gain is enhanced, and the maximum electron's energy 523.5 MeV is received at γ=1047(red curve), for $a_0 = 15$ (corresponding $I_0 = 4.86 \times 10^{20} W/cm^2$ and laser wavelength is $0.8\mu m$). Other normalized laser parameters are as: $w_0 = 300$, $\tau = 100$, $\phi_0 = 0$, $b_0 = 0.5$, $b_{0l} = 0.5$, $\beta = 0.0005$. The intensified level of interaction results in more forces acting on the electrons, causing them to move at greater speeds and hence attain higher ultimate energies. Moreover, increased intensity generates more advantageous resonance conditions, enhancing energy transfer efficiency and propelling electrons to higher energies [[107],35]. In another paper Kant *et.al*[155]. also investigate the effect of field parameter with different field

parameters and found energy gain is increased with increasing the value laser intensity. Other results are obtained as; for $a_0 = 8$, the gain is 141.5 MeV for $\gamma = 283$ (blue curve), for $a_0 = 10$ is 296.5 MeV correspond to $\gamma = 593$(black curve), and 437.9 MeV for $a_0 = 12$ (corresponding $\gamma = 875.8$ green curve). Furthermore, we may say that, when the intensity is increased, the impact of deceleration caused by phase mismatches or nonlinear interactions diminishes compared to the overall acceleration offered by the more powerful laser beam. This enables electrons to sustain or enhance their acceleration over greater distances. Therefore, the observed continuous increase in final energy underscores the direct relationship between the laser field's intensity and electron acceleration.
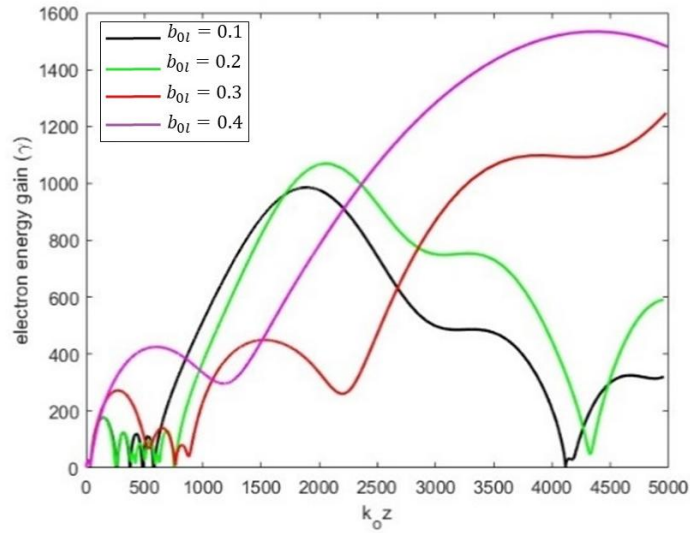
Figure3.17 graphical representation of electron energy gain over longitudinal position for several normalised magnetic field parameters of laser as $b_{0l} = 0.1, 0.2, 0.3, 0.4$ for this laser field parameter $a_0 = 15$, $b_0 = 0.7$, $\beta = 0.0001$.

In Figure 3.17 Graphical data show that the maximum energy gain is increased with the increasing normalised magnetic field parameters of laser. By using optimised parameters, 767 MeV energy is received for the optimized and normalised val`ue of the magnetic field b_{0l}=0.4(magenta curve), other

normalized laser parameters are as: $w_0 = 300, \tau = 100, \phi_0 = 0, b_0 = 0.7, \beta = 0.0001$.

When electrons synchronize with the electromagnetic field, they experience maximum energy gain in each undulator period. Consequently, changes in magnetic field strength directly affect both resonance conditions and energy gain. As the magnetic field strength increases, energy transfer from the laser pulse to electrons is more efficient, tightening focussing and electron beam confinement. So, external magnetic field in inverse free electron laser acceleration plays an important role in shaping the electron trajectories and optimizing their interaction with the electromagnetic field. This helps to energy transfer from the laser or microwave field to electrons, allowing them to gain energy and emit coherent radiation. The precise control of magnetic field of laser is essential for maximizing the efficiency and output of the IFEL system. Chen *et.al.* [166]emphasized that resonance conditions are crucial for efficient energy transfer in vacuum environments. Our results align with this, as changes in the magnetic field strength directly influence resonance conditions and thus the energy gain. The tighter focusing and enhanced confinement of the electron beam, as the magnetic field strength increases.
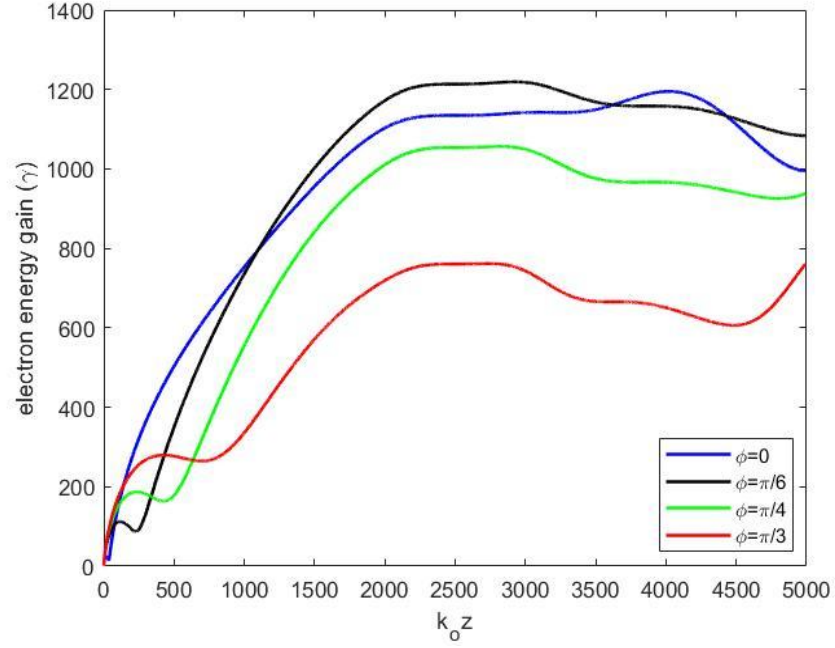
Figure 3.18 Electron energy with (k_0z) for various values of the initial phase of laser $\phi_0 = 0, \pi/6, \pi/4, \pi/3$, while the other parameters are as $a_0 = 15, b_0 = 0.7, \beta = 0.0004, b_{0l} = 0.5 \; and \; \tau = 100$

Figure 3.18 illustrates the variation in the energy gain γ concerning the initial laser phase, . It is observed that the change in the initial energy is first increased slightly and then continuously decreased for $\phi_0 = \pi/6$ to $\phi_0 = \pi/3$. So, we can say, that the initial phase allowing for precise controlling of the timing, phase stability, and resonance conditions during the acceleration process and our findings are consists with some previous studies[165], [167]. it helps to enhance acceleration efficiency and get specific electron beam properties for diverse applications in high-energy physics and particle beam technologies by deliberately modifying the beginning phase.
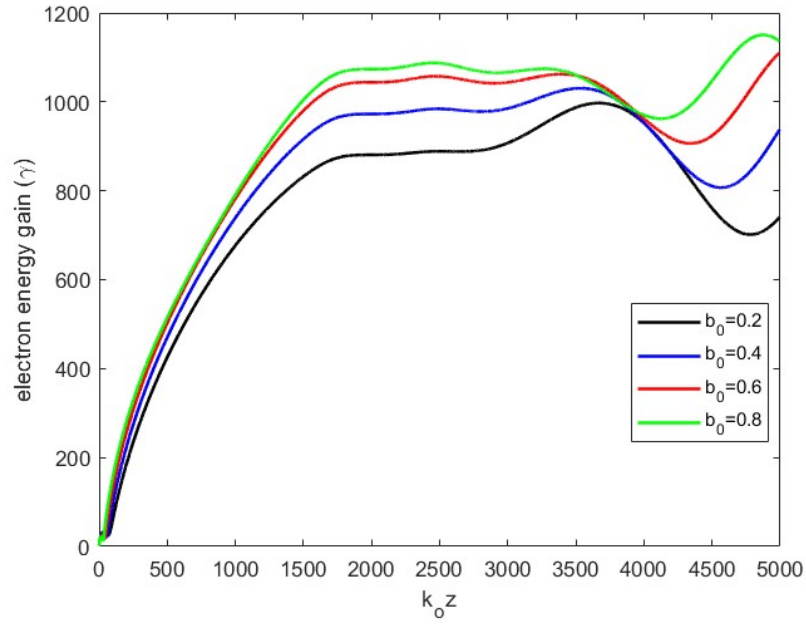
Figure 3.19 Illustrates the changes in electron energy gain with a longitudinal position $(k_o z)$ for different values of the amplitude of the wiggler magnetic field. The variation in wiggler magnetic field amplitude is optimised as $b_0 = 0$. 0.2, 0.4, 0.6, 0.8 other field vaiables are similar as in Figure 3.16.

Figure 3.19 illustrates the amplitude of the wiggler magnetic field have a crucial role in influencing the motion of electrons. A greater magnetic field amplitude results in more pronounced transverse oscillations and, as a result, a greater electron acceleration and energy gain. It is essential to calibrate the amplitude to match resonance conditions with electromagnetic waves to ensure efficient energy transfer. In addition, higher amplitudes result in a broader energy spectrum, whereas lower amplitudes produce a more monochromatic electron beam. This tuning is essential for regulating the generated radiation's quality and optimising the IFELA's efficiency and beam quality. Our findings are agree with previous research by Chen [166], which emphasized the importance of optimizing magnetic field amplitude for maximizing energy gain and achieving the desired energy spectrum in vacuum-based chirped pulse acceleration systems.

3.3.4 Conclusion

Electron acceleration is analysed numerically using a chirp laser and a helical magnetic wiggler. It is observed that the electron's acceleration strongly depends upon chirp parameters, initial laser phase, and laser field parameters. The peak energy is observed approximately $\sim$ 767MeV for optimised field parameters. Static magnetic field helps to maintain the resonance longer to improve the final energy gain. it is also observed that the presence of linear chirp strongly affects the final energy. It is also found, that the optimisation of the initial phase of the laser pulse is also very crucial to generating specific and desirable electron energy gain.

Chapter 3.4

IFEL electron acceleration due to two laser pulses incident at an oblique angle

3.4.1 Introduction

Advancements in laser technique [168], particularly the effective and efficient creation of sub-cycle pulses in microwaves [169], far-infrared [170], and ultrafast [171] realms, offer to make experimental procedures of many theories for THz radiation[172] generation and laser acceleration of electrons [173], [174], [175], [176]. Since the invention of the laser, the interaction between the laser and plasma has been an important part of speeding up particles. Using a long-pulse laser, the first plasma accelerators were made around the middle of the 1980s. Since the chirped pulse amplification (CPA) technique had not been introduced yet, there were no short-pulse lasers. Tajima and Dawson [12] proposed the beat-wave method to accelerate particles. In this method, two pulses with a slight difference in frequency are used, and when the frequency difference of both lasers is equal to the frequency of the plasma, a plasma wave of enhanced amplitude is generated. There are a lot of problems that need to be solved before any of these laser-based plasma acceleration systems can be considered possible. One of the problems is that the plasma (or gas) medium that the accelerating slow waves need to travel through may be unstable or cause scattering. In addition, since positron acceleration is a need for lepton colliders, their quick destruction in plasma or gas might be troublesome.

A different method of electron acceleration is to employ laser beams in a vacuum at the far-field limit [142], [177], [178], [179], i.e., in regions that are distant in comparison to the vacuum wavelength from physical borders, hence minimizing material degradation, plasma generation, and plasma instabilities. As an electron acceleration medium, a vacuum offers several benefits over

plasma. In a vacuum, laser-plasma interaction issues, such as instabilities, do not exist.

Inverse free-electron laser (IFEL) is yet another type of laser accelerator that has garnered significant attention over the last few decades. In an IFEL, a laser transfers its energy to e-beam when travels through a magnetic undulator. The magnetostatic field of the undulator is converted into an electromagnetic wave that beats with a laser. Accelerating the electrons in the beam requires maintaining a constant relative phase of the electrons about the beat wave. This synchronism may be maintained in an IFEL by adjusting either the undulator period or the magnetic field, or both factors simultaneously.

Numerical analysis of inverse free electron laser acceleration using crossing two lasers incident at an oblique angle is presented in this paper. Bobin [180]is first who introduced the idea of using beat wave in IFELA in the presence of stationary plasma and accelerate electron up to the 100 MeV energies over the short distance then Cai *et.al.* [181]use Bobin's idea, they use moving plasma and generate electric field gradient of ~1MeV/cm. We expand here concept IFELA using crossing of two lasers incident on an oblique angle under the influence of helical wiggler magnetic field in vacuum. The selection of helical undulator is based on certain qualities of helical undulator over the other wiggler magnetic fields. In order to connect electronic motion to laser beams, IFEL accelerators have thus far relied on planar undulators. Using a helical undulator magnetic field causes the electrons to move in a helical pattern, allowing for continued energy transfer when coupled with a similar kind circularly polarized [59]. So due to ability of generating a magnetic field with helical trajectory, helical magnetic wiggler produces transverse motion in the electron beam match proper resonance condition. This alignment improves the interaction in between the electron beam and electric field, leading to enhance the efficiency and effectiveness in energy transfer and acceleration procedure.

A frequency chirp is also introduced to obtain better results. The crossing of two chirped laser beams was investigated by Gupta *et al.* [182] presented that the final electron energy gain is higher than the unchirped one.

Middha *et al.* [183] compared the effects of linear chirp and quadratic chirp in vacuum using a Gaussian laser pulse in vacuum. As the electron's longitudinal momentum increases the intensity of the laser has puts a big effect on how much energy the electron gains when it is accelerated by a laser in a vacuum. When compared to a single laser, using two lasers that are crossed has several advantages when it comes to accelerating electrons in a vacuum. Due to constructive interference, the resultant field amplitude increases, resulting in a greater electron energy gain than in previous examples. To present a technique for electron acceleration utilizing two chirped lasers, we highlight prior work and obtain further findings. Two high-intensity chirped lasers with the same amplitude and frequency that intersect at an arbitrary angle in a vacuum cause laser intensity modulation. Electrons are injected externally at an angle δ relative to the z-direction (figure 1-a), which is accelerated by the resulting field. The IFELA mechanism plays a vital role in the field of particle acceleration physics. Our research presented a new method that considers the combined impact of intersecting laser beams in IFELA, while also taking into account the influence of a helical wiggler magnetic field in a vacuum. The use of a helical wiggler enables the sustained maintenance of the resonance condition over a greater distance and for a longer duration. By utilizing vacuum instead of plasma, the issue of obstruction in extracting more energy from electrons due to plasma instabilities is eliminated. The intersection of two lasers and the application of the chirp effect contribute to the amplification of energy and the enhancement of beam quality to a higher degree. The frequency chirp contributes significantly to the enhancement of electron energy during this action.

3.4.2 Electron acceleration by obliquely incident laser beams

Schematic layout of two Gaussian lasers crossing at an angle $\boldsymbol{\theta}$ and $-\boldsymbol{\theta}$ about the propagation axis (z-axis) shown in Figure 3.20 (a), a schematic of the helical magnetic wiggler is presented in Figure 3.20(b).
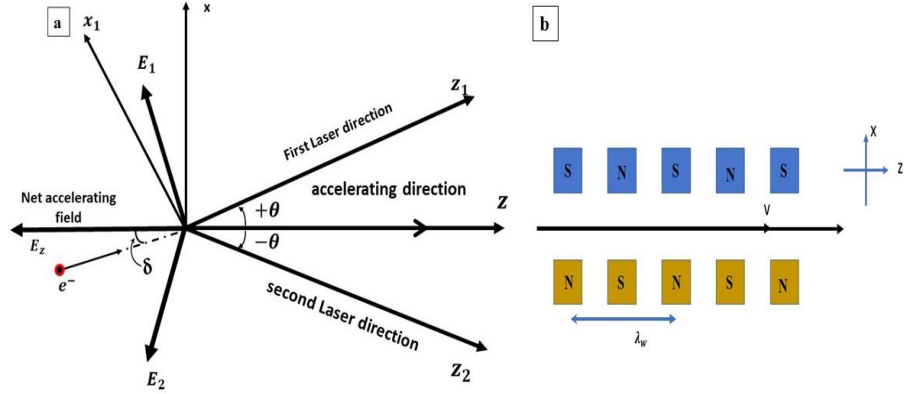
Figure 3.20 schematic layout of (a) crossing of two lasers incident on an oblique angle (b) helical wiggler magnetic field.

3.4.3 Electric fields of laser beams with magnetic wiggler

Two frequency-chirped laser pulses are used to study the crossing of lasers. Both lasers are incident at θ and $-\theta$ angles to the propagation axis (z-axis) both lasers are crossing at z=0, electric field equation of the first laser is as follows:

$$E_{x1} = \frac{E_{01}}{f_1} \cos(\phi_1) \exp\left[-\frac{(t-z_1/c)^2}{\tau_0^2} - \frac{r_1^2}{r_0^2 f_1^2}\right] \tag{3.4.1}$$

$$E_{z1} = -\frac{2E_{01}x_1}{K_0 r_0^2 f_1^2}\left[\sin(\phi_1) - \frac{z_1}{R_d}\cos(\phi_1)\right] \times \exp\left[-\frac{(t-z_1/c)^2}{\tau_0^2} - \frac{r_1^2}{r_0^2 f_1^2}\right] \tag{3.4.2}$$

Where $\phi_1 = k_0 z_1 - \omega_0(t)t + (z_1 r_1^2/R_d r_0^2 f_1^2) - \tan^{-1}(z_1/R_d) + \phi_0$ where ϕ_0 is a constant, $f_1^2 = 1 + (z_1/R_d)^2$, $\omega_0(t) = \omega_{00}[1 - \alpha t]$ for a linear chirp, $k_0 = \omega_0(z)/c$, $R_d = k_0 r_0^2/2$. here, r_0 is the minimum value of the laser spot, ω_{00} represents laser frequency at $z = 0$, and α is chirp parameters and ψ_0 is the initial phase of a periodic frequency chirp. R_d is Rayleigh length, $x_1 = x\cos\theta - z\sin\theta$, $y_1 = y$, $z_1 = x\sin\theta + z\cos\theta$, τ_0 is the laser pulse duration. laser's magnetic field may be measured using the Maxwell equation as

$$\nabla \times \vec{E} = -\delta\vec{B}_0/\delta t \tag{3.4.3}$$

The helical magnetic wiggler is given by: -

$$\vec{B}_w = B_w \cos(k_w z)\,\hat{\jmath} + B_w \sin(k_w z)\,\hat{k} \qquad (3.4.4)$$

Total magnetic field $\vec{B} = \vec{B}_0 + \vec{B}_w$

3.4.4 Electron acceleration

The equations defining the momentum and energy of electrons may be expressed as: -

$$\frac{dp_x}{dt} = v_z e B_w \cos(k_w z) \qquad (3.4.5)$$

$$\frac{dp_y}{dt} = v_x e B_w \sin(k_w z) \qquad (3.4.6)$$

$$\frac{dp_z}{dt} = -eE_z - ev_x B_w \cos(k_w z) \qquad (3.4.7)$$

$$\frac{d\gamma}{dt} = \frac{e}{mc^2}[v_x v_y B_w \sin(k_w z) - v_z E_z] \qquad (3.4.8)$$

Here, γ is given by $\sqrt{(1 + p^2/m_0^2 c^2)}$ known as the relativistic factor. where $p^2 = (p_x^2 + p_y^2 + p_z^2)$ and -e and m_0 are the charge and rest mass of an electron respectively. γ_0 is the initial energy of the electron. An electron is injected at an optimal angle δ with final momentum written as: -

$$p_o \sin(\delta)\,\hat{x} + p_0 \cos(\delta)\hat{z} \qquad (3.4.9)$$

All field parameters are normalized as follows:

$$a_0 \rightarrow \frac{eE_0}{m_0\,\omega_0 c}, \qquad \tau' \rightarrow \omega_0 \tau, \qquad r_0' \rightarrow \frac{\omega_0 r_0}{c}, \qquad z' \rightarrow \frac{\omega_0 z}{c}$$

$$\beta_z \rightarrow \frac{v_z}{c}, \qquad t' \rightarrow \omega_0 t, \qquad p_z' \rightarrow \frac{p_z}{m_0 c}, \qquad k' \rightarrow \frac{ck}{\omega_0}$$

3.4.5 Numerically analysis and discussion

To illustrate the IFELA scheme, we analyzed the dynamics of the electron under the influence of the crossing of two linearly chirped Gaussian laser beams. The helical magnetic wiggler profile was also introduced to study the effect of a helical magnetic wiggler.
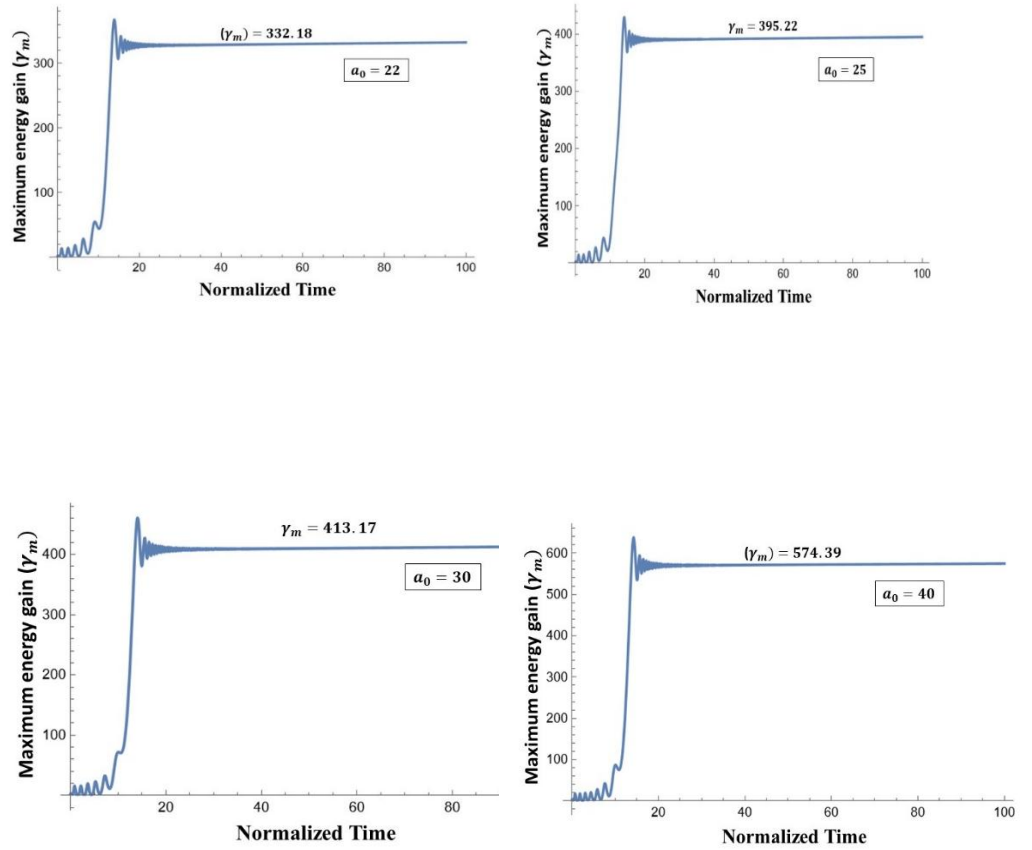
Figure3.21 (a-d) Change in electron's energy v/s normalized time for different values of laser field parameters $a_0 = 22, 25, 30$, and 40, other field parameters $b_0 = 0.6$, $\tau_0 = 1500$, $\gamma_0 = 1.9$, and crossing angle $\theta = 50^0, \delta = 10^0, \alpha = 0.06$ (linear chirp).

Figure 3.21 (a–d) presents a simulation curve for various values of laser field parameters using a linear chirp $\alpha = 0.06$. The ultimate energy gain is shown to grow with a greater laser field parameter, reaching the MeV region. The maximum energy gain is approximately 287 MeV (correspond to $\gamma_m =$

574.39)for $a_0 = 40$. If we further increase laser field parameter a_0, the energy gain will increase and reach approximately $\gamma = 658.31$ (329 MeV) for $a_0 = 50$, and by optimizing the other laser field parameters. We observed energy enhancement by comparing previously observed by singh *et. al.* [142], [184], who demonstrate IFELA phenomena using tightly focused laser pulse in the conjunction with planar and helical undulator. In another study bobin and cai investigate beat wave IFEL using plasma medium and shows the energy enhancement of electron to several hundred MeV[15], [16]. Our study focused on optimizing IFELA performance by employing crossing of two lasers in helical wiggler field. Helical undulator gives better results than planar undulator. In this analysis, the other field parameters are chosen as: $b_0 = 0.6$, $k_0 = 0.96$, $k_w = 0.99$, $\tau_0 = 1500$, $\delta = 70^0$, $\theta = 50$, $\alpha = 0.06$, $\phi_0 = 75^0$. The maximum energy gain achieved in this mechanism is 329 MeV using helical magnetic wiggler with optimised value.
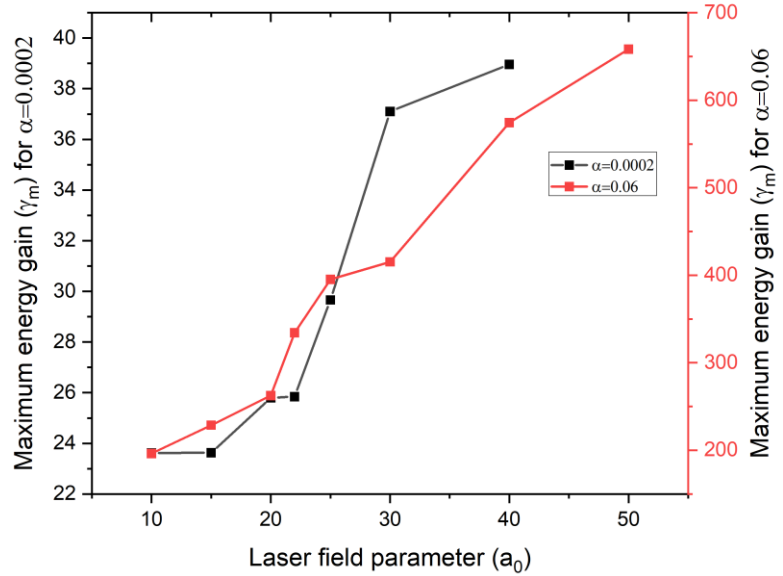
Figure 3.22 Variation in peak value of energy gain v/s the small linear chirp parameter α, where α is known as $\alpha = 0.0002$ (black curve) and while choosing a linear chirp parameter $\alpha = 0.06$ (red curve), all field values are optimized.

In Figure 3.22, we comparatively show peak value of energy gain in the presence of a very small chirp parameter $\alpha = 0.0002$ (black curve) and in the presence of optimised value of linear chirp *i.e.-* $\alpha = 0.06$. Figure 3 shows that in the case of linear chirp, parameter $\alpha = 0.06$, particles maintain proper resonance condition and capture electrons for a long time which helps enhance energy gain (γ_m) but while we use a small value of chirp pulse in the presence of helical magnetic wiggler, due to the lack of proper phasing between the electrons and laser pulse do not maintain in proper resonance condition in result the value of final energy gain is less. Singh et. al. [185] and some other researchers [153], [165] also investigated the effect of frequency chirp and found the similar results. The maximum energy gain (γ_m) more than 1.5 times, as compared to using a poor frequency chirp $\alpha = 0.0002$ while other laser parameters are used as:$b_0 = 0.8$, $k_0 = 0.96$, $k_w = 0.99$, $\tau_0 = 2000$, $\delta = 5^0$, $\theta = 20$, $\phi_0 = 10^0$. we saw the maximum energy gain is increased approximately 20 times more as compared to the small, chirped laser pulse. Thus, we can say that the optimization of the laser field parameter a_0 and the frequency chirp parameter plays an important role in achieving the maximum energy gain. In a previous study, Middha *et.al.* [15] observed the same kinds of results for using different values of frequency chirp and compared it with unchirped laser pulse, in our case we used a helical wiggler magnetic field, but they didn't.
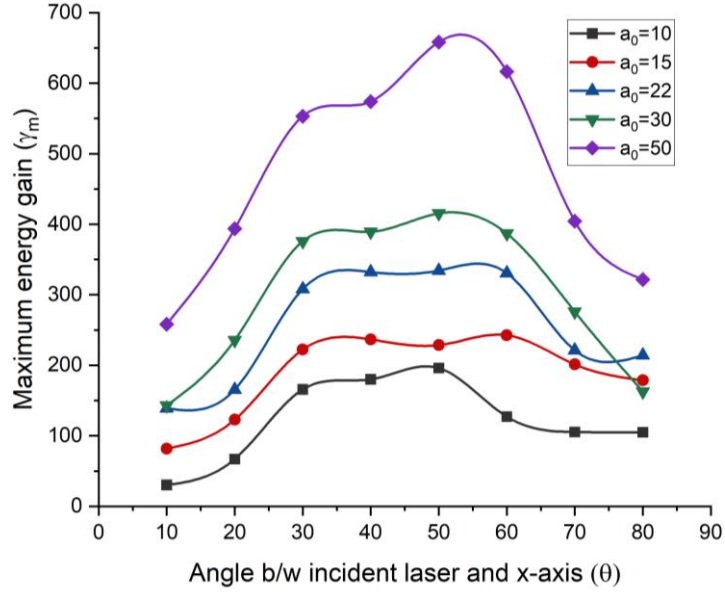
Figure 3.23 Variation in relativistic energy gain (maximum value-γ_m) with different values of incident angle θ with x-axis, for different values of laser intensities $(a_0 = 10,15,22,30,50)$. Other parameters $b_0 = 0.6, k_0 = 0.96, k_w = 0.99, \tau_0 = 1500, \delta = 70^0, \alpha = 0.06, \phi_0 = 75^0$.

Change in the maximum's electron energy gain γ_m with the incident angle of laser with x-axis for several laser field parameters is presented in figure 3.23. The value of incident angle (θ) is optimized for the better results. The various curves are plotted for the different values of laser field parameter $a_0 = 10$(black curve), 15(red curve), 22(blue curve), 30(green curve), 50(violet curve) and $b_0 = 0.6, k_0 = 0.96, k_w = 0.99, \tau_0 = 1500\ fs, \delta = 70^0, \alpha = 0.06, \phi_0 = 75^0$. First, the graph shows that the value of maximum energy gain is overall increased as we increase the value of laser field intensity. approximately 335 MeV corresponding to $\gamma_m \sim 658$ at $a_0 = 50$. This observation shows that the value of maximum energy gain is increased approximately 3.5 times more as we increased the value of laser field intensity by 5 times (*i.e.,* 10 to 50). Second, we can see the maximum energy gain in increased with increasing the value of θ (half of the crossing angle between both incident laser pulses) and reaching a maximum value for an optimum value of θ due to the proper phase matching between these two lasers. Electron's energy is higher within the range 30^0 to

60^0 of the incident angle between lasers and the x-axis. After an optimum value of θ net energy gain starting fall off. At this particular angle of 50 degree, the electron remains in the accelerating phase due to the fact that here, due to the effective interaction electron's energy gain is maximum. Overall observation shows that the incident angle between the lasers affects the interaction length, acceleration gradient, phase matching and beam quality. It is also necessary to optimize the laser field parameters for best results.
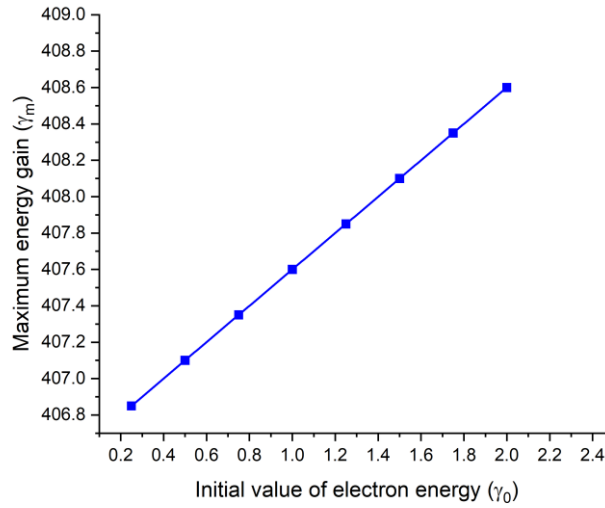
Figure 3.24 Maximum electron energy gain γ_m v/s initial value of electron energy γ_0.

Figure 3.24 shows the variation in Maximum electron energy gain (γ_m) with the initial value of electron energy (γ_0). It is illustrated that the value of maximum energy gain γ_m is directly proportional to the value of the initial value of electron energy (γ_0). The energy of the resultant electron is contingent upon the energy of the pre-accelerated electron; so, to achieve an electron with greater energy, one must enhance the energy of the pre-accelerated electron.
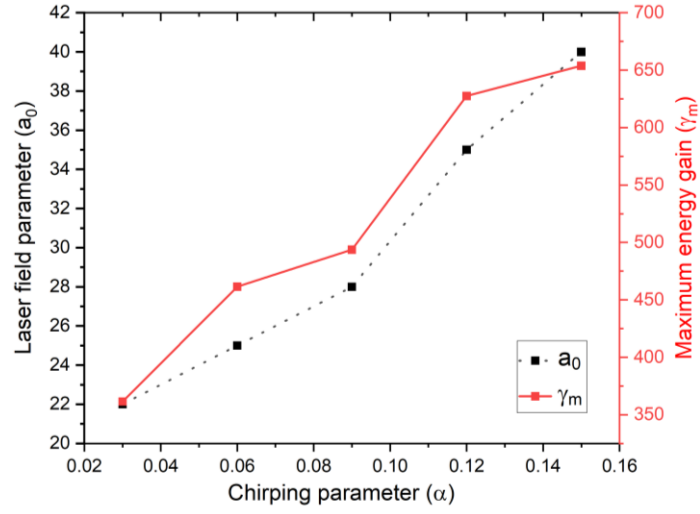
Figure 3.25 Variation of electron's maximum energy with chirping parameter α for different values of laser field parameters a_0.

In Figure 3.25, the variation of the peak value of the electron's energy is depicted v/s the chirping parameter α, where the value of α is optimized as $\alpha = 0.03, 0.06, 0.09, 0.12, 0.15$ for the different values of laser field parameters (a_0), *i.e.,* 22, 25, 28, 35, 40. The remained parameters are taken as $b_0 = 0.6, k_0 = 0.96, k_w = 0.99, \tau_0 = 1500, \delta = 70^0, \alpha = 0.06, \phi_0 = 75^0$. It is observed that the change chirping parameter of a laser pulse leads to a significant amount of energy gain in electrons. A positive linear chirp helps to maintain the interaction for longer time which helps to enhance the electron's final energy[186]. Inverse free electron laser (IFEL) acceleration could improve particle physics research, cancer treatment, and X-ray free electron lasers (XFELs) for materials science and biology. Additionally, it can facilitate scientific and technological advancements in high-energy physics investigations, advanced imaging, nuclear fusion research, and materials science.

3.4.6 Conclusion

Finally, we use mathematical simulation to investigate the IFEL acceleration effects when two chirped Gaussian laser beams hit each other at an

angle and there is a helical magnetic wiggler present. It has found the final energy gain depends on the optimizations of laser field parameters. In this paper, a maximum energy gain of 329 MeV is reported. The effect of linear chirp was also investigated, and it was observed that the final energy gain increased in the presence of linear chirp in the investigation. Energy of the pre-accelerated electron on the final output was also investigated, and a direct and positive relation was found between them, i.e., the high energy of the pre-accelerated electron heaving more final energy gain of the output electron.

Chapter 3.5

Inverse free electron laser acceleration using helical and planar wiggler field

3.5.1 Introduction

Since the beginning of the 20th century, particle accelerators have been extensively used in the field of science. Enrico Fermi realized in the '30s that the future of physics depended on the creation of equipment that could create and manage extremely high-quality particle beams[187]. Since then, there has been significant development in both the scientific and technological aspects of these machines. Particle accelerators have played and continue to play a crucial role in several industrial applications, including light sources, neutron sources, nuclear waste conversion, medical diagnostics and treatment, and a multitude of others. Radiofrequency (RF) is still the most efficient way to accelerate particles, but it is no longer the best way to do so. Because in RF technology the high energy barriers move higher to higher as particle accelerators become more powerful. In other words, we can say the conventional particle accelerators are restricted by their breakdown limit at a high electric field gradient, which is about 100MV/m. Fourth-order X-ray free electron lasers are costly and huge, highly complex, and high-energy particle accelerators[116], [117], [188]. On the behalf of medium requirement, there are several types of particle acceleration schemes: the first one is acceleration in a medium like in plasma or gas, the second is near field and the third one is vacuum acceleration or known as far-field i.e., there is no medium required in it. Advancement in the field of laser technology, the use of it to accelerate particles in a vacuum offers considerable potential for the future of compact particle accelerators [56], [189], [190]. Over the last few years, scientists in several labs have been looking into how high-power lasers could be used in a vacuum to speed up particles.

some advantages of vacuum acceleration:

Vacuum acceleration doesn't require any kind of media like plasma and gas, so it eliminates the various types of plasma instabilities or problems with gas. The particle is directly accelerated in a vacuum without contacting any physical boundary, or we can say the particles don't have any kind of wall contact and this removes the wall breaking issue due to the high energy gradient. Because the accelerated particles are not required to stay near a metallic barrier for the same reason, there are no substantial emittance or intensity limitations imposed by the beam's interaction with the surrounding wall, such as coherence beam perturbation or beam breakup. There are a lot of mechanisms to accelerate particles with high energy using a medium (Plasma Wakefield Acceleration, plasma beat wave acceleration) and without a medium like Radiofrequency acceleration (RF-Acceleration), free electron laser (FEL) acceleration, inverse free electron laser (IFEL) acceleration, beat wave acceleration in a vacuum, X-ray free electron acceleration, direct-laser acceleration (DLA), and so on.

In this chapter, we try to understand the basics of a special type of vacuum particle accelerator to transfer energy from laser radiation to particle, known as Inverse Free Electron Laser (IFEL) Acceleration. A short analysis of tightly focused Gaussian laser under the influence of planar and helical magnetic undulator is also investigated for understanding the concept.

3.5.2 Inverse free electron acceleration (IFELA)

In an IFEL acceleration (we call it IFELA) a laser beam interacts with electrons in a periodic wiggler magnetic field, also known as an undulator. In 1972, Palmer conceived of the phenomena of IFEL acceleration. In an IFEL acceleration, relativistic electrons propagate along with a laser beam throughout a magnetic wiggler. Also, the wiggler creates a small periodic transverse velocity parallel to the electric field vector of the EM- wave. When the electron's transverse velocity changes sign simultaneously with laser field, i.e., resonance conditions for FEL are $\gamma = \left[\frac{(1+K^2)\lambda_w}{2\lambda_l}\right]^{\frac{1}{2}}$ match, efficient energy exchange occurs. Where $\lambda_w, \lambda_l, K = eB_w k_w/2\pi mc$ are wiggler wavelength, laser wavelength, and undulator parameters, respectively. In undulator

parameter B_w, m, c define the wiggler magnetic field's peak value, electron's mass, and speed of light, respectively.

This allows energy to be transferred from the waves to the electrons. In IFELA, net energy is transmitted from the wave to the electrons. This is the exact opposite of the phenomenon known as Free Electron Laser (FEL) acceleration [191]. In FEL energy is transferred from the e-beam to the radiation pulse and generates coherent, ultra-short duration (up to a few fs) pulses combining unprecedented power density up to $100 W\,cm^{-2}$ [192]. Thus, the IFELA operates in the same way as the FEL acceleration. We had to add tapering to the undulator to keep the IFELA in sync with the desired energy. Schematic presentation of electron beam and laser moving between the undulator magnets is presented in figure 1.
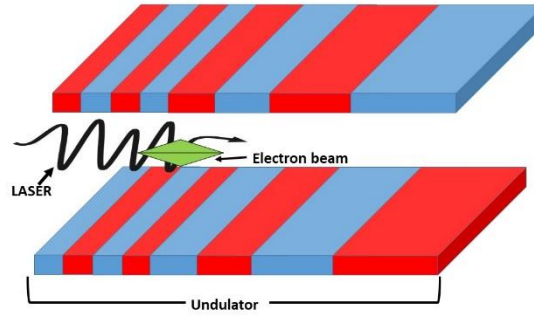
Figure 3.26 Schematic of the principle of IFELA

After Palmer invent this phenomenon in 1985 Courant et. al. demonstrated that the IFELA helps to accelerate a few MeV energy beams up to the hundreds of GeV energy and studied the effect of linear and helical wiggler magnetic field on the synchronization radiation loss of the beam. An experiment utilizing an ns-duration GW Co_2 the laser was conducted at Brookhaven National Laboratory (BNL) after Columbia University showed IFELA for the first time in 1992[150]. An experiment known as STaged ELectron Acceleration (STELLA) was carried out at BNL's Accelerator Test Facility (ATF)[193]. Employing a microwave IFEL accelerator, the net energy variation as a function of the relativistic injection stage of electron bunches has been seen

experimentally for the first time (MIFELA). At the UCLA Neptune Lab, a very high energetic IFEL experiment was conducted, in which an electron beam of 16 MeV was accelerated up to 55 MeV. The IFELA under the influence of square wave wiggler technique was presented, and it was demonstrated to have a twofold energy advantage over the standard IFEL with sinusoidal field wiggler[57]. The problem of phase instability of electrons related to the driving laser pulse and diffraction effects of laser beam disrupt the resonance state, hence preventing the high energy gain. To solve this issue, Kumar *et al.* investigated an IFEL scheme employing a frequency-chirped laser beam. In this approach, they evaluated a chirped Gaussian laser pulse in IFEL by considering more precise field expressions. The study illustrates that the mutual interaction of a tightly focused laser with a short pulse length is significantly more effective than the interaction of a narrower beam waist with an extended pulse length or a wider beam waist with a longer pulse. Furthermore, they achieve GeV energy gain from a 10 MeV electron by optimising laser input variables and considering tapering and chirp phenomena.[58]. A very intriguing feature of the IFELA beam is that the electrons become micro-bunched on the size of the driving wavelength.

Utilizing an IFEL to generate a micro-bunched electron beam offers several benefits. The IFEL micro-bunching may be accomplished at very high beam energies.Moreover, the micro-bunching enables a natural syncronisation between between the lasers used for kinetic energy and micro-bunched e-beam on the order of the laser wavelength.

3.5.2.1 Inverse free electron acceleration using planar and helical undulator.

3.5.2.1.1 Electron's motion in an IFELA

In IFELA a relativistic electron and laser's EM wave co-propagate to each other in the direction of the undulator axis and interact with each other and exchange the radiation with the EM wave. The dynamics of the electron in the undulator follow the Lorentz equation of motion given below.

$$\frac{dp_i}{dt} = -[qE + (v_i \times B_i)/c] \qquad (3.5.1)$$

$$\frac{d}{dt}(\gamma mc) = -q\beta_i.E_i \qquad (3.5.2)$$

Where $i = x, y, z$. $\vec{E}_i$ and are represents electric and magnetic fields of laser respectively and $\vec{B}_w$ denotes wiggler's magnetic field, $'m_e'$ and $'e'$ are the mass and charge of an electron. $'c'$ Defines the speed of light in a vacuum and $\left(\sqrt{1 - v^2/c^2}\right)^{-\frac{1}{2}}$, and $q = e$ is the charge of an electron.

3.5.2.1.2 The tightly focused laser field profile

Figure 3.27 shows a simplified schamatic of a tightly focused Gaussian laser beam.
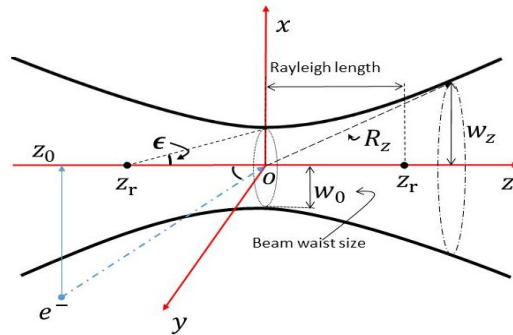
Figure 3.27 Schematic layout of a tightly focused laser beam

In figure3.27, w_z is beam's waist parameter at an arbitrary point z on the beam's axis and

$$w_z = w_0 \left(1 + \frac{z^2}{z_r^2}\right)^{\frac{1}{2}}$$

Where, $w_0 = $ beam's radius; and $z_r = \frac{kw_0^2}{2}$ (Rayleigh length)

For numerical analysis using simulation, electric field components of the tightly focused laser beam are expressed as [194]:

$$E_x = E_0 \left\{ \begin{array}{c} S_0 + \epsilon^2[\xi^2 S_2 - \rho^4 s_3/4] \\ +\epsilon^4 \left[\begin{array}{c} \frac{s_2}{8} - \frac{\rho^2 s_3}{4} - \frac{\rho^2(\rho^2 - 16\xi^2)s_4}{16} - \\ \rho^4(\rho^2 + 2\xi^2)S_5/8 + \rho^8 S_6/32 \end{array} \right] \end{array} \right\} \tag{3.5.3}$$

$$E_y = E_0 \xi \nu \{\epsilon^2 S_2 + \epsilon^4[\rho^2 S_4 - \rho^4 S_5/4]\} \tag{3.5.4}$$

$$E_z = E_0 \xi \left\{ \begin{array}{c} \epsilon C_1 + \epsilon^3[-C_2/2 + \rho^2 C_3 - \rho^4 C_4/4] \\ +\epsilon^5[-3C_3/8 - 3\rho^2 C_4/8 + 17\rho^4 C_5/16 - 3\rho^6 C_6/8 + \rho^8 C_7/32] \end{array} \right\} \tag{3.5.5}$$

And the related magnetic field is obtained by using Maxwell's equation.

$$\partial\vec{B}/\partial t = -\nabla \times \vec{E} \tag{3.5.6}$$

Where $\epsilon = \frac{w_0}{z_r}$; $\xi = x/w_0$

Other parameters used in equations are:

$$E = E_0(\, w_0/w)\exp[-r^2/w^2]\,, \; E_0 = kA_0,$$
$$S_n = (w_0/w)^n \sin(\psi + n\psi_G)\,; \quad n = 1,2,3,.$$

$$C_n = (w_0/w)^n \cos(\psi + n\psi_G)$$

Again, $k = \omega/c, r^2 = x^2 + y^2$ and $\rho = r/w_0$. A_0 Is vector potential, ω is the frequency and ψ read as

$$\psi = \psi_0 + \psi_p - \psi_R + \psi_G$$

where, ψ_0 is an initial steady phase. ; $\psi_p = \eta = \omega t - kz$ is the plane wave phase, the Guoy phase $\psi_G = (z/z_r)$, which changes from π to $-\pi$ while z changes from $-\infty$ to $+\infty$,

$\psi_R = kr^2/2R$, radius of the wavefront, where $R_z = z + z_r^2/z$ is Rayleigh length.

3.5.2.1.3 Profile of helical magnetic wiggler

Here we consider a wave that is moved in the z-direction, parallel to the axis of undulator. The simplest profile of helical wiggler magnetic field is chosen as.

$$\vec{B}_x = B_0 \cos(k_w z) \qquad\qquad (3.5.7)$$

$$\vec{B}_y = B_0 \sin(k_w z) \qquad\qquad (3.5.8)$$

here, $k_w = 2\pi/\lambda_w$ is wave propagation constant of wiggler and λ_w is wiggler wavelength B_0 is peak wiggler field strength.

3.5.2.1.4 Profile of planar magnetic wiggler

A planar wiggler magnetic field profile considering tapering effect is given as,

$$\vec{B}_y = B_0 \sin(k_w z) \quad \text{For} \quad z \leq z_0 \qquad (3.5.9)$$

$$\vec{B}_y = B_0 \quad\qquad \text{For} \quad z > z_0 \qquad (3.5.10)$$

3.5.2.2 Numerical study

As an explanation of the IFEL approach described above, we present simulations for the motion of a single particle by used laser beam.

Two alternative geometries of the wiggler magnet are included, the first one is planar and the other is helical. Here the laser field parameter $a_0 = 0.85 \times 10^{-9} \left[\lambda_0^2 I_0 \left(\frac{w}{cm^2} \right) \right]^{-\left(\frac{1}{2} \right)}$. where $\lambda_0 = 0.8 \mu m$ (wavelength of laser), and I_0 is laser intensity.

3.5.2.2.1 Planar wiggler field

The interaction between a planar magnetic wiggler field and a highly concentrated laser beam is examined here. The planar wiggler magnetic field is according to eq. (9) and (10). In the simulation model, we specify a group of

laser and planer wiggler field variables that are essential for the experimental procedure and compare various normalized values of a laser field a_0.
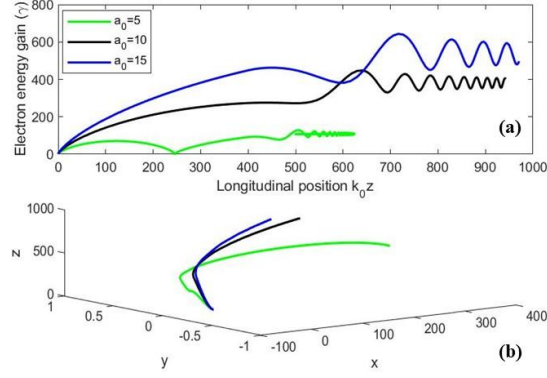
Figure 3.28 (a) Represent the electron energy gain γ v/s kz_0 for different laser field parameters $a_0 = 5$ (green curve), $a_0 = 10$ (black curve), and $a_0 = 10$ (blue curve) respectively. Normalised Beam waist size $kw_0 = 300$, $\tau = 100$, $\psi_0 = 0$ respectively. The maximum value of the normalized magnetic wiggler $b_0 = 0.5$. (b) The corresponding electron trajectory of an electron is shown. Figure 3.28 (a) Show how laser field parameters play a crucial role in electron acceleration. As laser field amplitude increases, the value of energy also increases (see figure 3). Figure (b) Present a 3-D trajectory of the electron's motion.

3.5.2.2.2 Helical wiggler field

The wiggler fields are described by equations (7) and (8).
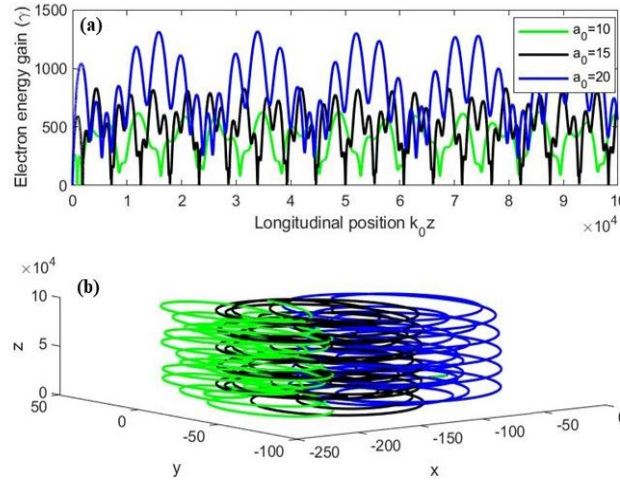
Figure 3.29 (a) shows electron energy gain (γ) v/s longitudinal position (k_0z) for different values of laser field parameter $a_0 = 10$, $a_0 = 12$, and $a_0 = 14$ respectively. Other laser beam parameters as beam-waist size $w_0 = 300$, the initial phase of laser $\psi_0 = 0$, laser pulse duration $\tau = 100$, the normalized value of magnetic wiggler field $b_0 = 0.5$, tapering point $k_0z_t = 2000$ respectively. Figure 4 (b) shows the 3-D orientation of the electron.

Figure 3.29 (a) Present graphical representation of electron energy gain γ v/s longitudinal position k_0z. Graphical data shows maximum energy gain γ is enhanced with the laser field parameter. A 3-d trajectory of electron under the wiggler is shown in (b).

3.5.3. Conclusion

In this chapter, comparative investigation (numerically) of the dynamics of a single electron with a tightly concentrated laser beam in the presence of a planer and helical undulator is conducted. To enhance the electron acceleration in the IFEL accelerator, several laser parameter effects are examined. For laser field descriptions, a more precise fifth-order correction in the diffraction angle is considered, which implies the laser beam is concentrated on a few micron-sized spots. Observations indicate that electron energy gain is greater for helical wigglers than for planar wigglers. The gain is proportional to the power of the

laser's field. In a planar wiggler, our research demonstrates that the electron achieves its maximum energy gain early but is unable to sustain it for an extended period, and the same is true for the influence of the wiggler magnetic field. under the same conditions, it has been found that the maximal energy gain of a helical wiggler exceeds that of a planar wiggler.

Chapter 4

Simulation study of two color Laser Wakefield acceleration

4.1 Introduction

Laser-Plasma based particle acceleration agents [9] represent the forefront of next-generation accelerator technology, offering accelerating gradients exceeding 100 GV/m—orders of magnitude higher than conventional radiofrequency (RF) accelerators. This breakthrough has been driven by rapid advancements in ultra-intense laser systems and concurrent experimental progress in laser-driven plasma acceleration, which have enabled the development of compact and high-performance accelerators[46], [195]. Experimental results have confirmed the production of high-quality electron bunches with normalized transverse emittance reaching micron and even sub-micron scales[101],[102], a critical parameter for applications in free-electron lasers, compact light sources, and future collider concepts. To further enhance beam quality—especially in terms of emittance and stability—innovative schemes such as two-colour laser wakefield acceleration[198] and electron-beam-driven plasma wakefield acceleration[199], [200], have been developed. In the two-colour laser wakefield scheme, a long-wavelength laser pulse (typically in the infrared range) first drives a strong nonlinear plasma wave through partial ionization of a high-Z gas, forming a wakefield with large longitudinal electric fields. A second, temporally delayed, short-wavelength laser pulse (such as a frequency-doubled 400 nm pulse) then ionizes the inner-shell electrons of the remaining bound states within the wake's accelerating phase. This precisely timed injection of electrons into the accelerating phase enables the generation of electron bunches with ultra-low emittance, due to minimal residual momentum at the time of ionization. This controlled injection process also reduces ti ming jitter and energy spread, leading to improved beam reproducibility and quality. The same ionization-based injection principle was

initially proposed in Reference[201], laying the foundation for the modern two-colour LWFA approach. These developments underscore the importance of integrated laser-plasma engineering and precise pulse synchronization in shaping the next generation of particle accelerators.

4.2 Particle in cell simulation

EPOCH [202] and cpl PIC [203] codes are used for 2D-PIC simulation. The plasma profile chosen in the simulation is shown in Figure 4.1. The peak value of electron plasma density is 8×10^{18} cm^{-3}. Dimensions of the simulation box is $250 \, c/\omega_p \times 450 \, c/\omega_p$, utilised for a 2D simulation travelling at the speed of light, c. The simulation box is partitioned into 2000 cells along the x and 500 cells along z axis. Each cell have 16 macro-particles.
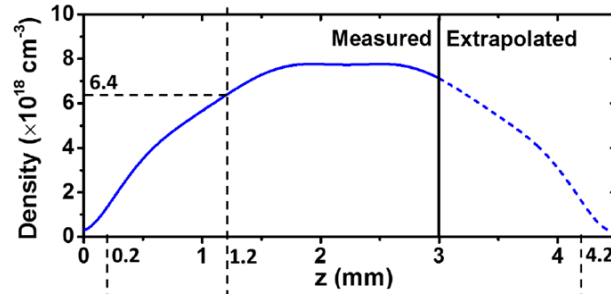
Figure 4.1 Plasma density for Electron profile utalised in the PIC-simulation[204].

4.3 Simulation results

4.3.1 Single-color laser wakefield acceleration

A laser of 2.1J energy is chosen for single color. Normalized vector potential $a_{L1} = 1.83$, with 30 femtoseconds pulse duration. Intensity of the laser is $I_{L1} = 7.2 \times 10^{18}$ W/cm^2. 50 μm is the waist size of the beam. The laser beam has a waist size of 50 μm, denoted as $2w_{L1} = 50 \, \mu$m. A plasma

channel of 4.2 mm in length is used, the laser is focused at 1.2 mm.
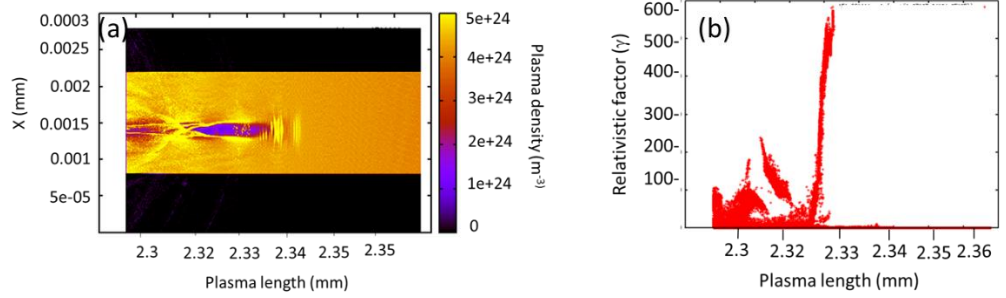
Figure 4.2 Simulation of Wakefield using a single colour laser. (a) Two-dimensional representation of the plasma density profile acquired at 2.3 mm, (b) relativistic factor (γ) of the electron bunch measured at 2.3 mm.

The 2D picture of the plasma density distribution and confined electrons in plasma bubble are depicted in Figure 4.2(a). The relativistic factor of an accelerated electron is illustrated in Figure 4.2(b). In a plasma channel that is 2.3 mm in length, γ = 600 is attained in a single colour laser scheme. Nevertheless, the numerical noise becomes the prevalent factor, as illustrated in Figure 4.2 (b).

4.3.2 Two-color laser wakefield acceleration

For two-color laser Wakefield simulation: the driving laser have $a_{L1} = 1.74$ with the energy of 1.9 Joule, pulse duration $\tau_{L1} = 30$ fs, intensity $I_{L1} = 6.5 \times 10^{18}\ W cm^{-2}$, $0.8 \mu m$ wavelength, spot size $2w_{L1} = 50\ \mu m$ with plane polarization while The trailing laser operates at a frequency of $\omega_2 = 7.854\omega_p$ characterised by the following parameters: $a_{L2} = 1.8$ with the energy of 82.8 mJ; $I_{L2} = 2.8 \times 10^{19}\ W/cm^2$, pulse duration $\tau_{L2} = 30$ fs, wavelength of 400 nm, and a spot size of $2w_{L2} = 5\ \mu m$ with plane polarisation. The initial laser is concentrated at a depth of 1.2 mm within the plasma channel.

4.3.2.1 Second-laser with plane-polarization
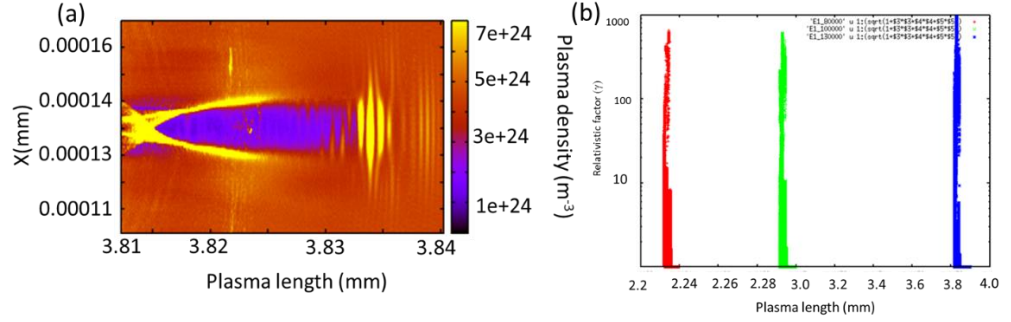
Figure 4.3 (a) Two-dimensional snapshot of the plasma density profile captured at 3.82 mm. (b) Relativistic factor (γ) of the electron bunch recorded at 2.3 mm, 2.29 mm, and 3.82 mm, respectively.

Figure 4.3(a) expresses the two-dimensional plasma density and the the position of trapped electrons in the plasma bubble. In 3.8 mm propagation, the relativistic factor increases to 1000 (Figure 4.3(b)). In the two-color instance, numerical noise is minimised, and the simulation proceeds smoothly until the termination of the plasma channel.

4.3.2.2 Second-laser with circular-polarization
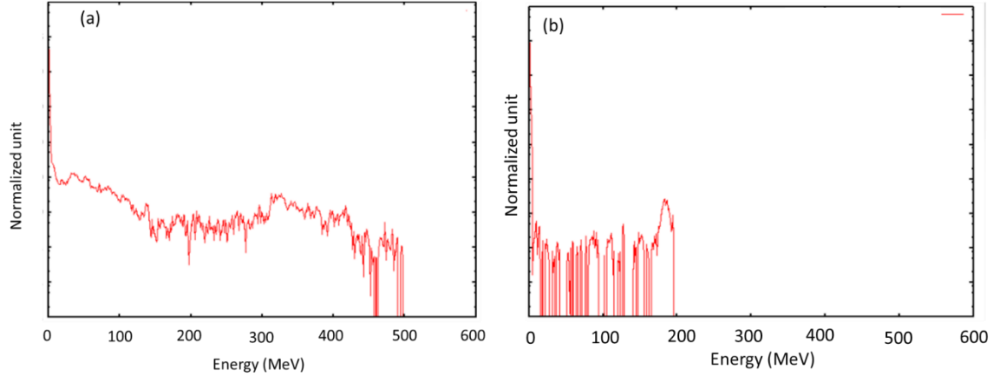
Figure 4.4 Electron-energy spectra (a) when second laser has plane-polarization, (b) second laser has circular-polarized.

Figure 4.4 shows electron energy spectra. In figure 4.4 (a) both lasers are plane polarized and in figure 4.4(b) only second laser has circularly polarised. In our study, we saw that for circular polarized case, numerical noise

becomes high while the number of trapped electrons in the plasma bubble is less.

4.4 Effect of time delay between two lasers

It has been noticed that the charge of the electron bunch that has been accelerated is quite low. In order to increase the charge that is per electron bunch, we carried out a simulation that involved a time delay between two lasers. In one instance, the 2ω beam is introduced approximately 100 fs to 300 fs before the 1ω beam. We noted that at these delays, there is a potential for an additional charge to be introduced into the plasma bubble, as evidenced by experimental observations. Additional instances include -50 fs and -100 fs, when the injection beam is introduced near the conclusion of the first and second plasma waves, respectively. An extra charge is detected at -100 fs, corresponding to the second wake bubble of the primary laser pulse. The findings are not included herein.

4.5 Summary

We reported preliminary simulation findings on two-color LWFA system in this paper. Outcomes are compared to single-color LWFA. The effect of second laser polarisation on electron acceleration is examined. 2D density plots can estimate it roughly. Also examined is the influence of time delay between both lasers on electron bunch acceleration. For a single colour laser, the electron beam energy was less than 200 MeV and the spectrum was quasi-monoenergetic. Two-color lasers boost electron beam energy to 600 MeV in a 4 mm plasma channel. More simulations are needed to determine how laser time delay affects electron acceleration.

Chapter 5

Effect of frequency-chirped ionization laser on accelerated electron beam characteristics in plasma wakefield acceleration

5.1 Introduction

Plasma-based acceleration methods utilise electric fields reaching tens of GV/m, much beyond the electric fields of existing metallic cavity accelerators (100 MV/m)[166], [205] and dielectric waveguide accelerators (1 GV/m)[206]. In last few years, plasma-based accelerator have considerably progressed in producing high energetic and powerful e-bunches [207], [208], [209], [210], [211], [212], [213], [214], [215], [216]. The pursuit of ultra-low emittance and GeV plasma-based acceleration agents will drive the development of compact linear colliders[217], which will facilitate investigations in high energy physics. Furthermore, new table-top X-ray coherent sources[117], [218] will become a reality. These sources will facilitate physical, chemical, and biological research at an atomic level.

Laser and electron beam-driven based plasma wakefield accelerations (LWFA and PWFA) are promising particle acceleration technologies[219], [220]. A short laser pulse or ultra-relativistic electron beam creates a plasma wake in an underdense plasma. The witness beam of trailing electrons is accelerated to ultra-relativistic energies by the space charge. In centimetre-scale plasma, wakefield accelerators (WFA) have achieved GeV energy with minimum energy spread[221]. Beam-driven PWFA accelerated electrons to 42 GeV in a meter-long plasma channel[222]. For such tremendous development in recent years, several strategies have improved witness beam properties.

Numerous schemes have been helps to enhance electron-beam characteristics, including self-injection schemes[223], [224], [225], [226], density profile tailoring [227], [228], [229], [230], multiple laser-pulse injection

[120], [231], [232], two-color laser wakefield acceleration[136] and ionization-induced injection[233], [234], [235], [236]. Along with various combinations of these methods. Hybrid plasma accelerators utilising an e-beam as a driver to generate a plasma bubble, combined with a low-intensity laser for ionisation injection, may serve as an alternative to enhance the properties of electron bunches. Recent studies indicate that the output of electron beam-plasma accelerators meets the requirements for free electron lasers[199], [237], [238]. Further enhancement in the brightness of electron bunches is necessary to achieve a significant reduction in FEL gain length, thereby facilitating the development of compact XFELs[239] at shorter wavelengths [240].

The use of chirping in frequency in optical lasers results in asymmetry in laser pulses[241], which directly influences Wakefield generation and electron acceleration[242], [243]. Here we investigates the impact of frequency-chirp in ionisation lasers on the characteristics of witness bunches in the TH injection scheme[199].

5.2 Simulation method

The hybrid approach of PWFA [199], [237], [244], [245], [246], Laser-mediated ionisation electron sources are used with electron-beam plasma blow-out cavities. A combination of low ionisation threshold (LIT) gas Lithium (Li) and high ionisation threshold (HIT) gas Helium (He). An electron beam, functioning as a driver, ionises only LIT gas and induces a plasma wakefield within the plasma. The HIT gas maintains a neutral state during the passage of the electron beam.

An accurately synchronised optical laser pulse trails the electron beam and is concentrated into the plasma bubble, which ionises the HIT gas. This phase of the plasma explosion creates optimal conditions for the acceleration of laser-ionized electrons. Laser pulses of modest strength with femtosecond durations are employed for electron ionisation and their injection in a plasma bubble. The tunnelling ionisation rates of He and Li ions are derived using ADK theory [244]. A driving e-beam density is $n_{b0} = 7.1 \times 10^{17}$ cm^{-3}, is used. The

beam energy $\langle E_d \rangle = 200$ MeV, and the driving beam sizes are $k_p \sigma_{b,z} 1.26$ and $k_p \sigma_{b,r} 0.53$ are chooses for study[237]. The beam's normalised emittance $\varepsilon_r = 15$ µm , the waist size of the ionisation laser pulse at the focal point is $w_0 = 8$ µm, and the pulse length ~ 12 µm. The plasma density $n_0 = 3.3 \times 10^{17}$ cm⁻³.

5.3 Simulation results and discussion

FBPIC (Fourier-Bessel PIC) code is employed to conduct the simulations in cylindrical geometry, utilising the azimuthal Fourier decomposition algorithm [247]. The mesh resolution was determined to be $\Delta z = \lambda_0/16$ and $\Delta r = \lambda_0/8$ n the longitudinal and transverse orientations, respectively. The normalised charge per unit length of the driving beam $\Lambda \equiv (n_b/n_0)k_p^2 \sigma_{b,r}^2$ and the condition $k_p r_m \gg 1$ A determine the radius of the bubble region as a relativistic charged particle beam with n_b≫n_0 passes through the plasma. For a laser wavelength of around 800 nm, the laser intensity is $I_0 \approx 7 \times 10^{14}$ W/cm² resulting in an electric field of approximately $E_0 \approx 72$ GV/m. This electric field is adequate to ionise the HIT gas.
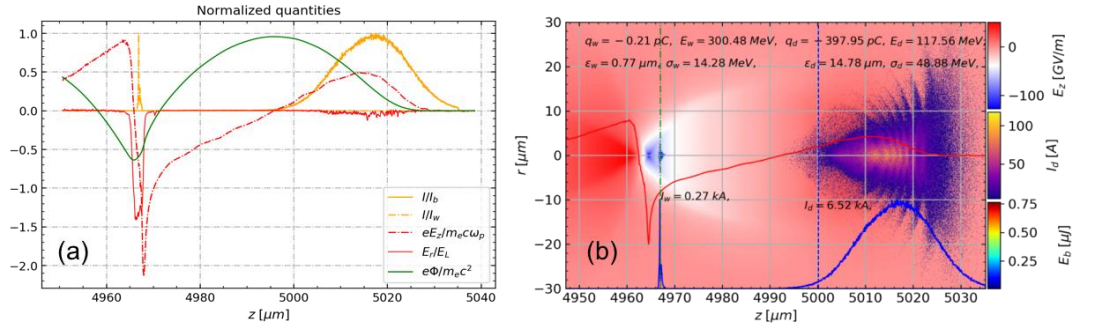
Figure 5.1 (a) Normalized profiles of wake potential (green-line), wakefield (red-lines) and current (orange-lines) distributions at time t = 16 ps. (b) 2D snapshot of electron density (background and ionized electrons), current-profile (blue-line) and plasma wakefield distributions (red-line) at t = 16 ps. These results are for an unchirped ionization-laser of 8 fs FWHM long pulse used.

For an unchirped laser, Figure 5.1(a) depicts the fluctuation of normalised wake potential, wakefield, and current at t = 16 ps. Figure 5.1(b) depicts baseline and ionised electron density distribution in 2D. The witness-bunch is shown by the vertical green-dashed line in figure 5.1(b) and the ionising laser by the blue-dashed line. In plasma bubbles, ionisation injection occurs at wake-potential peak. Backward electrons trap at the wakefield minimum and accelerate. Ionised electrons were trapped in plasma blowout's second half. At two separate acceleration instants, the wake-potential difference between the ionisation position and the end of acceleration cavity in figure 5.1(b) exceeds 1. With relative energy spread $\Delta E/E$ of 4.7 % the accelerated beam with peak electron energy of 300 MeV in 5 mm long plasma channel is obtained where ΔE is the FWHM of the peak energy, and E is the centre energy in energy spectra. The bunch length is of 5fs; the normalised emittance and bunch-charge are respectively 0.77 μm and 0.21 pC.
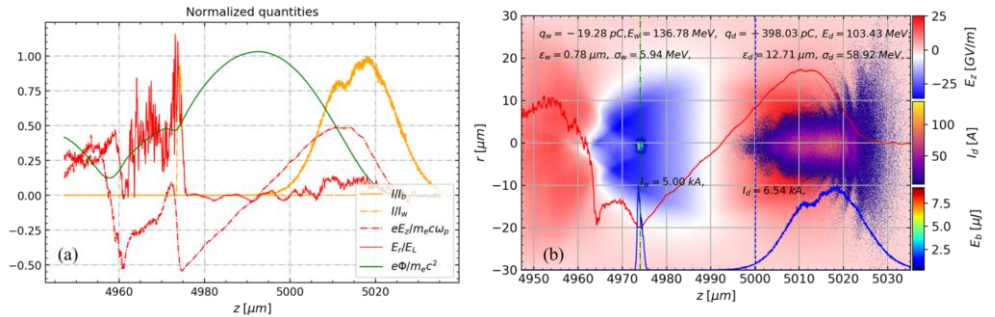
Figure 5.2 (a) Normalised distributions of wake potential (green line), wakefield (red lines), and current profile (orange lines) at time t = 16 ps. 5.2 (b) Two-dimensional representation of electron density (including background and ionised electrons), current profile (blue line), and plasma wakefield distributions (red line) at t = 16 ps. The results pertain to a negative-chirped ionisation laser, $\phi^{(2)} = -1.0 \times 10^{-4}$, The parameters of the witness bunch, including beam energy, beam emittance, and energy spreads of both the witness bunch and the driving beam, are illustrated in Figure 5.2(b).

107

Figure 5.2 (a) illustrates the profiles of normalised currents, wakefields, and wake potential produced during 5 mm of laser propagation in underdense plasma utilising a negatively chirped pulse in the ionisation laser. Figure 5.2 (b) illustrates the two-dimensional representation of electron density (including background and ionised electrons) of the plasma bubble, wakefield, and current profile at 5 mm along the plasma for a negatively chirped pulse. The specified negative chirp results in a potential difference greater than 1, as illustrated in figure 5.2 (a). Consequently, the ionization-induced injection transpires throughout the entire region, resulting in a substantial quantity of trapped electrons. Nonetheless, the effective injection persists for merely a few hundred micrometres, as the wakefield potential difference within the plasma disrupts the conditions necessary for ionization-induced injection. Furthermore, the injection length can be improved by regulating the negative-chirp parameter. Figure 5.2 (b) illustrates that the trapped charge is amplified by two orders of magnitude in the presence of a negative-chirped laser, resulting in a total charge of $Q \approx 19.28$ pC and a peak current amplification of 5 kA, accompanied by a 136 MeV energy gain. The energy spread remains nearly constant, namely $\Delta E_{rms}/E = 4\%$ in 5 mm long plasma cavity. The accelerated bunch measures 7 fs in length and has a normalised emittance of $0.78 \mu m$.
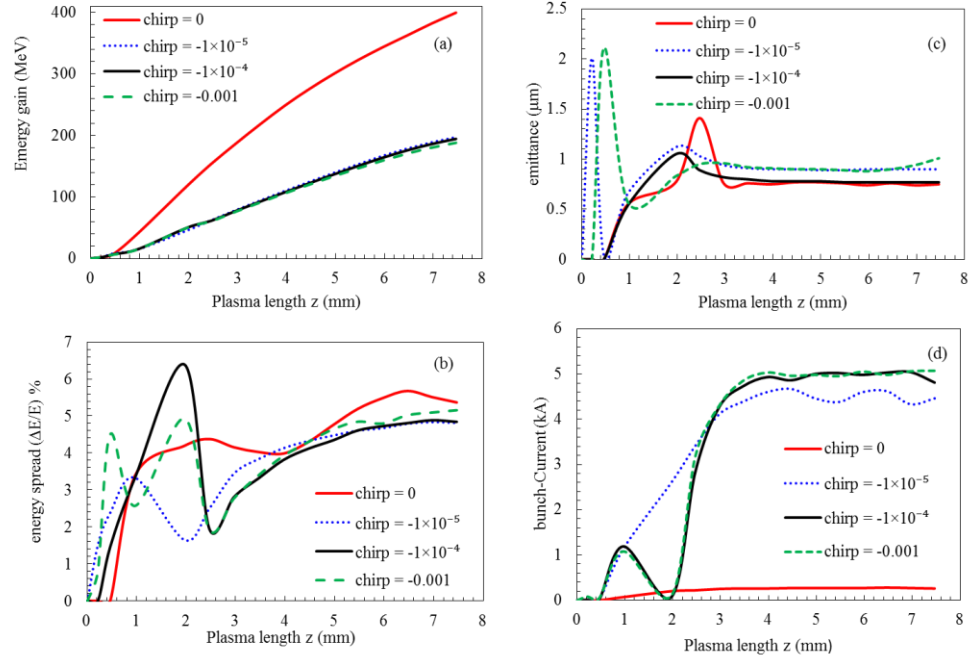
Figure 5.3 Shows time variation of witness-bunch properties; (a) energy-gain, (b) energy-spread, (c) beam-emittance, (d) bunch-current, respectively corresponding to different frequency chirp in ionization laser.

To examine the parametric scaling, we monitor the changes in witness-bunch characteristics to assess the impact of the negative frequency-chirp variables. Figure 5.3 (a) illustrates the energy gain achieved along the plasma length for various frequency-chirp configurations. It is observed that in the un-chirp scenario where $\phi^{(2)} = 0$, the energy gain reaches a maximum of approximately 400 MeV within a 7.5 mm long plasma channel. In the case of negative-chirp with $\phi^{(2)} = -1.0 \times 10^{-4}$, the energy gain is reduced to half of that of the unchirped case, resulting in 200 MeV. Figure 5.3 (b) illustrates the temporal progression of the energy spread within the accelerated electron bunch. The energy spread evolution for negative-chirp $\phi^{(2)} = -1.0 \times 10^{-4}$ (black-line) is marginally lower compared to the un-chirped case $\phi^{(2)} = 0$ (red-line). Initially, the observation of transverse oscillations resulting from the finite transverse momentum spread of the accelerated electrons leads to an initial

increase in the energy spread. The frequency-chirp $\phi^{(2)} = -1.0 \times 10^{-4}$ (black-line) yields the lowest energy-spread value. The beam emittance represents a critical parameter of the accelerated electron bunch. A similar trend in emittance growth has been noted initially for both unchirped and chirped cases, as illustrated in figure 5.3(c). For $\phi^{(2)} = 0$ (red-line), the normalised emittance exhibits an initial increase followed by a saturation phase. Nonetheless, in the case of finite negative-chirp $\phi^{(2)}$, a reduction in emittance is noted at the conclusion of the simulation. Figures 5.3(d) and 3(e) illustrate the temporal evolution of current and charge for the accelerated electron bunch in conjunction with the plasma length. The injected charge for the negative-chirped pulse reaches 60% of the total charge. Figure 5.3(e) illustrates that electrons are captured from the initial position in contrast to the unchirped laser scenario. Two injections are noted for the negative-chirped pulse; the first is recorded at approximately 0.5 μm, while the second injection takes place at 2 μm. At a later stage, trapped electrons encounter a reduced accelerating wakefield in comparison to those injected earlier, leading to a lower energy gain relative to the unchirped scenario.

The group of witnesses produced through ionization-induced injection methods is expected to play a significant role in the development of compact light sources, such as betatron X-ray sources. The enhanced brightness characteristics of such electron bunches indicate their potential to meet the Pellegrini criterion $\varepsilon_n < \gamma \lambda_r / 4\pi$ [248] while also contributing to a significant increase in the FEL parameter ρ_{FEL} in future applications. Consequently, these characteristics position the ionization-injected driver as an optimal choice for FEL lasing, facilitating the attainment of higher power within a reduced undulator. The low emittance and high brightness characteristics of the beam generated by TH methods allow for an estimation of a reduced 1D FEL gain length, expressed as $L_g = \epsilon^{5/6} / I_p^{1/2}$ [249], This configuration is expected to yield exceptionally high FEL power levels. Nonetheless, the synchronisation of the electron beam with a laser pulse system presents a significant challenge for the experimental realisation. This issue is present in external injection as well,

where electron beams injected from outside, produced in linacs, are utilised in laser based accelerators. While this study offers a detailed theoretical and simulation-based investigation of the influence of negatively chirped ionisation lasers on electron bunch characteristics within the Trojan-horse injection framework, it is important to acknowledge that the present work lacks experimental validation. Future experimental studies are essential to corroborate the simulation results presented here and to explore the practical feasibility of implementing chirped laser pulses in real-world wakefield acceleration setups.

Additionally, a more comprehensive parameter space analysis—considering varying plasma densities, laser intensities, and chirp magnitudes—could further deepen the understanding of how chirp influences both the phase space dynamics and energy spread of the accelerated bunch. The integration of 3D PIC simulations and beam diagnostics in experimental configurations could provide a more robust foundation for optimizing injection schemes using chirped ionisation lasers. Despite these limitations, the current findings clearly demonstrate the promising potential of negative chirp as a control parameter for enhancing electron injection rates and bunch charge. This work thus lays the groundwork for both theoretical advancements and experimental pursuits aimed at realizing compact, high-brightness electron sources for next-generation accelerators.

5.4. Conclusion

This study presents a comprehensive investigation of the accelerated bunch characteristics in the Trojan-horse injection method[199], recognised for its promise in generating low-emittance, high-brightness electron bunches. We investigate the impact of a negatively chirped ionisation laser beam on the accelerated electrons bunch. Our research demonstrates that manipulating the frequency chirp in ionisation lasers allows for the regulation of accelerated electron bunch characteristics. The application of negative frequency-chirp in ionisation laser pulses significantly enhances the number of trapped electrons,

hence increasing the overall bunch charge in comparison to unchirped laser pulses. The net energy gain is diminished in the scenario of negative chirped ionisation lasers relative to unchirped laser pulses. Negative-chirped ionisation laser pulses are effective in increasing the quantity of trapped electrons. These pulses capture electrons two orders of magnitude higher and achieve a peak current one order of magnitude more than the unchirped laser pulse in the Trojan horse approach. Consequently, an enhanced electron injection rate across a reduced distance, facilitated by a negatively-chirped ionisation laser, can effectively produce ultra-short, high-charge electron bunches. These findings underscore several benefits of employing frequency chirp in ionisation lasers.

Chapter 6 (6.1)

Optimizing laser wakefield acceleration through plasma density profile analysis

6.1.1. Introduction

Particle acceleration has been an important part of modern physics for a long time, leading to progress in both basic study and real-world applications. Standard techniques, like vacuum electron acceleration [144], [178], [250], which employs electromagnetic fields inside the vacuum tubes to speed up particles to very high speeds, have helped scientists make discoveries in many areas. Particle physicists and engineers now have more tools at their disposal, such as inverse free electron laser acceleration (IFEL), which uses the coherent radiation emitted by high-energy electrons in a magnetic undulator[142], [156], and beat wave acceleration[143], [183], which utilizes the interference pattern of multiple laser beams to create accelerating gradients. But even though these ways work, they often have problems with size, cost, and effectiveness.

Laser wakefield acceleration (LWFA) has become a potential alternative in recent years. It uses the interaction between intense laser pulses and plasma to achieve acceleration gradients that have never been seen before over very short distances[251]. By using an intense laser wave to create a plasma wakefield, LWFA could speed up particles in a compact way while also introducing high-gradient forces[148]. By providing compact, high-energy solutions with significant implications for scientific research, medicinal applications, and industrial technologies, laser wakefield acceleration (LWFA) techniques revolutionise particle acceleration physics.

Laser wakefield acceleration (LWFA) is an innovative technique for accelerating particles in the field of plasma physics. This phenomenon involves the utilization of intense laser pulses to generate highly potent electric fields within the plasma, enabling the rapid acceleration of charged particles to tremendous energy levels over extremely short distances[12], [252]. Singh *et*

al.[253] have examined a two-colour laser wakefield acceleration method to amplify the produced wakefield. Aniculaesei *et al.*[254] introduces a straightforward and potent experimental technique that utilizes a sequence of plasma profiles customized longitudinally to regulate the phase relationship between the electron bunch and the wakefield. As a result, this method allows for precise control over the characteristics of the accelerated electron bunch. Sprangle[255] conducted a study on GeV acceleration by utilizing a plasma channel that tapered and increased the plasma density as distance increased. The findings revealed that, by doing so, the phase velocity of the accelerated field back to the pulse can matched with the speed of light. This approach prevents electron's dephasing and leads to enhanced energy gain. Hubbard *et al.*[256] examine the simulation and development of channel-guided laser wakefield acceleration devices, focusing on their stability. The study also includes an examination of a numerical model. In a study, The wakefields generated by Bessel-Gaussian and Gaussian laser pulses were examined by Fallah et al. [257]. They found that, under certain conditions, the Bessel-Gaussian laser pulse can accomplish an energy gain of up to 90 MeV. Also, Fallah *et al.*[258] examined the impact of Gaussian, super-Gaussian, and cosine-Gaussian laser pulses in a separate investigation. 800 MeV energy was attained through the utilization of Cosine-Gaussian laser pulses. Tooley *et al.*[259] develop the plasma density gradient injection threshold. Sub-femtosecond bunches are injected in particle-in-cell simulations, confirming this condition. Changing the plasma density profile permits precise control over bunch charge, length, and separation within a bunch train. Massimo *et al.*[260] examined how density transition factors affect the characteristics of electron beams accelerated by laser wakefields, employing particle-in-cell simulations (PIC) code CALDER-CIRC. They offered theoretical and numerical analysis of the injection process and electron beam parameters. An increase in the charge of electron bunches was achieved by Gupta *et al.*[261] through the utilization of a flattened Gaussian laser pulse. Gopal *et al.*[262] investigated the impact of pulse duration on LWFA utilizing a skewed laser pulse. They established that by optimizing the

pulse duration, the quality of accelerated electron bunches can be improved. In addition, the pulse profile plays a crucial role in the formation of numerous nonlinear phenomena that result from the laser-plasma interaction. Xia *et al.* studied laser wakefield acceleration in axially inhomogeneous underdense plasma[263]. Furthermore, the high-energy electrons are expelled due to this nonlinearity, which obviates the necessity for a supplementary extractor. Akou *et al.* [264] present a study on the creation of plasma wake using an asymmetric laser pulse. The findings indicate that asymmetrical and positively chirped Gaussian pulse with a quickly increasing time can generate a significantly larger wake wave. The significance of optimizing the laser pulse length to produce an effective wakefield is determined by Sharma *et al.*[265], who investigated the relationship between frequency modulation and pulse length. Asri *et al.* [266] investigated circularly polarized (CP) Gaussian pulses of laser featuring varying sense rotations.

In this chapter, we investigate the novel approach of LWFA using different values of plasma density profiles. This work systematically investigates the impact of various density profiles on energy gain, generated wakefield, and wake potential. In section 6.1.2 we studied the governing equations of the LWFA mechanism. Analytical expressions are derived for the longitudinal wake-potential, wakefield produced by the laser pulse, and electron energy gain. discussion of the density modulation on wake-potential, wakefield and energy gain is studied, and results are present in section 6.1.3. In section 6.1.4 of the paper conclusion part is concluded.

6.1.2. Numerical analysis

6.1.2.1 Mathematical equations

In this study, we analyze the behaviour of em-waves in a uniform plasma with external magnetic field (B = B_0 $\hat{\jmath}$) under conditions of weak nonlinearity. In plasma, the following equations describe laser's interaction with plasma in the nonlinear regime with an external magnetic field:

$$m_0 \frac{\partial \vec{v}}{\partial t} + (\vec{v}.\vec{\nabla})\vec{p} = -e\{\vec{E} + \vec{v} \times (\vec{B} + \overrightarrow{B_0})\} \qquad (6.1.1)$$

$$\vec{\nabla} \times \vec{B} = \mu_0 \vec{J} + \mu_0 \epsilon_0 \frac{\partial \vec{E}}{\partial t} \tag{6.1.2}$$

$$\frac{\partial \vec{B}}{\partial t} = -\vec{\nabla} \times \vec{E} \tag{6.1.3}$$

Current density $\vec{J}$ due to electron motion is given by.

$$\vec{J} = -n_e e \vec{v} \tag{6.1.4}$$

$$\frac{\partial n_e}{\partial t} + \vec{\nabla}.(n_e \vec{v}) = 0 \tag{6.1.5}$$

where, n_e is plasma density and $\vec{v}$ is the electron's velocity.

From the Gauss's law for electro-statics

$$\vec{\nabla}.\vec{E} = \frac{e}{\epsilon_0}(n_i - n_e) \tag{6.1.6}$$

Where $\vec{P} = \gamma m_0 v$ relativistic momentum of electrons is, m_0 is electron's rest mass. γ is given by.

$$\gamma = 1 / \sqrt{1 - \frac{V^2}{C^2}} = \sqrt{1 + \left(\frac{P}{mc}\right)^2} \tag{6.1.7}$$

If a laser pulse is assumed to propagate in the Z-direction, then its electric field should be oriented along the x-dir., while the magnetic field must be oriented along the y-direction. $v_\parallel$ and $v_\perp$ represent the velocity components parallel and perpendicular (in the x-direction) to the laser's direction.

Using equations (1)-(6) and velocity components, we get

$$\frac{\partial n_e}{\partial t} + \frac{\partial(n_e v_\parallel)}{\partial z} = 0 \tag{6.1.8}$$

$$\frac{\partial \emptyset}{\partial z} = \frac{m}{e}\frac{dv_\parallel}{dt} + \frac{m}{e}v_\parallel\frac{\partial v_\parallel}{\partial z} + (B + B_0)v_\perp \tag{6.1.9}$$

$$-\frac{eE}{m} = \frac{dv_\perp}{dt} + v_\parallel\frac{\partial v_\perp}{\partial z} - \frac{ev_\parallel(B+B_0)}{m} \tag{6.1.10}$$

The given equations form a system of differential equations, expressed in terms of z and t, that describe the wake-field Φ. To minimize the influence of the

independent variables (z and t), we assume that the system is static and does not change over time. We introduce a novel variable, denoted as ξ, which is a function of both space and time. Specifically, ξ is defined as the difference between the spatial coordinate 'z' and the product of the group velocity of plasma "v_g" and time 't', *i.e.* $\xi(z,t) = z - v_g t$, here $v_g = c\sqrt{(1 - (\omega_p^2/\omega^2))}$ and $\omega_p = e\sqrt{(n_e/m\epsilon_0)}$ plasma frequency.

So, $\frac{\partial}{\partial z} \equiv \frac{\partial}{\partial \xi}$ and $\frac{\partial}{\partial t} = -v_g \frac{\partial}{\partial \xi}$

If n_0 is the initial electron density in plasma and n_e' is number density perturbation due to EM-laser pulse, then net e^- density is:-

$n_e = n_0 + n_e'$.

Using equations (8), (9) and (10) in terms of new variable ξ we get.

$$-v_g \frac{\partial n_e'}{\partial \xi} + n_0 \frac{\partial v_\parallel}{\partial \xi} + v_\parallel \frac{\partial n_e'}{\partial \xi} + n_e' \frac{\partial v_\parallel}{\partial \xi} = 0 \qquad (6.1.11)$$

$$\frac{\partial \emptyset}{\partial \xi} = -v_g \frac{\partial v_\parallel}{\partial \xi} + v_\parallel \frac{\partial v_\parallel}{\partial \xi} + (B + B_0)v_\perp \qquad (6.1.12)$$

$$-\frac{eE}{m} = -v_g \frac{\partial v_\perp}{\partial \xi} + v_\parallel \frac{\partial v_\perp}{\partial \xi} - \frac{ev_\parallel(B+B_0)}{m} \qquad (6.1.13)$$

The expression for the net electric field encountered by plasma electrons is.

$$\vec{E} = Ei - \frac{\partial \phi}{\partial \xi} \hat{k} \qquad (6.1.14)$$

Using equations from (1)-(13)

$$\left(\frac{\partial^2 \emptyset}{\partial \xi^2}\right) + k_P{}^2 \emptyset - \left[\left\{\frac{e(\beta^2-1)}{2mv_g{}^2}\right\}\left(E^2 + 2B_0 E v_g\right)\right] = 0 \quad (6.1.15)$$

Here $\beta = c/v_g$ and $k_p = \omega_p/v_g$, $\emptyset$ is wake-potential.

Eq. (14)'s last term also indicates the force term that drives the wakefield and is connected with pondermotive force.

Longitudinal wakefield is obtained by using given equation:-

$$\vec{E}_w = -\frac{\partial \Phi}{\partial z}\hat{k} \tag{6.1.16}$$

Relativistic factor ($\Delta\gamma$) in the terms of $\eta = k_p(\xi - L/2)$ is given as:

$\Delta\gamma = -e/k_p mc^2\{1 - 1/\beta\}\int E_w d\eta$, Energy gained by electrons is calculated by

$$\Delta W = m_0 c^2 \Delta\gamma \tag{6.1.17}$$

The Gaussian Laser Pulse's field distribution profile is selected below.

$$E^2 = E_0{}^2 \exp\left[-\frac{2\left(\xi - \frac{L}{2}\right)^2}{r_0{}^2}\right], \quad 0 \le \xi \le L. \tag{6.1.18}$$

Here E_0 is the maxi. value of the Gaussian electric field amplitude and r_0 is beam waist radius.

Using eq. (15), (16) and (17) we calculate wake potential (Φ), wakefield (E_w) and electron energy gain (ΔE). In our study, we incorporate the error function (Erf) to describe the spatial distribution of plasma electron density within generated wakefield, a crucial factor influencing particle acceleration dynamics. By leveraging the mathematical formulation of the erf function, our study provides insights into the complex interplay between intense laser pulses and plasma, advancing our understanding of LWFA as a promising particle acceleration mechanism. For the given profile in equation (18) wakefield (E_w), wake potential (Φ), and electron energy gain (ΔE) Are obtained as

$$\mathbb{E}_w = -\frac{ee^{-\frac{1}{8}k_P^2 w_0^2}\sqrt{\frac{\pi}{2}}(-1+\beta^2)\text{Cos}\left[\frac{1}{2}(L-2\xi)k_P\right]\left(\text{Erf}\left[\frac{2L-ik_P w_0^2}{2\sqrt{2}w_0}\right]+\text{Erf}\left[\frac{2L+ik_P w_0^2}{2\sqrt{2}w_0}\right]\right)w_0\mathbb{E}_0^2}{4m_0 v_g^2}\bigg/10^9 \tag{6.1.19}$$

$$\phi_w = -\frac{1}{4k_P m_0 v_g^2}ee^{-\frac{1}{8}k_P^2 w_0^2}\sqrt{\frac{\pi}{2}}(-1+\beta^2)\left(\text{Erf}\left[\frac{2L-ik_P w_0^2}{2\sqrt{2}w_0}\right]+\text{Erf}\left[\frac{2L+ik_P w_0^2}{2\sqrt{2}w_0}\right]\right)\text{Sin}\left[\frac{1}{2}(L-2\xi)k_P\right]w_0\mathbb{E}_0^2/10^6$$

$$\tag{6.1.20}$$

$$\Delta \mathbb{E}_{10} = \frac{1}{4}\sqrt{\frac{\pi}{2}} \, \mathrm{Re}\left[\frac{1}{k_P m_0 v_g^2} \, e \, e^{-\frac{1}{8}k_P^2 w_0^2}\beta(1+\beta)\left(\mathrm{Erf}\left[\frac{2L-ik_P w_0^2}{2\sqrt{2}w_0}\right] + \mathrm{Erf}\left[\frac{2L+ik_P w_0^2}{2\sqrt{2}w_0}\right]\right)\left(\mathrm{Sin}\left[\frac{Lk_P}{2}\right] - \mathrm{Sin}\left[\frac{1}{2}(L-2\xi)k_P\right]\right)w_0 \mathbb{E}_0^2\right]/10^9$$

$$(6.1.21)$$

Equations (19), (20) and (21) are expressions of generated wakefield, wake-potential, and energy gain respectively.

6.1.3. Results and discussion

For analytical investigation, we choose a practical laser pulse of wavelength $10.6 \mu m$. All laser and plasma parameters are optimized for the best output.

Terms $(e/m\omega_p c)$, (e/mc^2) and $(e/mk_p c)$ defines normalise values of produced wakefield, wake potential, and external magnetic field, respectively.

6.1.3.1 Effect of density modulation on laser wakefield
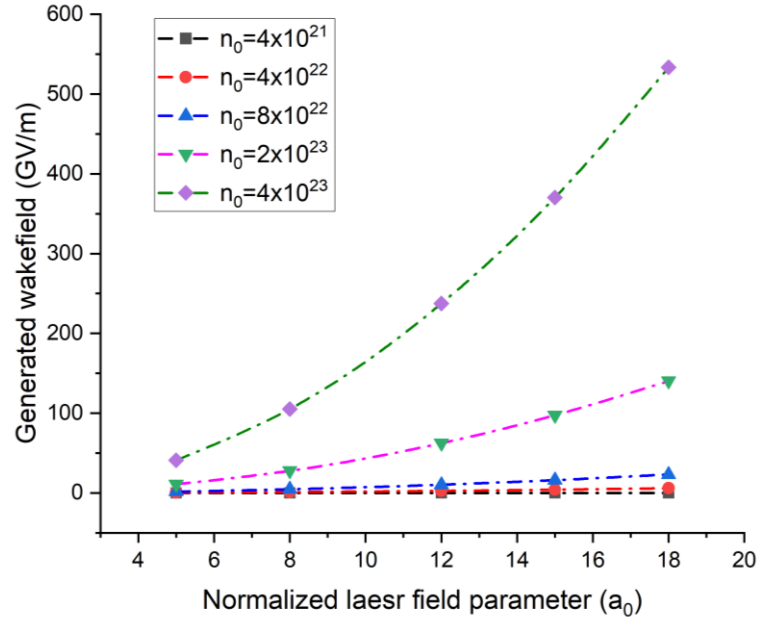
Figure: 6.1 Evaluation of generated laser wakefield with laser field parameter (a_0) in the presence of different plasma density profiles such as $n_0 =$

4×10^{21}(black curve), $n_0 = 4 \times 10^{21}$ (red curve), $n_0 = 8 \times 10^{22}$(blue curve), $n_0 = 2 \times 10^{23}$(pink curve), $n_0 = 4 \times 10^{23}$ (green curve). The normalized laser field parameters are optimized as: $a_0 = 5$, 8, 12, 15, 18. The other field parameters are laser pulse length (L)= $36 \mu m$, beam waist size w_0=$30 \mu m$.

Figure 6.1 depicts a visual representation of the wakefield when compared to the laser field parameter. The findings are derived from the implementation of equation (19). The impact of increasing plasma density on the laser wakefield is observed when using a Gaussian laser pulse. In Figure 6.1, the black curve represents the minimum and maximum values of the plasma wakefield, which are 0.0045 GV/m and 0.0589 GV/m, respectively, for a_0 values of 5 and 18. The plasma density profile is optimized at a value of $n_0 = 4 \times 10^{21}$(black curve). The laser wakefield achieves its highest value of 533.32 GV/m when the plasma density is $n_0 = 4 \times 10^{23}$ and the laser field parameter is $a_0 = 18$. Conversely, the lowest value of the generated wakefield is 41.15 GV/m, which corresponds to a laser field parameter of $a_0 = 5$. The maximum amplitude of the wakefield created by different plasma density profiles, with $n_0 = 4 \times 10^{22}$(red curve), $n_0 = 8 \times 10^{22}$(blue curve), $n_0 = 2 \times 10^{22}$(pink curve), and $n_0 = 2 \times 10^{23}$(green curve) are 0.235 GV/m, 5.845 GV/m, and 23.156 GV/m, respectively. Figure 6.1 present the impact of the plasma density on the generated wakefield. The max. value of wakefield increas according to the increase in both the plasma's density n_0 and the laser's pulse parameter a_0. Furthermore, it is noted that within the optimal range of laser field intensity a_0 and a lower plasma density profile, there are no discernible alterations in the laser wakefield value depicted in Figure 6.1 (black and red curve). For the moderate plasma density profile, the final wakefield rose in accordance with the blue and pink curves. However, when using high-density plasma, the wakefield increases drastically, as seen by the green curve in Figure 6.1. So, the plasma density significantly influences the efficiency and characteristics of laser wakefield acceleration. Higher plasma densities generally lead to stronger wakefields, shorter depletion lengths, and enhanced self-focusing effects, all of which can contribute to more efficient particle acceleration. However, the

interplay between plasma density, laser parameters, and other factors is complex and requires careful consideration for optimizing LWFA.

6.1.3.2 Effect of density modulation on wake potential

In the realm of LWFA, the term "wake potential" refers to the electrostatic potential that is produced behind an intense laser pulse as it travels through a plasma. Electrons and other charged particles are accelerated to high energies because of this potential, which is responsible for the acceleration. The properties of the wake potential, and consequently the acceleration of particles in LWFA, are significantly influenced by the plasma density, which has a substantial impact on the conditions under which it occurs.
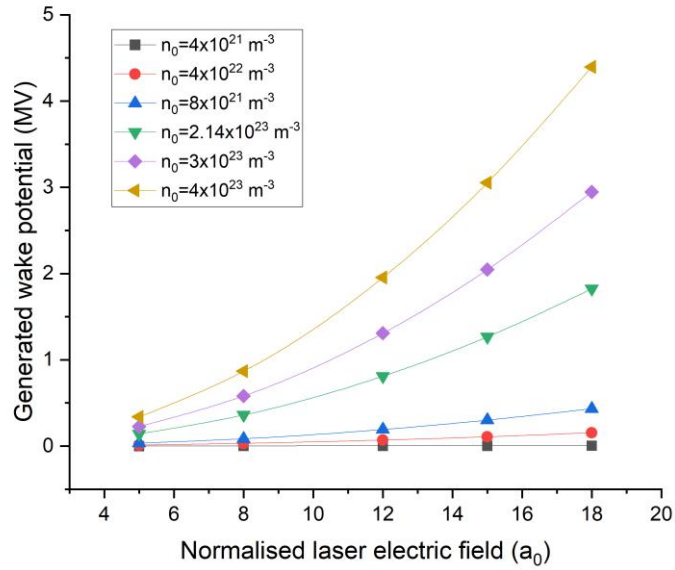
Figure 6.2 shows variation in wake potential with normalised laser electric field, for different values of plasma density profile as. $n_0 = 4 \times 10^{21}$(black curve), $n_0 = 4 \times 10^{22}$(red curve), $n_0 = 8 \times 10^{22}$(blue curve), $n_0 = 2.14 \times 10^{23}$(green curve), $n_0 = 3 \times 10^{23}$ (violet curve), $n_0 = 4 \times 10^{23}$ (brown curve). The normalized laser field parameters are optimized as: $a_0 = 5, 8, 12,$

15, 18. The other field parameters are laser pulse length (L)= $36\mu m$, and beam waist size w_0=$30\mu m$.

We use a laser pulse heaving 10 μm wavelength and a beam waist size of 35 μm that is already accessible for experimentation to examine the impact of modulating plasma density. Equation (20) is used to analyse the effect of an increasing value of the plasma density profile on the wake potential. For various values of the laser field parameters, the wake potential is increased as the plasma density increases. Figure 6.2 displays a visual depiction of the outcomes. Figure 6.2 illustrates the comparison study that looked at the effect of both the plasma density profile and the laser field parameters on the wake potential at the same time; the results showed that the wake potential increased as the profiles of both parameters increased. We have maximized the wake potential by optimizing all the laser and plasma field parameters.

For a plasma density profile, $n_0 = 4 \times 10^{21}$, the wake potential increases from 0.0003 to 0.0049 as the laser electric field parameter (a_0) increases from 5 to 18, indicating a direct relationship between the two variables. As illustrated in Figure 2, the maximum wake potential of 4.395 is achieved with a plasma density of $n_0 = 4 \times 10^{23}$ and a matching laser field parameter (a_0) of 18, while the minimum wake potential related to this plasma density profile is 0.339 for the laser field parameter $a_0 = 5$. The other maximum wake potential values, which are 0.155 MV, 0.433, 1.823 and 2.947 MV, correspond to plasma densities of $n_0 = 4 \times 10^{22}$, $n_0 = 8 \times 10^{22}$, $n_0 = 2.14 \times 10^{23}$, and $n_0 = 3 \times 10^{23}$, respectively. Figure 2 illustrates visually how the wakefield increases as the plasma density profile and laser field parameter, which are both important in LWFA, grow. When the plasma density is lower, for a given range of laser field parameters $(a_0 = 5$ to $a_0 = 8)$, small gains become apparent. Figure 2 shows that the resultant wakefield is increased for moderate plasma densities. The wakefield shows a dramatic increase as the laser intensity increases for high and specified values of the plasma density profile.

6.1.3.3 Effect of density modulation on energy gain

Density modulation in laser wakefield acceleration (LWFA) involves deliberately altering plasma density in the direction of the laser. Modulating this process can exert a substantial influence on the energy acquisition of accelerated electrons. The effect of density modulation on energy gain in Laser Wakefield Acceleration (LWFA) is described below.

(a) Electron energy gain by due to Gaussian pulse

(b) Electron energy gain by due to Gaussian puls

(c) Electron energy gain by due to Gaussian puls

(d) Electron energy gain by due to Gaussian pul

Electron energy gain by due to Gaussian pulse
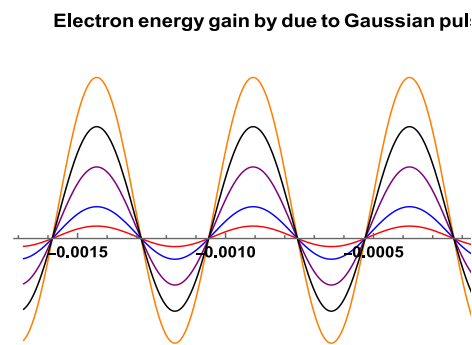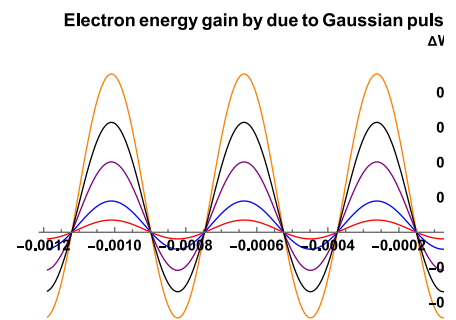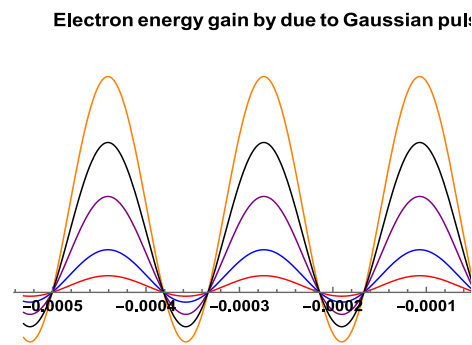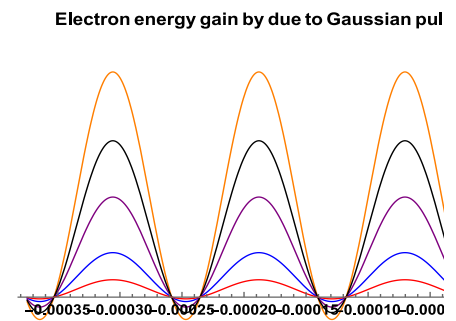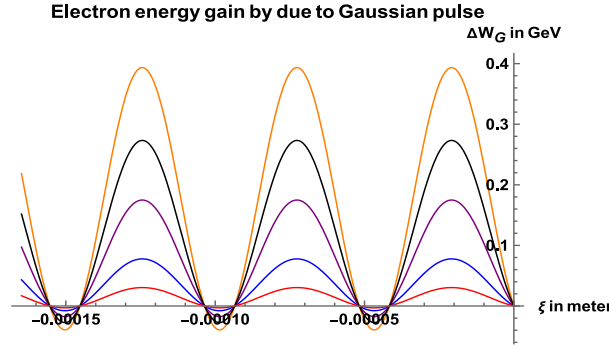
(e)

Figure 6.3 (a)-(e) present graphical variation in energy gain and propagation distance ξ by using various plasma density profiles. (a) plasma density $n_0 = 4 \times 10^{21}$, (b) plasma density $n_0 = 8 \times 10^{21}$, (c) plasma density $n_0 = 4 \times 10^{22}$ (d) plasma density $n_0 = 8 \times 10^{22}$ (e) plasma density $n_0 = 4 \times 10^{23}$. Other parameters are optimised as laser pulse length $L = 40 \times 10^{-6}$m, and beam waist size $w_0 = 40 \times 10^{-6}$m. in all (a)-(e) curves we choose laser field parameters a_0=5(red curve), 8(blue curve), 12(violet curve), 15(black curve), 18(orange curve).

The graphical representation in Figure 6.3 illustrates that final energy gain is significantly affected by the plasma density and laser field parameters. The optimization of plasma density profiles occurs within the range of 10^{21} to 10^{23}. The electron can achieve a minimum energy of 0.031 GeV and peak value of energy of 0.393 GeV when the plasma density is $n_0 = 4 \times 10^{23}$ and laser field parameter is $a_0 = 5$ and $a_0 = 18$, respectively. The result is displayed in Figure 3(e). When the laser field parameter is increased from 5 to 18, the maximum increase in energy gain ranges from 0.002GeV to 0.029GeV for a specific plasma density profile $n_0 = 4 \times 10^{21}$ in Figure 6.3(a), from 0.003GeV to 0.045GeV for plasma density $n_0 = 8 \times 10^{21}$ in Figure 6.3(b), from 0.009 GeV to 0.125GeV for plasma density $n_0 = 4 \times 10^{22}$ in figure 6.3(c), and from 0.015 GeV to 0.195GeV for plasma density $n_0 = 8 \times 10^{22}$ in figure 6.3(d). So, it is

analysed that the final energy gain is enhanced by increasing the value of laser field parameters and plasma density simultaneously. Plasma density directly impacts electron energy gain in LWFA by influencing the strength of the wakefield, acceleration gradient, and dephasing length. Higher densities lead to stronger wakefields, enabling electrons to gain more energy over shorter distances while limiting their accelerating length. Conversely, lower densities allow for longer dephasing lengths, sustaining acceleration over larger distances. However, finding the optimal density is crucial, as excessively high densities can lead to nonlinear effects and wave-breaking, affecting electron energy gain. Therefore, careful control of plasma density alongside laser parameters is essential for maximizing electron acceleration efficiency in LWFA.
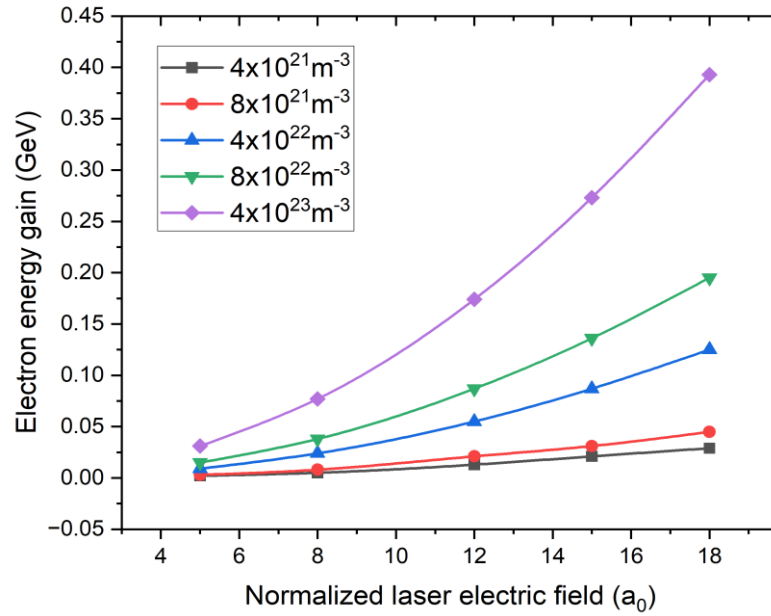
Figure 6.4 Comparative study of electron energy gain vs. laser field parameter for various plasma densities $n_0 = 4 \times 10^{21}$(black curve), $n_0 = 8 \times 10^{21}$(red

curve), $n_0 = 4 \times 10^{22}$(blue curve), $n_0 = 8 \times 10^{22}$(green curve), and $n_0 = 4 \times 10^{23}$(violet curve). Other field parameters are the same as Figure 6.3

Figure 6.4 illustrates the electron energy gain and laser field parameters for different increasing values of plasma densities in laser wakefield acceleration (LWFA), a consistent trend emerges where the overall energy gain increases with both higher plasma density and more intense laser field parameters. As plasma density increases, the strength of the wakefield grows, leading to higher acceleration gradients experienced by electrons, thus enhancing their energy gain. Similarly, increasing laser field parameters such as intensity, duration, and wavelength amplify the ponderomotive force by the laser pulse on the plasma, intensifying the wakefield and resulting in greater energy gains for accelerated electrons. The combination of higher plasma density and stronger laser fields synergistically enhances the efficiency of electron acceleration, leading to an overall increase in energy gain. This trend underscores the importance of optimizing both plasma density and laser field parameters to achieve the desired levels of electron energy gain in LWFA experiments.

6.1.4 Conclusion

In conclusion, our comparative investigation has provided valuable insights into the effect of plasma density profiles on laser wakefield acceleration (LWFA). Through systematic analysis, we have elucidated the relationship between plasma density, generated wake potential, and energy gain in the LWFA process. Our findings demonstrate that variations in plasma density significantly influence the efficiency and effectiveness of particle acceleration within the wakefield. Higher plasma densities tend to yield stronger wake potentials, resulting in enhanced energy gain for accelerated particles. This underscores the importance of plasma density as a crucial parameter in optimizing LWFA performance. Moreover, our study highlights the potential for tailoring plasma density profiles to achieve desired acceleration outcomes. By strategically adjusting plasma and laser parameters, such as plasma density

profile or laser field parameter, we manipulate the characteristics of the generated wakefield and wake potential, thereby optimizing energy gain up to the 393 MeV. Furthermore, our results emphasize the importance of comprehensive modelling and experimental validation in LWFA research. Accurate characterization of plasma density profiles is essential for predicting and understanding the dynamics of particle acceleration within the wakefield accurately.

Chapter 6.2

Enhanced laser wakefield acceleration through slanting plasma density profile

6.2.1 Introduction

Laser wakefield acceleration, commonly known as wakefield acceleration or simply LWFA, is a game-changing scientific notion that has transformed particle acceleration. It's a technology that uses powerful laser pulses to produce electric fields that are capable of propelling electrons to extremely high energy across very small distances[267], [268]. Particle accelerators have traditionally been large facilities spanning kilometres, requiring enormous amounts of energy to drive particles to high speeds. Laser wakefield acceleration, on the other hand, provides a small and energy-efficient option. Scientists have identified a technique to utilise the wakefield formed by a strong laser pulse travelling through a plasma medium by using plasma physics concepts. As a laser beam passes through the plasma it generates a longitudinal laser wakefield. As the wakefield passes through the plasma, electrons in plasma channel "surf" on the electric field, accumulating enormous amount of energy over a small distance. Electrons may be accelerated to energies equivalent to or even exceeding those attained in conventional accelerators in just a few centimetres. Laser wakefield acceleration is an appealing and promising technique due to its amazing acceleration gradient. This phenomenon is proposed by Tajima and Dawson in 70's[52]. Gupta *et al.*[269] studied that periodic plasma density modulation improves self-trapping and injection, but magnetic field-assisted self-injection improves energy gain. 2-D Particle-in-cell (PIC) simulation helps to clarify the hypothesised process. Askari *et al.*[270] demonstrated LWFA by short intense Gaussian laser pulse and found that, energy gain can be enhanced by increasing the laser intensity. Pukhov *et al.*[271] have studied the plasma density profile to enhance the maximum gain of energy with improved beam quality. Ke *et al.*[272] proposed

a technique aimed at enhancing the efficiency of e-beam in a laser-driven wakefield accelerator by utilizing shock induced plasma-density modulation. The approach employed by the researchers yields enhanced beam quality through efficient manipulation of plasma density, resulting in reduced energy dispersion, increased charge, and improved electron beam emittance. Sadler *et al.*[273] introduced a potentially effective approach to surpassing the dephasing limit in the context of multiple-laser pulses based wakefield acceleration. Ding *et al.*[274] examines the nonlinear scaling actions of plasma wavelength within the context of a laser wakefield accelerator. The authors examine the correlation between plasma density and laser field parameters, with particular emphasis on the influence of laser intensity on the plasma wavelength. The first optical plasma waveguide-based LWFA experiment was conducted by Miao *et al.*[275] and drive a beam of electrons with 5 GeV energy gain. Additionally, one can observe proof of pump depletion-induced dephasing, which is a result of the extended optical guiding distance. In a study, Sharma *et al.*[276] examined LWFA excitation within an under-dense plasma, specifically focusing on the effects of laser pulses with positive and negative frequency chirps. The findings indicate that the phenomenon of laser wakefield is boosted by positive chirp. Rajput *et al.*[277] focuses on the electron dynamics along a plasma density ramp in a downward direction. This study utilizes a circularly polarised (CP) laser pulse while considering the influence of an azimuthal magnetic field. Kaur *et al.* [278] use VORPAL code (2D-PIC simulations) to investigate how implementing a linear-upward density ramp in the bubble phase of LWFA and it affects the dephasing length and accelerated particles energy. Bulanov *et al.*[279] performed 1-D Particle-in-Cell (PIC) simulations to examine a laser pulse propagating downward across a plasma density ramp. These simulation results showed that the density ramp broke the plasma wave. This rupture injected several electrons into the system. Although electrons accelerate to gain energy, the energy distribution inside the electron bunch is highly dispersed. The dephasing effect in LWFA with uniform plasma density is discussed by Dong *et al.*[280] in terms of its limitations on acceleration length and electron

beam peak energy. Rajput *et al.*[267] examines the phenomenon of electron acceleration using interaction of a radially polarised laser with an obliquely incident magnetic field during the process of ionisation in gases with lower densities. The electron acquires additional energy because of resonance when subjected to an external magnetic field that is applied at an oblique angle in the transverse direction relative to its propagation direction, leading to its excitation at higher energy levels on the order of Giga electron Volts (GeV). In a study, Ariniello *et al.*[281] provide a theoretical analysis of the transverse beam dynamics within a plasma ramp of arbitrary shape.

6.2.2 Electron acceleration using down slanting plasma density profile.

We examine the behaviour of a linearly polarised laser pulse as it propagates through a plasma medium characterised by a downward slanted density profile in positive z direction. the plane polarised electric field vector associated with the pulse is given by the expression[282]:-

$$\vec{E}(r,z,t) = E_0(r,z,t)\cos(k_0 z - \omega_0 t)\hat{x} \qquad (6.2.1)$$

The unit vector of polarization direction denoted as $\hat{x}$, is a key component in the analysis of laser pulses. $E_0(r,z,t)$, k_0, and ω_0 represent the amplitude, laser propagation constant, and the frequency of the laser, respectively.

We have considered a plasma with slanting down density variation given by $n = n_0 e^{-k_r \xi}$. n_0 denotes ambient plasma density. k_r slanting density modulation parameter.

From the definition of Lorentz force

$$\frac{\partial \vec{V}}{\partial t} = -\frac{e}{m}\left(\vec{E} + \vec{E_w}\right) - \frac{e}{mc}\left(\vec{V} \times \vec{B}\right) - \frac{1}{2}\vec{\nabla}.\left(\vec{V}.\vec{V}\right) + \vec{V} \times \left(\vec{\nabla} \times \vec{V}\right) \quad (2a)$$

From equation of continuity $\frac{\partial n}{\partial t} + \vec{\nabla}.\left(n\vec{V}\right) = 0$ \qquad (2b)

The velocity of plasma electrons, denoted as $\vec{V}$. The rest mass of the electrons is represented by m, while the density of plasma electrons is denoted as n. Moreover, the electric wakefield denoted as E_w generated because of the

interaction with between the laser pulse. It is noted that $\vec{B}$ represents the magnetic field vector associated with laser pulse.

Term $\xi = z - v_g t$ is introduced, where $v_g = c\sqrt{1 - (\omega_p/\omega_0)^2}$ is the group velocity of plasma electrons. ω_0 is the frequency of electromagnetic pulse, and ω_p is plasma frequency given by $\omega_p = \sqrt{4\pi n_0 e^2/m}$. Additionally, m refers to the rest mass of the electron. It is assumed that $\omega_0 \gg \omega_p$, $\vec{V_g}$ is marginally lesser in magnitude when compared to the speed of light.

We study plasma wave excitation using the quasi-static approximation (QSA), assuming that plasma-pulse interaction is shorter than the normal laser pulse alteration duration due to non-linear self-effect.[283]. Plasma electrons perceive a laser field that depends on ξ. Perturbative expansion of Eq. (2a) and substitution of Eq. (1) describes first-order velocity. Reflecting the plasma electron's transverse quiver motion.

$$V_x^{(1)} = ac \sin k_0\xi \qquad\qquad (6.2.3)$$

Here $a = eE_0(r,z,t)/m\omega_0 c$ is normalized value of electric field amplitude of laser pulse. second-order slow axial velocity element calculated using Eq. (6.2.3).

$$\Rightarrow V_g \frac{\partial V_x^{(2)}}{\partial \xi} = \frac{e}{m} E_{wz} + \frac{1}{4}\frac{\partial}{\partial \xi}(a^2 c^2) \qquad\qquad (6.2.4)$$

Using quasi static approximation, Maxwell's equation can be written as

$$\frac{V_g}{c}\frac{\partial E_{wz}}{\partial \xi} = \frac{4\pi}{c}J_z - \frac{1}{r}\frac{\partial}{\partial r}(rB_{w\theta}) \qquad\qquad (6.2.5)$$

Here J_z denotes the axial current density.

Considering that the $B_{w\theta}$. The second part on the RHS of Eq. (5) is neglected.

So, $\frac{V_g}{c}\frac{\partial E_{wz}}{\partial \xi} = \frac{4\pi}{c}J_z$

Differentiating equation (5) w.r.t. ξ and using equation (4) we get

$$\frac{1}{k_p^2}\frac{\partial^2 E_{wz}}{\partial \xi^2} + e^{-k_r\xi} E_{wz} = -\frac{m c^2}{4e}e^{-k_r\xi}\frac{\partial}{\partial \xi}(a^2) \qquad\qquad (6.2.6)$$

In above equation $k_p = \omega_p/v_p$ represent the wave number while v_p indicates plasma wave's phase velocityThe laser pulse group velocity is considered to be

close to the plasma wave phase velocity. Eq. (6) describes how an axial wakefield is generated in a plasma that is under dense and uniform.

Let the pulse profile is $a = a_r \sin\frac{\pi\xi}{L}$, $a_r = a_0 e^{-\left(\frac{r^2}{r_0^2}\right)}$ where r $<< r_0$ (6.2.7)

$$\frac{1}{k_p^2}\frac{\partial^2 E_{wz}}{\partial\xi^2} + e^{-k_r\xi}\,E_{wz} = -\frac{m\,c^2}{4e}e^{-k_r\xi}\frac{\pi a_0^2}{L}\sin\frac{2\pi\xi}{L} \qquad (6.2.8)$$

6.2.3 Result and discussion

In the current investigation, we have undertaken an examination of a solitary laser pulse with a wavelength of $0.63\mu m$, which is subsequently propagate through a plasma medium characterised by a density of $1.8 \times 10^{24} m^{-3}$. The plasma frequency ω_p and corresponding wavelength λ_p exhibit values of $7.5 \times 10^{13}\,Rad/sec$ and $24.91\mu m$, respectively.

Generated wakefield is normalized by $e/mc\omega_p$. k_p is used for normalisation of the pulse length (L) and propagation distance (ξ). Laser Propagation constants (k_0) and slanting density modulation parameter k_r are normalized by $1/k_p$. The graphical presentation of equation (8) are as follows.

6.2.3.1 Effect of slanting density modulation parameter
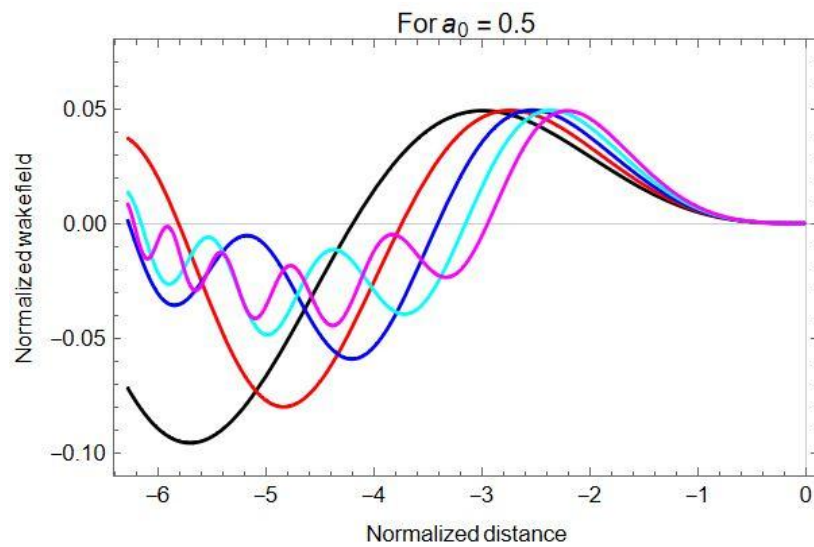
Figure 6.5 Comparison of Normalized wakefield for various values of slanting density modulation parameter $k_r = 0.1\,k_p$ (*black*), $k_r = 0.3\,k_p$ (*red*), $k_r = 0.5k_p$ (*blue*), $k_r = 0.7\,k_p$ (*cyan*), $k_r = 0.9k_p$ (*magenta*).
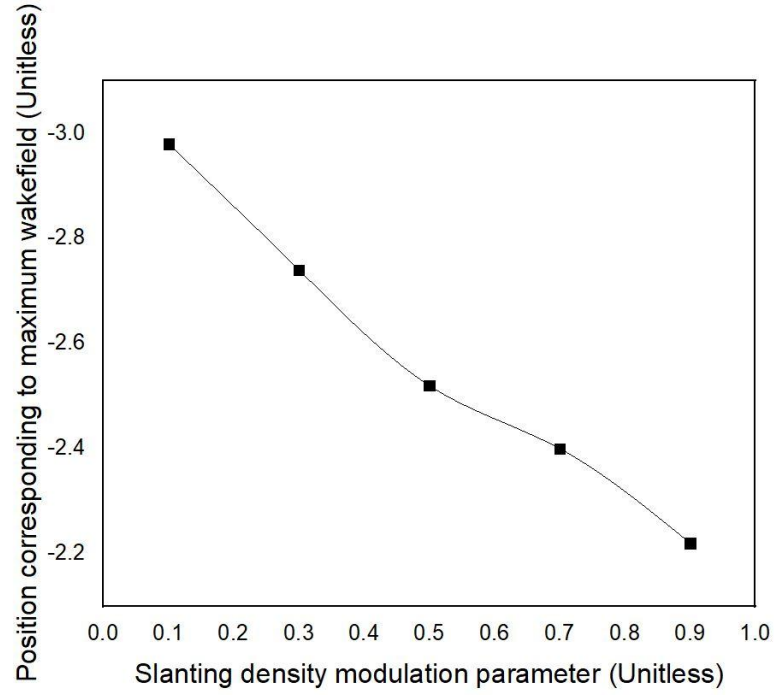
Figure 6.6 variation of maximum wakefield position with slanting density modulation parameter

Figure 6.6 shows variation of normalised wakefield E_{wz} with normalised distance $(k_p \xi)$ for different slanting density modulation parameters. The figure shows that the value of maximum wakefield remain constant with increasing slanting density modulation parameters. But, the position corresponding to maximum wakefield shift towards the $\xi = 0$ *i.e.* the starting point of laser pulse. The peak value of normalised wakefield is 0.049 for all value. The same variation is shown in figure 6.5.

6.2.3.2 Effect of laser field amplitude on laser wakefield
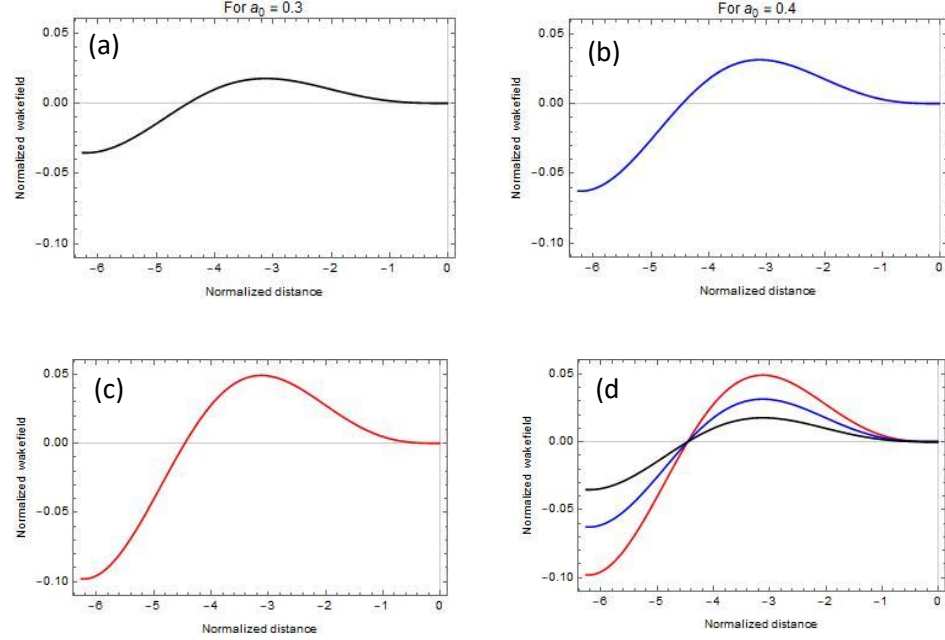
Figure 6.7 Evaluation of the normalised wakefield as the function of normalised distance, (a) laser field parameter $a_0 = 0.3$, (b) laser field parameter $a_0 = 0.4$, (c) laser field parameter $a_0 = 0.5$, (d) graphical comparison for different values of laser field parameter i.e. $a_0 = 0.3$ (black) $a_0 = 0.4$ (blue) $a_0 = 0.5$ (red). Other field parameters are the same for all graphs. Slanting density modulation parameter $k = 0.01$, laser pulse length $L_n = 6.283$.

In figure 6.7, the variation of normalised wakefield (E_{wz}) with the normalised distance($k_p \xi$) is shown. For this study, we use laser field parameter $a_0 = eE/m\omega_0 c = 0.3$ in fig (a), 0.4 in Fig (b), and 0.5 in Fig (c). for this, we use normalised laser pulse length $L_n = 6.283$, and normalised propagation constant $k = 0.01$. In all graphs, it observed that the normalised wakefield increased with normalised distance ($k_p \xi$) and attained a peak value of 0.017 (for $a_0 = 0.3$), 0.031 (for $a_0 = 0.4$), and 0.049 (for $a_0 = 0.5$) at the normalised position 3.12, 3.13, and 3.16, respectively. In fig (d) we compare plots for different values of laser field parameters. Wakefield amplitude varies

as the square of the laser field parameter. It is concluded that normalised wakefield amplitude is strongly influenced by laser field parameters.

6.2.3.3 Effect of pulse length
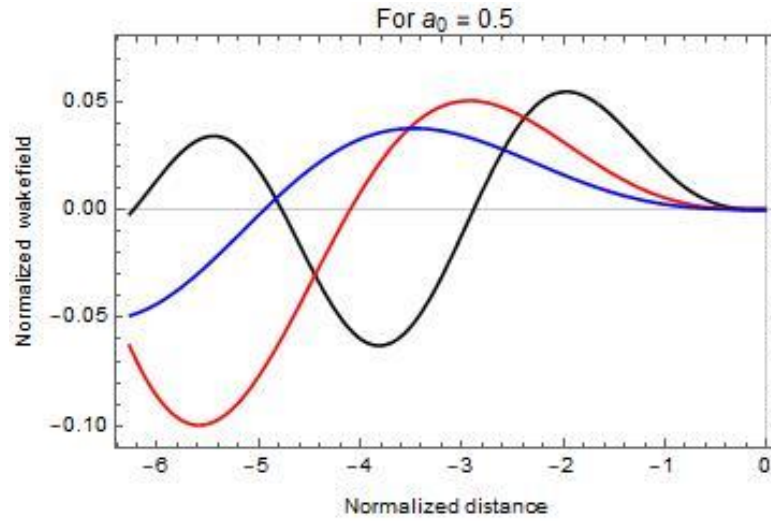
Figure 6.8 Variation in longitudinal wakefield for different values of normalised laser pulse length L_n= 3(black), 6(rad), and 9(blue). Other parameters are the same as those used in the above figure.

Figure 6.8, presents the graphical representation of variation in normalized wakefield with normalised pulse length of 3(black), 6(rad), and 9(blue). The maximum normalized generated wakefield, as determined through analysis of the data, is estimated to be approximately 0.054 (black curve corresponds to $L_n = 3$ at normalised distance 1.96). Other peak values of normalised wakefields are 0.049 (rad curve corresponds to $L_n = 6$ at normalised distance 2.93) and 0.037 (blue curve corresponds to $L_n = 9$ at normalised distance 3.54). It is shown that the maximum value of wakefield is decreases as we increase laser pulse length. This analysis shows that the optimisation of the laser pulse length is very crucial to generating maximum normalised wakefield.

6.2.4 Conclusion

Effect of laser field parameter, normalised propagation constant of laser and normalised pulse length in laser wakefield acceleration investigated in this scheme using a plasma having slanting density profile. It's observed that the normalised wakefield is affected by laser field parameters and normalised laser pulse length. The position that corresponds to the largest wakefield shifts towards $\xi=0$, which is the initial point of the pulse with an increase in the slanting density modulation parameter. The maximum value of the normalized wakefield is consistently 0.049 across all values of the slanting density modulation parameter. The wakefield's highest value exhibits a negative correlation with the lengthening of the laser pulse. This research demonstrates the critical importance of optimizing the length of the laser pulse for achieving the largest normalized wakefield. The maximum obtained laser wakefield amplitude with the optimised parameter is 6.97 GV/m. The current investigation holds significant value for researchers seeking to identify optimal laser pulses capable of generating efficient and energy-conscious Laser Wakefield Acceleration (LWFA) mechanisms.

Chapter 7

Summary and Conclusion

This thesis has conducted a numerical and simulation-based analysis of laser-plasma wakefield acceleration.

This thesis presents a comprehensive numerical exploration of the comparative analysis of single-electron dynamics utilizing a tightly focused laser beam in the context of planar and helical undulators. The primary objective was to optimize the electron's energy in the Inverse Free Electron Laser (IFEL) accelerator by examining the effects of various laser attributes. We concluded that a more accurate fifth-order modification of the diffraction angle is necessary to characterize the laser field. This adjustment signified that the emphasis need to be on micron-scale spot dimensions. Research demonstrates that the presence of a helical wiggler leads to a significantly greater enhancement in electron energy acquisition compared to a planar wiggler. The helical wiggler design attained a maximum energy of 1.331 GeV when the laser field intensity was optimized and the tapering parameters were suitably adjusted. In contrast, the planar wiggler arrangement attained a maximum energy of 300 MeV, a markedly inferior value. The research indicates a clear association between the energy acquired by electrons and the strength of the laser field. It is crucial to recognize that while electrons can achieve their peak energy gain sooner in the planar wiggler configuration, they cannot sustain it for a prolonged duration. This directly reflects prior findings regarding the impact of the wiggler magnetic field. Moreover, with same laser and wiggler parameters, the helical wiggler design achieves a superior maximum energy gain compared to the planar wiggler arrangement. Furthermore. An examination of the impact of the second laser's polarization on electron acceleration is conducted. The findings of this study demonstrate that the two-color laser scheme enhances electron beam energy by up to 600 MeV within a plasma channel measuring 4 mm in length. This differs from the monochromatic laser system, which yields less than 200 MeV. Moreover, the impact of the temporal delay between the two lasers on electron acceleration requires deeper examination through modeling, a pursuit recommended for

future research. This research elucidates the complex dynamics of electron acceleration in IFEL accelerators and offers essential insights for optimizing laser and wiggler combinations to enhance energy yield. This research has facilitated advancements in particle acceleration technologies.

References

[1] F. Gianotti and T. Virdee, "The discovery and measurements of a Higgs boson," *Philos. Trans. R. Soc. Math. Phys. Eng. Sci.*, vol. 373, Jan. 2015, doi: 10.1098/rsta.2014.0384.

[2] D. Strickland and G. Mourou, "Compression of amplified chirped optical pulses," *Opt. Commun.*, vol. 56, no. 3, pp. 219–221, Dec. 1985, doi: 10.1016/0030-4018(85)90120-8.

[3] W. Scharf and J. V. Siebers, *Biomedical Particle Accelerators*. American Inst. of Physics, 1994.

[4] B. Martinez, E. d'Humières, and L. Gremillet, "Synchrotron radiation from ultrahigh-intensity laser-plasma interactions and competition with Bremsstrahlung in thin foil targets," *Phys. Rev. Res.*, vol. 2, no. 4, p. 043341, Dec. 2020, doi: 10.1103/PhysRevResearch.2.043341.

[5] P. Sprangle, E. Esarey, and J. Krall, "Laser driven electron acceleration in vacuum, gases, and plasmas," *Phys. Plasmas*, vol. 3, no. 5, pp. 2183–2190, May 1996, doi: 10.1063/1.871673.

[6] C. Joshi, "The Los Alamos Laser Acceleration of Particles Workshop and Beginning of the Advanced Accelerator Concepts Field," *AIP Conf. Proc.*, vol. 1507, pp. 61–66, Dec. 2012, doi: 10.1063/1.4773677.

[7] R. B. Palmer, "Interaction of Relativistic Particles and Free Electromagnetic Waves in the Presence of a Static Helical Magnet," *J. Appl. Phys.*, vol. 43, no. 7, pp. 3014–3023, Nov. 2003, doi: 10.1063/1.1661650.

[8] J. A. Edighoffer, W. D. Kimura, R. H. Pantell, M. A. Piestrup, and D. Y. Wang, "Observation of inverse \ifmmode \check{C}\else \v{C}\fi{}erenkov interaction between free electrons and laser light," *Phys. Rev. A*, vol. 23, no. 4, pp. 1848–1854, Apr. 1981, doi: 10.1103/PhysRevA.23.1848.

[9] E. Esarey, C. B. Schroeder, and W. P. Leemans, "Physics of laser-driven plasma-based electron accelerators," *Rev. Mod. Phys.*, vol. 81, no. 3, pp. 1229–1285, Aug. 2009, doi: 10.1103/RevModPhys.81.1229.

[10] G. Malka, E. Lefebvre, and J. L. Miquel, "Experimental Observation of Electrons Accelerated in Vacuum to Relativistic Energies by a High-Intensity Laser," *Phys.*

Rev. Lett., vol. 78, no. 17, pp. 3314–3317, Apr. 1997, doi: 10.1103/PhysRevLett.78.3314.

[11] C. Joshi, "Plasma-based accelerators: then and now," *Plasma Phys. Control. Fusion*, vol. 61, no. 10, p. 104001, Aug. 2019, doi: 10.1088/1361-6587/ab396a.

[12] T. Tajima and J. M. Dawson, "Laser Electron Accelerator," *Phys. Rev. Lett.*, vol. 43, no. 4, pp. 267–270, Jul. 1979, doi: 10.1103/PhysRevLett.43.267.

[13] P. Chen, J. M. Dawson, R. W. Huff, and T. Katsouleas, "Acceleration of Electrons by the Interaction of a Bunched Electron Beam with a Plasma," *Phys. Rev. Lett.*, vol. 54, no. 7, pp. 693–696, Feb. 1985, doi: 10.1103/PhysRevLett.54.693.

[14] J. D. Lawson, "Lasers and Accelerators," *IEEE Trans. Nucl. Sci.*, vol. 26, no. 3, pp. 4217–4219, Jun. 1979, doi: 10.1109/TNS.1979.4330749.

[15] T. Plettner *et al.*, "Visible-Laser Acceleration of Relativistic Electrons in a Semi-Infinite Vacuum," *Phys. Rev. Lett.*, vol. 95, no. 13, p. 134801, Sep. 2005, doi: 10.1103/PhysRevLett.95.134801.

[16] P. Mora and B. Quesnel, "Comment on ``Experimental Observation of Electrons Accelerated in Vacuum to Relativistic Energies by a High-Intensity Laser''," *Phys. Rev. Lett.*, vol. 80, no. 6, pp. 1351–1351, Feb. 1998, doi: 10.1103/PhysRevLett.80.1351.

[17] Y. I. Salamin and C. H. Keitel, "Subcycle high electron acceleration by crossed laser beams," *Appl. Phys. Lett.*, vol. 77, no. 8, pp. 1082–1084, Aug. 2000, doi: 10.1063/1.1289649.

[18] Y. I. Salamin and C. H. Keitel, "Electron Acceleration by a Tightly Focused Laser Beam," *Phys. Rev. Lett.*, vol. 88, no. 9, p. 095005, Feb. 2002, doi: 10.1103/PhysRevLett.88.095005.

[19] Z. Huang, G. Stupakov, and M. Zolotorev, "Calculation and optimization of laser acceleration in vacuum," *Phys. Rev. Spec. Top. - Accel. Beams*, vol. 7, no. 1, p. 011302, Jan. 2004, doi: 10.1103/PhysRevSTAB.7.011302.

[20] G. V. Stupakov and M. S. Zolotorev, "Ponderomotive Laser Acceleration and Focusing in Vacuum for Generation of Attosecond Electron Bunches," *Phys. Rev. Lett.*, vol. 86, no. 23, pp. 5274–5277, Jun. 2001, doi: 10.1103/PhysRevLett.86.5274.

[21] S. Kumar and M. Yoon, "Electron dynamics and acceleration study in a magnetized plasma-filled cylindrical waveguide," *J. Appl. Phys.*, vol. 103, no. 2, p. 023302, Jan. 2008, doi: 10.1063/1.2831223.

[22] S. Kumar and M. Yoon, "Electron acceleration in a warm magnetized plasma-filled cylindrical waveguide," *J. Appl. Phys.*, vol. 104, no. 7, p. 073303, Oct. 2008, doi: 10.1063/1.2988899.

[23] I. Wernick and T. C. Marshall, "Experimental test of the inverse free-electron-laser accelerator principle," *Phys. Rev. A*, vol. 46, no. 6, pp. 3566–3568, Sep. 1992, doi: 10.1103/PhysRevA.46.3566.

[24] A. van Steenbergen, J. Gallardo, J. Sandweiss, and J.-M. Fang, "Observation of Energy Gain at the BNL Inverse Free-Electron-Laser Accelerator," *Phys. Rev. Lett.*, vol. 77, no. 13, pp. 2690–2693, Sep. 1996, doi: 10.1103/PhysRevLett.77.2690.

[25] W. D. Kimura *et al.*, "First Staging of Two Laser Accelerators," *Phys. Rev. Lett.*, vol. 86, no. 18, pp. 4041–4043, Apr. 2001, doi: 10.1103/PhysRevLett.86.4041.

[26] R. B. Yoder, T. C. Marshall, and J. L. Hirshfield, "Energy-Gain Measurements from a Microwave Inverse Free-Electron-Laser Accelerator," *Phys. Rev. Lett.*, vol. 86, no. 9, pp. 1765–1768, Feb. 2001, doi: 10.1103/PhysRevLett.86.1765.

[27] J. Singh, J. Rajput, N. Kant, and S. Kumar, "Comparative study of inverse free-electron laser interaction based on helical and planar wiggler," *Optik*, vol. 260, p. 169017, Jun. 2022, doi: 10.1016/j.ijleo.2022.169017.

[28] J. P. Duris, P. Musumeci, and R. K. Li, "Inverse free electron laser accelerator for advanced light sources," *Phys. Rev. Spec. Top. - Accel. Beams*, vol. 15, no. 6, p. 061301, Jun. 2012, doi: 10.1103/PhysRevSTAB.15.061301.

[29] N. Sudar *et al.*, "High Efficiency Energy Extraction from a Relativistic Electron Beam in a Strongly Tapered Undulator," *Phys. Rev. Lett.*, vol. 117, no. 17, p. 174801, Oct. 2016, doi: 10.1103/PhysRevLett.117.174801.

[30] N. Sudar *et al.*, "Demonstration of Cascaded Modulator-Chicane Microbunching of a Relativistic Electron Beam," *Phys. Rev. Lett.*, vol. 120, no. 11, p. 114802, Mar. 2018, doi: 10.1103/PhysRevLett.120.114802.

[31] A. Pukhov and J. Meyer-ter-Vehn, "Laser wake field acceleration: the highly non-linear broken-wave regime," *Appl. Phys. B*, vol. 74, no. 4, pp. 355–361, Apr. 2002, doi: 10.1007/s003400200795.

[32] J. Faure *et al.*, "A laser–plasma accelerator producing monoenergetic electron beams," *Nature*, vol. 431, no. 7008, Art. no. 7008, Sep. 2004, doi: 10.1038/nature02963.

[33] C. G. R. Geddes *et al.*, "High-quality electron beams from a laser wakefield accelerator using plasma-channel guiding," *Nature*, vol. 431, no. 7008, pp. 538–541, Sep. 2004, doi: 10.1038/nature02900.

[34] V. I. Veksler, "Coherent principle of acceleration of charged particles," 1956, doi: 10.5170/CERN-1956-025.80.

[35] A. Caldwell, K. Lotov, A. Pukhov, and F. Simon, "Proton Driven Plasma Wakefield Acceleration," *Nat. Phys.*, vol. 5, no. 5, pp. 363–367, May 2009, doi: 10.1038/nphys1248.

[36] E. Esarey, P. Sprangle, J. Krall, and A. Ting, "Overview of plasma-based accelerator concepts," *IEEE Trans. Plasma Sci.*, vol. 24, no. 2, pp. 252–288, Apr. 1996, doi: 10.1109/27.509991.

[37] R. Bingham and R. Trines, "Introduction to Plasma Accelerators: the Basics," *CERN Yellow Rep.*, vol. 1, pp. 67–67, Feb. 2016, doi: 10.5170/CERN-2016-001.67.

[38] L. M. Gorbunov and V. I. Kirsanov, "Excitation of plasma waves by an electromagnetic wave packet," 1987.

[39] S. V. Bulanov, V. I. Kirsanov, and A. S. Sakharov, "Excitation of ultrarelativistic plasma waves by pulse of electromagnetic radiation," *ZhETF Pisma Redaktsiiu*, vol. 50, p. 176, Aug. 1989.

[40] P. Sprangle, E. Esarey, and A. Ting, "Nonlinear theory of intense laser-plasma interactions," *Phys. Rev. Lett.*, vol. 64, no. 17, pp. 2011–2014, Apr. 1990, doi: 10.1103/PhysRevLett.64.2011.

[41] H. Hamster, A. Sullivan, S. Gordon, W. White, and R. W. Falcone, "Subpicosecond, electromagnetic pulses from intense laser-plasma interaction,"

Phys. Rev. Lett., vol. 71, no. 17, pp. 2725–2728, Oct. 1993, doi: 10.1103/PhysRevLett.71.2725.

[42] H. Dewa *et al.*, "Experiments of high energy gain laser wakefield acceleration," *Nucl. Instrum. Methods Phys. Res. Sect. Accel. Spectrometers Detect. Assoc. Equip.*, vol. 410, no. 3, pp. 357–363, Jun. 1998, doi: 10.1016/S0168-9002(98)00164-8.

[43] C. E. Clayton *et al.*, "Self-guided laser wakefield acceleration beyond 1 GeV using ionization-induced injection," *Phys. Rev. Lett.*, vol. 105, no. 10, p. 105003, Sep. 2010, doi: 10.1103/PhysRevLett.105.105003.

[44] A. Maksimchuk *et al.*, "Studies of laser wakefield structures and electron acceleration in underdense plasmasa)," *Phys. Plasmas*, vol. 15, p. 056703, May 2008, doi: 10.1063/1.2856373.

[45] W. P. Leemans *et al.*, "GeV electron beams from a centimetre-scale accelerator," *Nat. Phys.*, vol. 2, no. 10, Art. no. 10, Oct. 2006, doi: 10.1038/nphys418.

[46] X. Wang *et al.*, "Quasi-monoenergetic laser-plasma acceleration of electrons to 2 GeV," *Nat. Commun.*, vol. 4, no. 1, Art. no. 1, Jun. 2013, doi: 10.1038/ncomms2988.

[47] H. T. Kim *et al.*, "Enhancement of Electron Energy to the Multi-GeV Regime by a Dual-Stage Laser-Wakefield Accelerator Pumped by Petawatt Laser Pulses," *Phys. Rev. Lett.*, vol. 111, no. 16, p. 165002, Oct. 2013, doi: 10.1103/PhysRevLett.111.165002.

[48] S. P. D. Mangles *et al.*, "Monoenergetic beams of relativistic electrons from intense laser–plasma interactions," *Nature*, vol. 431, no. 7008, Art. no. 7008, Sep. 2004, doi: 10.1038/nature02939.

[49] M. Hogan *et al.*, "Plasma wakefield acceleration experiments at FACET," *New J. Phys.*, vol. 12, p. 055030, May 2010, doi: 10.1088/1367-2630/12/5/055030.

[50] A. Aschikhin *et al.*, "The FLASHForward facility at DESY," *Nucl. Instrum. Methods Phys. Res. Sect. Accel. Spectrometers Detect. Assoc. Equip.*, vol. 806, pp. 175–183, Jan. 2016, doi: 10.1016/j.nima.2015.10.005.

[51] E. Adli *et al.*, "Acceleration of electrons in the plasma wakefield of a proton bunch," *Nature*, vol. 561, no. 7723, Art. no. 7723, Sep. 2018, doi: 10.1038/s41586-018-0485-4.

[52] T. Tajima and J. M. Dawson, "Laser electron accelerator," *Phys. Rev. Lett.*, vol. 43, no. 4, pp. 267–270, 1979, doi: 10.1103/PhysRevLett.43.267.

[53] P. Musumeci, M. Westfall, R. K. Li, A. Murokh, A. Tremaine, and I. V. Pogorelsky, "High-gradient high-energy-gain inverse free electron laser experiment using a helical undulator," *AIP Conf. Proc.*, vol. 1299, no. November, pp. 747–751, 2010, doi: 10.1063/1.3520424.

[54] G. Strickland, D.; Mourou, "COMPRESSION OF AMPLIFIED CHIRPED OPTICAL PUI~SES I)onna STR[CKLAND and Gerard MOUROU."

[55] D. Cline, L. Shao, X. Ding, Y. Ho, Q. Kong, and P. Wang, "First Observation of Acceleration of Electrons by a Laser in a Vacuum," vol. 2013, no. January, pp. 1–6, 2013.

[56] I. Gadjev *et al.*, "An inverse free electron laser acceleration-driven Compton scattering X-ray source," *Sci. Rep.*, vol. 9, no. 1, Dec. 2019, doi: 10.1038/s41598-018-36423-y.

[57] Z. Parsa and M. P. Pato, "Inverse free electron laser acceleration with a square wave wiggler," no. June, pp. 179–194, 2008, doi: 10.1063/1.52968.

[58] S. Kumar, D. N. Gupta, H. K. Malik, D. Singh, J. Lee, and M. Yoon, "Effect of a tightly focused chirped Gaussian laser pulse on electron acceleration in helical undulator," *Phys. Plasmas*, vol. 27, no. 4, Apr. 2020, doi: 10.1063/1.5120769.

[59] J. Duris *et al.*, "High-quality electron beams from a helical inverse free-electron laser accelerator," *Nat. Commun.*, vol. 5, 2014, doi: 10.1038/ncomms5928.

[60] J. Rosenzweig, "A Helical Undulator Wave-guide Inverse Free-Electron Laser," pp. 858–864, 2004, doi: 10.1063/1.1842634.

[61] M. Dunning, E. Hemsing, C. Hast, T. O. Raubenheimer, S. Weathersby, and D. Xiang, "Demonstration of Cascaded Optical Inverse Free-Electron Laser Accelerator," vol. 244801, no. June, pp. 1–5, 2013, doi: 10.1103/PhysRevLett.110.244801.

[62] P. Musumeci *et al.*, "High energy gain of trapped electrons in a tapered, diffraction-dominated inverse-free-electron laser," *Phys. Rev. Lett.*, vol. 94, no. 15, Apr. 2005, doi: 10.1103/PhysRevLett.94.154801.

[63] J. P. Duris, P. Musumeci, and R. K. Li, "Inverse free electron laser accelerator for advanced light sources," *Phys. Rev. Spec. Top. - Accel. Beams*, vol. 15, no. 6, Jun. 2012, doi: 10.1103/PhysRevSTAB.15.061301.

[64] Y. I. Salamin, G. R. Mocken, and C. H. Keitel, "Electron scattering and acceleration by a tightly focused laser beam," *Phys. Rev. Spec. Top. - Accel. Beams*, vol. 5, no. 10, pp. 9–22, 2002, doi: 10.1103/PhysRevSTAB.5.101301.

[65] Y. I. Salamin, "Electron acceleration from rest in vacuum by an axicon Gaussian laser beam," *Phys. Rev. - At. Mol. Opt. Phys.*, vol. 73, no. 4, pp. 1–6, 2006, doi: 10.1103/PhysRevA.73.043402.

[66] J. T. Moody *et al.*, "Ultrashort laser pulse driven inverse free electron laser accelerator experiment," *Phys. Rev. Accel. Beams*, vol. 19, no. 2, 2016, doi: 10.1103/PhysRevAccelBeams.19.021305.

[67] N. Sudar *et al.*, "High Efficiency Energy Extraction from a Relativistic Electron Beam in a Strongly Tapered Undulator," *Phys. Rev. Lett.*, vol. 117, no. 17, pp. 1–5, 2016, doi: 10.1103/PhysRevLett.117.174801.

[68] J. Duris, P. Musumeci, M. Babzien, S. Custodio, M. Fedurin, and K. Kusche, "Helical inverse free electron laser accelerator for efficient production of high quality electron beams Helical inverse free electron laser accelerator for efficient production of high quality electron beams," vol. 060001, no. October, 2016, doi: 10.1063/1.4965630.

[69] R. Khullar and G. Mishra, "Effects of Staggered Undulator Magnetic Field Contributions on Inverse Free Electron Laser Accelerator," *IEEE Trans. Plasma Sci.*, vol. 49, no. 2, pp. 729–733, 2021, doi: 10.1109/TPS.2020.3046314.

[70] R. B. Palmer, "Interaction of relativistic particles and free electromagnetic waves in the presence of a static helical magnet," *J. Appl. Phys.*, vol. 43, no. 7, pp. 3014–3023, 1972, doi: 10.1063/1.1661650.

[71] S. Mirzanejhad, F. Sohbatzadeh, M. Asri, and E. S. Toosi, "Electron bunch acceleration in an inverse free-electron laser with a helical magnetic wiggler and axial guide field," *Phys. Plasmas*, vol. 13, no. 12, 2006, doi: 10.1063/1.2402508.

[72] S. Agarwal, N. Kant, and J. Rajput, "Magnetic Field Assisted Electron Acceleration Due to Inverse Free Electron Laser," *J. Phys. Conf. Ser.*, vol. 1531, no. 1, 2020, doi: 10.1088/1742-6596/1531/1/012042.

[73] K. P. Singh, "Acceleration of electrons by a circularly polarized laser pulse in the presence of an intense axial magnetic field in vacuum," *J. Appl. Phys.*, vol. 100, no. 4, 2006, doi: 10.1063/1.2234549.

[74] R. Khazaeinezhad and M. Esmaeilzadeh, "Electron acceleration in the inverse free electron laser with a helical wiggler by axial magnetic field and ion-channel guiding," *Chin. Phys. C*, vol. 36, no. 9, pp. 879–885, 2012, doi: 10.1088/1674-1137/36/9/015.

[75] F. Amiranoff *et al.*, "Laser particle acceleration: beat-wave and wakefield experiments," *Plasma Phys. Control. Fusion*, vol. 38, no. 12A, p. A295, Dec. 1996, doi: 10.1088/0741-3335/38/12A/022.

[76] Y.-D. Jung and I. Murakami, "Quantum effects on magnetization due to ponderomotive force in cold quantum plasmas," *Phys. Lett. A*, vol. 373, no. 10, pp. 969–971, Mar. 2009.

[77] J. P. Palastro, J. L. Shaw, P. Franke, D. Ramsey, T. T. Simpson, and D. H. Froula, "Dephasingless Laser Wakefield Acceleration," *Phys. Rev. Lett.*, vol. 124, no. 13, p. 134802, Mar. 2020, doi: 10.1103/PhysRevLett.124.134802.

[78] N. E. Andreev, S. V. Kuznetsov, and I. V. Pogorelsky, "Monoenergetic laser wakefield acceleration," *Phys. Rev. Spec. Top. - Accel. Beams*, vol. 3, no. 2, p. 021301, Feb. 2000, doi: 10.1103/PhysRevSTAB.3.021301.

[79] F. Amiranoff *et al.*, "Observation of Laser Wakefield Acceleration of Electrons," *Phys. Rev. Lett.*, vol. 81, no. 5, pp. 995–998, Aug. 1998, doi: 10.1103/PhysRevLett.81.995.

[80] A. R. Maier *et al.*, "Decoding Sources of Energy Variability in a Laser-Plasma Accelerator," *Phys. Rev. X*, vol. 10, no. 3, p. 031039, Aug. 2020, doi: 10.1103/PhysRevX.10.031039.

[81] T. Mehrling, J. Grebenyuk, F. S. Tsung, K. Floettmann, and J. Osterhoff, "Transverse emittance growth in staged laser-wakefield acceleration," *Phys. Rev. Spec. Top. - Accel. Beams*, vol. 15, no. 11, p. 111303, Nov. 2012, doi: 10.1103/PhysRevSTAB.15.111303.

[82] J. Osterhoff *et al.*, "Generation of Stable, Low-Divergence Electron Beams by Laser-Wakefield Acceleration in a Steady-State-Flow Gas Cell," *Phys. Rev. Lett.*, vol. 101, no. 8, p. 085002, Aug. 2008, doi: 10.1103/PhysRevLett.101.085002.

[83] H. K. Malik, S. Kumar, and Y. Nishida, "Electron acceleration by laser produced wake field: Pulse shape effect," *Opt. Commun.*, vol. 280, no. 2, pp. 417–423, Dec. 2007, doi: 10.1016/j.optcom.2007.08.013.

[84] "High energy-gain laser wakefield acceleration," presented at the IEEE Particle Accelerator Conference, IEEE, May 1997, pp. 648–650. doi: 10.1109/PAC.1997.749793.

[85] "Theoretical investigation of external injection schemes for laser wakefield acceleration," Sep. 2010, doi: 10.3990/1.9789036530712.

[86] "Laser wakefield acceleration experiments at the university of Michigan," vol. 1086, no. 1, pp. 184–189, Jan. 2009, doi: 10.1063/1.3080902.

[87] "Diagnostics for plasma-based electron accelerators," *Rev. Mod. Phys.*, vol. 90, no. 3, p. 035002, Aug. 2018, doi: 10.1103/REVMODPHYS.90.035002.

[88] M. Tzoufras *et al.*, "Beam Loading in the Nonlinear Regime of Plasma-Based Acceleration," *Phys. Rev. Lett.*, vol. 101, no. 14, p. 145002, Sep. 2008, doi: 10.1103/PhysRevLett.101.145002.

[89] T. P. Rowlands-Rees *et al.*, "Laser-Driven Acceleration of Electrons in a Partially Ionized Plasma Channel," *Phys. Rev. Lett.*, vol. 100, no. 10, p. 105005, Mar. 2008, doi: 10.1103/PhysRevLett.100.105005.

[90] B. B. Pollock *et al.*, "Demonstration of a Narrow Energy Spread, $\ensuremath{\sim}0.5\text{ }\text{ }\mathrm{GeV}$ Electron Beam from a Two-Stage Laser Wakefield Accelerator," *Phys. Rev. Lett.*, vol. 107, no. 4, p. 045001, Jul. 2011, doi: 10.1103/PhysRevLett.107.045001.

[91] G.-B. Zhang, N. A. M. Hafz, Y.-Y. Ma, L.-J. Qian, F.-Q. Shao, and Z.-M. Sheng, "Laser Wakefield Acceleration Using Mid-Infrared Laser Pulses*," *Chin. Phys. Lett.*, vol. 33, no. 9, p. 095202, Sep. 2016, doi: 10.1088/0256-307X/33/9/095202.

[92] P. Muggli *et al.*, "Status of the plasma wakefield acceleration experiment at the Stanford Linear Accelerator Center," in *PACS2001. Proceedings of the 2001 Particle Accelerator Conference (Cat. No.01CH37268)*, Jun. 2001, pp. 122–125 vol.1. doi: 10.1109/PAC.2001.987448.

[93] T. Kozawa, "Plasma wake field acceleration experiments in overdense regime driven by narrow bunches," SLAC National Accelerator Lab., Menlo Park, CA (United States), SLAC-REPRINT-1995-013, Jan. 1995. Accessed: Aug. 15, 2023. [Online]. Available: https://www.osti.gov/biblio/830175

[94] N. A. M. Hafz *et al.*, "Enhanced laser wakefield acceleration using dual-color relativistic pulses," *Plasma Phys. Control. Fusion*, vol. 62, no. 9, p. 095012, Jul. 2020, doi: 10.1088/1361-6587/aba481.

[95] K. V. Lotov and P. V. Tuev, "Plasma wakefield acceleration beyond the dephasing limit with 400 GeV proton driver," *Plasma Phys. Control. Fusion*, vol. 63, no. 12, p. 125027, Nov. 2021, doi: 10.1088/1361-6587/ac349a.

[96] A. Cianchi *et al.*, "Challenges in plasma and laser wakefield accelerated beams diagnostic," *Nucl. Instrum. Methods Phys. Res. Sect. Accel. Spectrometers Detect. Assoc. Equip.*, vol. 720, pp. 153–156, Aug. 2013, doi: 10.1016/j.nima.2012.12.012.

[97] A. Ferran Pousa, A. Martinez de la Ossa, R. Brinkmann, and R. W. Assmann, "Compact Multistage Plasma-Based Accelerator Design for Correlated Energy Spread Compensation," *Phys. Rev. Lett.*, vol. 123, no. 5, p. 054801, Jul. 2019, doi: 10.1103/PhysRevLett.123.054801.

[98] M. J. Hogan *et al.*, "Multi-GeV Energy Gain in a Plasma-Wakefield Accelerator," *Phys. Rev. Lett.*, vol. 95, no. 5, p. 054802, Jul. 2005, doi: 10.1103/PhysRevLett.95.054802.

[99] C. Joshi *et al.*, "Plasma wakefield acceleration experiments at FACET II," *Plasma Phys. Control. Fusion*, vol. 60, no. 3, p. 034001, Jan. 2018, doi: 10.1088/1361-6587/aaa2e3.

[100]   D. Strickland and G. Mourou, "Compression of amplified chirped optical pulses," *Opt. Commun.*, vol. 56, no. 3, pp. 219–221, Dec. 1985, doi: 10.1016/0030-4018(85)90120-8.

[101]   M. A. Gashti and S. Jafari, "Electron acceleration based on a laser pulse propagating through a plasma in the simultaneous presence of a helical wiggler and an obliquely applied external magnetic field," *Eur. Phys. J. Plus*, vol. 131, no. 6, Jun. 2016, doi: 10.1140/epjp/i2016-16210-8.

[102]   Y. I. Salamin, "Fields and propagation characteristics in vacuum of an ultrashort tightly focused radially polarized laser pulse," *Phys. Rev. - At. Mol. Opt. Phys.*, vol. 92, no. 5, Nov. 2015, doi: 10.1103/PhysRevA.92.053836.

[103]   J. X. Li, W. P. Zang, and J. G. Tian, "Electron acceleration in vacuum induced by a tightly focused chirped laser pulse," *Appl. Phys. Lett.*, vol. 96, no. 3, 2010, doi: 10.1063/1.3294634.

[104]   K. P. Singh and V. K. Tripathi, "Laser induced electron acceleration in a tapered magnetic wiggler," *Phys. Plasmas*, vol. 11, no. 2, pp. 743–746, 2004, doi: 10.1063/1.1635372.

[105]   D. N. Gupta, N. Kant, and K. P. Singh, "Electron acceleration by a radially polarized laser pulse in the presence of an intense pulsed magnetic field," *Laser Phys.*, vol. 29, no. 1, Jan. 2019, doi: 10.1088/1555-6611/aaef94.

[106]   D. N. Gupta, H. Suk, and M. S. Hur, "Realistic laser focusing effect on electron acceleration in the presence of a pulsed magnetic field," *Appl. Phys. Lett.*, vol. 91, no. 21, 2007, doi: 10.1063/1.2801392.

[107]   H. S. Ghotra and N. Kant, "Electron acceleration to GeV energy by a chirped laser pulse in vacuum in the presence of azimuthal magnetic field," *Appl. Phys. B Lasers Opt.*, vol. 120, no. 1, pp. 141–147, Jul. 2015, doi: 10.1007/s00340-015-6114-0.

[108]   N. Kant, J. Rajput, and A. Singh, "Enhanced electron acceleration by a chirped tightly focused laser in vacuum in the presence of axial magnetic field," *Eur. Phys. J. D*, vol. 74, no. 7, Jul. 2020, doi: 10.1140/epjd/e2020-100241-y.

[109] "Short-period high-strength helical undulator by laser-driven bifilar capacitor coil." Accessed: Aug. 16, 2024. [Online]. Available: https://opg.optica.org/oe/fulltext.cfm?uri=oe-27-21-29676&id=421861

[110] S. Kumar and M. Yoon, "Electron acceleration by a chirped circularly polarized laser pulse in vacuum in the presence of a planar magnetic wiggler," *Phys. Scr.*, vol. 77, no. 2, Feb. 2008, doi: 10.1088/0031-8949/77/02/025404.

[111] R. Singh and S. S. Gaur, "Electron Acceleration by a Radially Polarized Laser Pulse in an Azimuthal Magnetic Field," *J. At. Mol. Condens. Nano Phys.*, vol. 5, no. 2, pp. 149–157, Aug. 2018, doi: 10.26713/jamcnp.v5i2.810.

[112] R. Khullar, G. Sharma, and G. Mishra, "Effects of misaligned electron beam on inverse free electron laser acceleration \$," *Radiat. Phys. Chem.*, vol. 107, pp. 95–102, 2015, doi: 10.1016/j.radphyschem.2014.09.010.

[113] M. Nikrah and S. Jafari, "Electron energy and electron trajectories in an inverse free-electron laser accelerator based on a novel electrostatic wiggler," *Laser Phys.*, vol. 26, no. 6, Jun. 2016, doi: 10.1088/1054-660X/26/6/065005.

[114] M. Masumeh Amiri, "Electron Acceleration in the Inverse Free-Electron Laser with A Tapered Helical Magnetic Wiggler," *Int. J. Sci. Study*, vol. 367, p. 367, 2017, doi: 10.17354/ijssI/2017/55.

[115] K. P. Singh, "Electron acceleration by a linearly polarized laser pulse in the presence of a pulsed intense axial magnetic field in vacuum," 2006.

[116] T. Ishikawa *et al.*, "A compact X-ray free-electron laser emitting in the sub-ångström region," *Nat. Photonics*, vol. 6, no. 8, pp. 540–544, 2012, doi: 10.1038/nphoton.2012.141.

[117] H. S. Kang *et al.*, "Hard X-ray free-electron laser with femtosecond-scale timing jitter," *Nat. Photonics*, vol. 11, no. 11, pp. 708–713, 2017, doi: 10.1038/s41566-017-0029-8.

[118] E. D. Courant, C. Pellegrini, and W. Zakowicz, "High-energy inverse free-electron-laser accelerator," *Phys. Rev. A*, vol. 32, no. 5, pp. 2813–2823, 1985, doi: 10.1103/PhysRevA.32.2813.

[119]   A. V. Steenbergen, N. Synchrotron, L. Source, and J. C. Gallardo, "INVERSE FREE ELECTRON LASER ACCELERATOR DEVELOPMENT," pp. 616–620, 1998.

[120]   D. Umstadter, J. K. Kim, and E. Dodd, "Laser Injection of Ultrashort Electron Pulses into Wakefield Plasma Waves," *Phys. Rev. Lett.*, vol. 76, no. 12, pp. 2073–2076, Mar. 1996, doi: 10.1103/PhysRevLett.76.2073.

[121]   E. Esarey, R. F. Hubbard, W. P. Leemans, A. Ting, and P. Sprangle, "Electron Injection into Plasma Wakefields by Colliding Laser Pulses," *Phys. Rev. Lett.*, vol. 79, no. 14, pp. 2682–2685, 1997, doi: 10.1103/PhysRevLett.79.2682.

[122]   W. P. Leemans *et al.*, "Laser-driven plasma-based accelerators: Wakefield excitation, channel guiding, and laser triggered particle injection*." [Online]. Available: http://ojps.aip.org/pop/popcr.jsp

[123]   D. N. Gupta and C.-M. Ryu, "Electron acceleration by a circularly polarized laser pulse in the presence of an obliquely incident magnetic field in vacuum," *Phys. Plasmas*, vol. 12, no. 5, p. 053103, Apr. 2005, doi: 10.1063/1.1886829.

[124]   C. Sung, S. Ya. Tochitsky, S. Reiche, J. B. Rosenzweig, C. Pellegrini, and C. Joshi, "Seeded free-electron and inverse free-electron laser techniques for radiation amplification and electron microbunching in the terahertz range," *Phys. Rev. Spec. Top. - Accel. Beams*, vol. 9, no. 12, p. 120703, Dec. 2006, doi: 10.1103/PhysRevSTAB.9.120703.

[125]   L. H. Yu *et al.*, "High-gain harmonic-generation free-electron laser," *Science*, vol. 289, no. 5481, pp. 932–934, Aug. 2000, doi: 10.1126/science.289.5481.932.

[126]   C. Sung *et al.*, "Study of a THz IFEL prebuncher for laser-plasma accelerators," *AIP Conf. Proc.*, vol. 737, no. 1, pp. 922–928, Dec. 2004, doi: 10.1063/1.1842643.

[127]   C. M. S. Sears *et al.*, "HIGH-HARMONIC INVERSE FREE-ELECTRON-LASER INTERACTION AT 800 NM."

[128]   W. D. Kimura, P. Musumeci, D. C. Quimby, S. C. Gottschalk, and C. Pellegrini, "Conceptual Design for a 1-GeV IFEL Accelerator," *AIP Conf. Proc.*, vol. 737, no. 1, pp. 251–257, Dec. 2004, doi: 10.1063/1.1842550.

[129] M. S. Zolotorev and A. A. Zholents, "Transit-time method of optical stochastic cooling," *Phys. Rev. E*, vol. 50, no. 4, pp. 3087–3091, Oct. 1994, doi: 10.1103/PhysRevE.50.3087.

[130] A. A. Zholents and M. S. Zolotorev, "Femtosecond X-Ray Pulses of Synchrotron Radiation," *Phys. Rev. Lett.*, vol. 76, no. 6, pp. 912–915, Feb. 1996, doi: 10.1103/PhysRevLett.76.912.

[131] A. Maltsev and T. Ditmire, "Above Threshold Ionization in Tightly Focused, Strongly Relativistic Laser Fields," *Phys. Rev. Lett.*, vol. 90, no. 5, p. 053002, Feb. 2003, doi: 10.1103/PhysRevLett.90.053002.

[132] F. V. Hartemann *et al.*, "The chirped-pulse inverse free-electron laser: A high-gradient vacuum laser accelerator," *Phys. Plasmas*, vol. 6, no. 10, pp. 4104–4110, 1999, doi: 10.1063/1.873718.

[133] H. S. Ghotra and N. Kant, "Electron injection for enhanced energy gain by a radially polarized laser pulse in vacuum in the presence of magnetic wiggler," *Phys. Plasmas*, vol. 23, no. 1, p. 013101, Jan. 2016, doi: 10.1063/1.4939027.

[134] S. Mirzanejhad, F. Sohbatzadeh, M. Asri, and E. S. Toosi, "Electron bunch acceleration in an inverse free-electron laser with a helical magnetic wiggler and axial guide field," *Phys. Plasmas*, vol. 13, no. 12, 2006, doi: 10.1063/1.2402508.

[135] S. Kumar and M. Yoon, "Electron acceleration by a chirped circularly polarized laser pulse in vacuum in the presence of a planar magnetic wiggler," *Phys. Scr.*, vol. 77, p. 025404, Feb. 2008, doi: 10.1088/0031-8949/77/02/025404.

[136] J. Singh, J. Rajput, N. Kant, and S. Kumar, "Simulation study of two color laser Wakefield acceleration," presented at the AIP Conference Proceedings, Aug. 2021, p. 050043. doi: 10.1063/5.0053366.

[137] A. Mehta, N. Kant, V. Thakur, and J. Rajput, "Numerical study of nonlinear current density produced by beating of two chirped lasers in plasma with density-ripple," *J. Phys. Conf. Ser.*, vol. 1531, p. 012037, May 2020, doi: 10.1088/1742-6596/1531/1/012037.

[138] J. Singh, J. Rajput, and N. Kant, "Electron acceleration by cosh-Gaussian laser beam in the presence of axial magnetic field," *J. Phys. Conf. Ser.*, vol. 1531, no. 1, p. 012027, May 2020, doi: 10.1088/1742-6596/1531/1/012027.

[139] J. Rajput, N. Kant, and A. Singh, "Resonance assisted enhanced electron acceleration in the presence of self-generated magnetic fields due to circularly polarized laser in plasma," *AIP Conf. Proc.*, vol. 2136, no. 1, p. 060012, Aug. 2019, doi: 10.1063/1.5120958.

[140] J. Rajput, N. Kant, H. Singh, and V. Nanda, "Resonant third harmonic generation of a short pulse laser in plasma by applying a wiggler magnetic field," *Opt. Commun.*, vol. 282, no. 23, pp. 4614–4617, Dec. 2009, doi: 10.1016/j.optcom.2009.08.042.

[141] J. Rajput, H. Ghotra, and A. Pramanik, "Efficient electron acceleration by radially polarized Hermite-Cosh-Gaussian laser beam in an ion channel," *Eur. Phys. J. D*, vol. 77, Aug. 2023, doi: 10.1140/epjd/s10053-023-00740-3.

[142] J. Singh, J. Rajput, N. Kant, and S. Kumar, "Comparative study of inverse free-electron laser interaction based on helical and planar wiggler," *Optik*, vol. 260, p. 169017, Jun. 2022, doi: 10.1016/j.ijleo.2022.169017.

[143] K. Middha, V. Thakur, and J. Rajput, "Chirped Cosh-Gaussian Electron Acceleration in Vacuum Due to Two Lasers," *Iran. J. Sci.*, vol. 47, Oct. 2023, doi: 10.1007/s40995-023-01538-z.

[144] J. Rajput, A. Pramanik, P. Kumar, S. Gaur, R. Singh, and N. Kant, "Comparative study of electron acceleration by linearly and circularly polarized Hermite-cosh-Gaussian laser pulse in a vacuum," *J. Opt.*, vol. 52, Nov. 2022, doi: 10.1007/s12596-022-01000-0.

[145] J. Rajput, N. Kant, and A. Singh, "Electron energy enhancement by frequency chirped axicon Gaussian laser pulse in vacuum," *AIP Conf. Proc.*, vol. 1860, no. 1, p. 020005, Jul. 2017, doi: 10.1063/1.4990304.

[146] J. Rajput and N. Kant, "Electron acceleration to GeV energy by an axicon Gaussian laser pulse in a preformed ion channel," *Optik*, vol. 225, p. 165836, Jan. 2021, doi: 10.1016/j.ijleo.2020.165836.

[147] J. Rajput, N. Kant, and A. Singh, "Electron acceleration due to a circularly polarized laser pulse on a downward plasma density ramp in the presence of an azimuthal magnetic field," *AIP Conf. Proc.*, vol. 2006, no. 1, p. 030025, Aug. 2018, doi: 10.1063/1.5051281.

[148] G. Stupakov, "Generation of a wakefield undulator in plasma with transverse density gradient," *Phys. Plasmas*, vol. 24, no. 11, p. 113110, Nov. 2017, doi: 10.1063/1.4990048.

[149] R. B. Palmer, "Interaction of Relativistic Particles and Free Electromagnetic Waves in the Presence of a Static Helical Magnet," *J. Appl. Phys.*, vol. 43, no. 7, pp. 3014–3023, Jul. 1972, doi: 10.1063/1.1661650.

[150] I. Wernick and T. C. Marshall, "Experimental test of the inverse free-electron-laser accelerator principle," *Phys. Rev. A*, vol. 46, no. 6, pp. 3566–3568, Sep. 1992, doi: 10.1103/PhysRevA.46.3566.

[151] C. W. Roberson and P. Sprangle, "A review of free-electron lasers," *Phys. Fluids B*, vol. 1, no. 1, pp. 3–42, 1989, doi: 10.1063/1.859102.

[152] A. V. Steenbergen, J. Gallardo, J. Sandweiss, and J. Fang, "Observation of Energy Gain at the BNL Inverse Free-Electron-Laser Accelerator," *Phys. Rev. Lett.*, vol. 77, no. 20, p. 4280, 1996, doi: 10.1103/PhysRevLett.77.4280.2.

[153] A. L. Troha, F. V. Hartemann, D. J. Gibson, and E. C. Landahl, "The chirped-pulse inverse free-electron laser," in *PACS2001. Proceedings of the 2001 Particle Accelerator Conference (Cat. No.01CH37268)*, Jun. 2001, pp. 3978–3980 vol.5. doi: 10.1109/PAC.2001.988317.

[154] B. J. Galow, J. X. Li, Y. I. Salamin, Z. Harman, and C. H. Keitel, "High-quality multi-GeV electron bunches via cyclotron autoresonance," *Phys. Rev. Spec. Top. - Accel. Beams*, vol. 16, no. 8, pp. 1–6, 2013, doi: 10.1103/PhysRevSTAB.16.081302.

[155] N. Kant, J. Rajput, and A. Singh, "Electron acceleration from rest to GeV energy by chirped axicon Gaussian laser pulse in vacuum in the presence of wiggler magnetic field," *High Energy Density Phys.*, vol. 26, pp. 16–22, Mar. 2018, doi: 10.1016/j.hedp.2017.11.003.

[156] J. Singh, J. Rajput, N. Kant, and S. Kumar, "Electron acceleration in an inverse free electron laser with a tapered wiggler field," *J. Phys. Conf. Ser.*, vol. 2267, p. 012068, May 2022, doi: 10.1088/1742-6596/2267/1/012068.

[157] D. N. Gupta and H. Suk, "Combined role of frequency variation and magnetic field on laser electron acceleration," *Phys. Plasmas*, vol. 13, no. 1, pp. 1–6, 2006, doi: 10.1063/1.2164809.

[158] D. N. Gupta and H. Suk, "Electron acceleration to high energy by using two chirped lasers," *Laser Part. Beams*, vol. 25, no. 1, pp. 31–36, 2007, doi: 10.1017/S026303460707005X.

[159] J. X. Li, Y. I. Salamin, B. J. Galow, and C. H. Keitel, "Acceleration of proton bunches by petawatt chirped radially polarized laser pulses," *Phys. Rev. - At. Mol. Opt. Phys.*, vol. 85, no. 6, pp. 1–12, 2012, doi: 10.1103/PhysRevA.85.063832.

[160] Y. I. Salamin and N. M. Jisrawi, "Electron laser acceleration in vacuum by a quadratically chirped laser pulse," *J. Phys. B At. Mol. Opt. Phys.*, vol. 47, no. 2, 2014, doi: 10.1088/0953-4075/47/2/025601.

[161] F. Sohbatzadeh, S. Mirzanejhad, H. Aku, and S. Ashouri, "Chirped Gaussian laser beam parameters in paraxial approximation," *Phys. Plasmas*, vol. 17, no. 8, p. 083108, Aug. 2010, doi: 10.1063/1.3464478.

[162] Q. Song, X. Y. Wu, J. X. Wang, S. Kawata, and P. X. Wang, "Peculiarities of laser phase behavior associated with the accelerated electron in a chirped laser pulse," *Phys. Plasmas*, vol. 21, no. 5, 2014, doi: 10.1063/1.4879801.

[163] Z. Rajablou and F. Jahangiri, "Gain and bandwidth investigation in dual-pumped non-collinear optical parametric chirped pulse amplification," *J. Appl. Phys.*, vol. 121, no. 19, 2017, doi: 10.1063/1.4983766.

[164] K. Middha, V. Thakur, N. Kant, and J. Rajput, "Comparison of Linear and Quadratic Chirp in Beat Wave Acceleration in Vacuum," *J. Phys. Conf. Ser.*, vol. 2267, no. 1, 2022, doi: 10.1088/1742-6596/2267/1/012103.

[165] F. Sohbatzadeh, S. Mirzanejhad, and M. Ghasemi, "Electron acceleration by a chirped Gaussian laser pulse in vacuum," *Phys. Plasmas*, vol. 13, no. 12, p. 123108, Dec. 2006, doi: 10.1063/1.2405345.

[166] P. Chen, J. M. Dawson, R. W. Huff, and T. Katsouleas, "Acceleration of Electrons by the Interaction of a Bunched Electron Beam with a Plasma," *Phys. Rev. Lett.*, vol. 54, no. 7, pp. 693–696, Feb. 1985, doi: 10.1103/PhysRevLett.54.693.

[167] M. M. Amiri, "Effect of chirped pulse on electron acceleration in the inverse free-electron laser," *QUID Investig. Cienc. Tecnol.*, no. Extra 1, pp. 1271–1275, 2017.

[168] M. D. Perry *et al.*, "Petawatt laser pulses," *Opt. Lett.*, vol. 24, no. 3, pp. 160–162, Feb. 1999, doi: 10.1364/OL.24.000160.

[169] C. W. Domier, N. C. Luhmann Jr., A. E. Chou, W. Zhang, and A. J. Romanowsky, "Ultrashort-pulse reflectometry (invited)," *Rev. Sci. Instrum.*, vol. 66, no. 1, pp. 399–401, Jan. 1995, doi: 10.1063/1.1146358.

[170] R. R. Jones, D. You, and P. H. Bucksbaum, "Ionization of Rydberg atoms by subpicosecond half-cycle electromagnetic pulses," *Phys. Rev. Lett.*, vol. 70, no. 9, pp. 1236–1239, Mar. 1993, doi: 10.1103/PhysRevLett.70.1236.

[171] A. Bonvalet, M. Joffre, J. L. Martin, and A. Migus, "Generation of ultrabroadband femtosecond pulses in the mid-infrared by optical rectification of 15 fs light pulses at 100 MHz repetition rate," *Appl. Phys. Lett.*, vol. 67, no. 20, pp. 2907–2909, Nov. 1995, doi: 10.1063/1.114838.

[172] J. Rajput, N. Kant, and A. Singh, "Resonance assisted enhanced electron acceleration in the presence of self-generated magnetic fields due to circularly polarized laser in plasma," presented at the AIP Conference Proceedings, Aug. 2019, p. 060012. doi: 10.1063/1.5120958.

[173] J. Rajput, N. Kant, and A. Singh, "Electron energy enhancement by frequency chirped axicon Gaussian laser pulse in vacuum," *AIP Conf. Proc.*, vol. 1860, no. 1, p. 020005, Jul. 2017, doi: 10.1063/1.4990304.

[174] N. Kant, J. Rajput, and A. Singh, "Magnetic field assisted enhanced electron acceleration due to a chirped echelon phase modulated laser in vacuum," *Optik*, vol. 182, pp. 858–865, Apr. 2019, doi: 10.1016/j.ijleo.2019.01.096.

[175] J. Singh, J. Rajput, H. Ghotra, and N. Kant, "Electron Acceleration by a radially polarised cosh-Gaussian laser beam in vacuum," *Commun. Theor. Phys.*, vol. 73, May 2021, doi: 10.1088/1572-9494/ac02b6.

[176] J. Rajput, N. Kant, and A. Singh, "Electron acceleration due to a circularly polarized laser pulse on a downward plasma density ramp in the presence of an

azimuthal magnetic field," *AIP Conf. Proc.*, vol. 2006, no. 1, p. 030025, Aug. 2018, doi: 10.1063/1.5051281.

[177]   H. S. Ghotra, "Electron acceleration by higher-order cosh-gaussian laser pulses in vacuum," *Optik*, vol. 286, p. 170992, Sep. 2023, doi: 10.1016/j.ijleo.2023.170992.

[178]   J. Rajput, H. Ghotra, P. Kumar, S. Gaur, and N. Kant, "Radially Polarized Laser-Induced Electron Acceleration in Vacuum," *Iran. J. Sci.*, vol. 47, Jun. 2023, doi: 10.1007/s40995-023-01479-7.

[179]   D. Ramsey, P. Franke, T. T. Simpson, D. H. Froula, and J. P. Palastro, "Vacuum acceleration of electrons in a dynamic laser pulse," *Phys. Rev. E*, vol. 102, no. 4, p. 043207, Oct. 2020, doi: 10.1103/PhysRevE.102.043207.

[180]   J. L. Bobin, "Laser wiggler beat wave in a plasma," *Opt. Commun.*, vol. 55, no. 6, pp. 413–418, Oct. 1985, doi: 10.1016/0030-4018(85)90143-9.

[181]   S. Y. Cai and A. Bhattacharjee, "Inverse-free-electron-laser beat-wave accelerator," *Phys. Rev. A*, vol. 42, no. 8, pp. 4853–4861, Oct. 1990, doi: 10.1103/PhysRevA.42.4853.

[182]   D. N. Gupta and H. Suk, "Electron acceleration to high energy by using two chirped lasers," *Laser Part. Beams*, vol. 25, no. 1, pp. 31–36, Mar. 2007, doi: 10.1017/S026303460707005X.

[183]   K. Middha, V. Thakur, N. Kant, and J. Rajput, "Comparison of Linear and Quadratic Chirp in Beat Wave Acceleration in Vacuum," *J. Phys. Conf. Ser.*, vol. 2267, p. 012103, May 2022, doi: 10.1088/1742-6596/2267/1/012103.

[184]   J. Singh, J. Rajput, N. Kant, and S. Kumar, "Electron acceleration in an inverse free electron laser with a tapered wiggler field," *J. Phys. Conf. Ser.*, vol. 2267, no. 1, p. 012068, May 2022, doi: 10.1088/1742-6596/2267/1/012068.

[185]   K. P. Singh, "Electron acceleration by a chirped short intense laser pulse in vacuum," *Appl. Phys. Lett.*, vol. 87, no. 25, p. 254102, Dec. 2005, doi: 10.1063/1.2149984.

[186]   J. Rajput, N. Kant, and A. Singh, *Electron energy enhancement by frequency chirped axicon Gaussian laser pulse in vacuum*, vol. 1860. 2017. doi: 10.1063/1.4990304.

[187] P. Musumeci, "Acceleration of Electrons By Inverse Free Electron Laser Interaction.pdf," *PhD Thesis*, 2004.

[188] P. Emma *et al.*, "First lasing and operation of an ångstrom-wavelength free-electron laser," *Nat. Photonics*, vol. 4, no. 9, pp. 641–647, 2010, doi: 10.1038/nphoton.2010.176.

[189] W. P. Leemans *et al.*, "GeV electron beams from a centimetre-scale accelerator," *Nat. Phys.*, vol. 2, no. 10, pp. 696–699, 2006, doi: 10.1038/nphys418.

[190] V. D. Shiltsev, "High-energy particle colliders: past 20 years, next 20 years, and beyond," *Phys.-Uspekhi*, vol. 55, no. 10, pp. 965–976, 2012, doi: 10.3367/ufne.0182.201210d.1033.

[191] D. W. Workie, "Basic Physical Processes and Principles of Free Electron Lasers (FELs)," pp. 1–6.

[192] K. Ueda, "X-ray free-electron laser," *Appl. Sci. Switz.*, vol. 8, no. 6, May 2018, doi: 10.3390/app8060879.

[193] W. D. Kimura *et al.*, "First staging of two laser accelerators," *Phys. Rev. Lett.*, vol. 86, no. 18, pp. 4041–4043, 2001, doi: 10.1103/PhysRevLett.86.4041.

[194] J. Singh, J. Rajput, N. Kant, and S. Kumar, "Comparative study of inverse free-electron laser interaction based on helical and planar wiggler," *Optik*, vol. 260, no. March, p. 169017, 2022, doi: 10.1016/j.ijleo.2022.169017.

[195] W. P. Leemans *et al.*, "Multi-GeV Electron Beams from Capillary-Discharge-Guided Subpetawatt Laser Pulses in the Self-Trapping Regime," *Phys. Rev. Lett.*, vol. 113, no. 24, p. 245002, Dec. 2014, doi: 10.1103/PhysRevLett.113.245002.

[196] G. R. Plateau *et al.*, "Low-Emittance Electron Bunches from a Laser-Plasma Accelerator Measured using Single-Shot X-Ray Spectroscopy," *Phys. Rev. Lett.*, vol. 109, no. 6, p. 064802, Aug. 2012, doi: 10.1103/PhysRevLett.109.064802.

[197] R. Weingartner *et al.*, "Ultralow emittance electron beams from a laser-wakefield accelerator," *Phys. Rev. Spec. Top. - Accel. Beams*, vol. 15, no. 11, Nov. 2012, doi: 10.1103/PhysRevSTAB.15.111302.

[198] L.-L. Yu *et al.*, "Two-Color Laser-Ionization Injection," *Phys. Rev. Lett.*, vol. 112, no. 12, p. 125001, Mar. 2014, doi: 10.1103/PhysRevLett.112.125001.

[199] B. Hidding, G. Pretzler, J. B. Rosenzweig, T. Königstein, D. Schiller, and D. L. Bruhwiler, "Ultracold Electron Bunch Generation via Plasma Photocathode Emission and Acceleration in a Beam-Driven Plasma Blowout," *Phys. Rev. Lett.*, vol. 108, no. 3, p. 035001, Jan. 2012, doi: 10.1103/PhysRevLett.108.035001.

[200] K. Moon, S. Kumar, M. Hur, and M. Chung, "Longitudinal phase space dynamics of witness bunch during the Trojan Horse injection for plasma-based particle accelerators," *Phys. Plasmas*, vol. 26, no. 7, p. 073103, Jul. 2019, doi: 10.1063/1.5108928.

[201] L.-L. Yu *et al.*, "Low transverse emittance electron bunches from two-color laser-ionization injection," in *Laser Acceleration of Electrons, Protons, and Ions II; and Medical Applications of Laser-Generated Beams of Particles II; and Harnessing Relativistic Plasma Waves III*, SPIE, May 2013, pp. 54–62. doi: 10.1117/12.2021089.

[202] T. D. Arber *et al.*, "Contemporary particle-in-cell approach to laser-plasma modelling," *Plasma Phys. Control. Fusion*, vol. 57, no. 11, p. 113001, Nov. 2015, doi: 10.1088/0741-3335/57/11/113001.

[203] M. S. Hur and H. Suk, "Numerical study of 1.1 GeV electron acceleration over a-few-millimeter-long plasma with a tapered density," *Phys. Plasmas*, vol. 18, pp. 033102–033102, Mar. 2011, doi: 10.1063/1.3561781.

[204] S. Li *et al.*, "A laser-plasma accelerator driven by two-color relativistic femtosecond laser pulses," *Sci. Adv.*, vol. 5, no. 11, p. eaav7940, Nov. 2019, doi: 10.1126/sciadv.aav7940.

[205] T. Tajima and J. M. Dawson, "Laser Electron Accelerator," *Phys. Rev. Lett.*, vol. 43, no. 4, pp. 267–270, Jul. 1979, doi: 10.1103/PhysRevLett.43.267.

[206] X. L. Xu *et al.*, "Physics of Phase Space Matching for Staging Plasma and Traditional Accelerator Components Using Longitudinally Tailored Plasma Profiles," *Phys. Rev. Lett.*, vol. 116, no. 12, p. 124801, Mar. 2016, doi: 10.1103/PhysRevLett.116.124801.

[207] A. Pukhov and J. Meyer-ter-Vehn, "Laser wake field acceleration: The highly non-linear broken-wave regime," *Appl. Phys. B Lasers Opt.*, vol. 74, no. 4–5, pp. 355–361, 2002, doi: 10.1007/s003400200795.

[208] W. Lu, C. Huang, M. Zhou, W. B. Mori, and T. Katsouleas, "Nonlinear theory for relativistic plasma wakefields in the blowout regime," *Phys. Rev. Lett.*, vol. 96, no. 16, pp. 1–4, 2006, doi: 10.1103/PhysRevLett.96.165002.

[209] W. Lu *et al.*, "Generating multi-GeV electron bunches using single stage laser wakefield acceleration in a 3D nonlinear regime," *Phys. Rev. Spec. Top. - Accel. Beams*, vol. 10, no. 6, pp. 1–12, 2007, doi: 10.1103/PhysRevSTAB.10.061301.

[210] N. Naumova, I. Sokolov, J. Nees, A. Maksimchuk, V. Yanovsky, and G. Mourou, "Attosecond Electron Bunches," *Phys. Rev. Lett.*, vol. 93, no. 19, p. 195003, Nov. 2004, doi: 10.1103/PhysRevLett.93.195003.

[211] W. T. Wang *et al.*, "High-Brightness High-Energy Electron Beams from a Laser Wakefield Accelerator via Energy Chirp Control," *Phys. Rev. Lett.*, vol. 117, no. 12, p. 124801, Sep. 2016, doi: 10.1103/PhysRevLett.117.124801.

[212] M. R. Islam *et al.*, "Near-threshold electron injection in the laser–plasma wakefield accelerator leading to femtosecond bunches," *New J. Phys.*, vol. 17, no. 9, p. 093033, Sep. 2015, doi: 10.1088/1367-2630/17/9/093033.

[213] E. Brunetti *et al.*, "Low Emittance, High Brilliance Relativistic Electron Beams from a Laser-Plasma Accelerator," *Phys. Rev. Lett.*, vol. 105, no. 21, p. 215007, Nov. 2010, doi: 10.1103/PhysRevLett.105.215007.

[214] M. Mirzaie *et al.*, "Effect of injection-gas concentration on the electron beam quality from a laser-plasma accelerator," *Phys. Plasmas*, vol. 25, p. 043106, Apr. 2018, doi: 10.1063/1.5008561.

[215] S. Li *et al.*, "A laser-plasma accelerator driven by two-color relativistic femtosecond laser pulses," *Sci. Adv.*, vol. 5, no. 11, p. eaav7940, Nov. 2019, doi: 10.1126/sciadv.aav7940.

[216] S. R. Yoffe, Y. Kravets, A. Noble, and D. A. Jaroszynski, "Longitudinal and transverse cooling of relativistic electron beams in intense laser pulses," *New J. Phys.*, vol. 17, no. 5, pp. 1–13, May 2015, doi: 10.1088/1367-2630/17/5/053025.

[217] P. Azzi *et al.*, "Standard Model Physics at the HL-LHC and HE-LHC," Dec. 20, 2019, *arXiv*: arXiv:1902.04070. Accessed: May 06, 2024. [Online]. Available: http://arxiv.org/abs/1902.04070

[218] K. J. Kim, "Accelerator Challenges Beyond LCLS: Development of Ultra-High-Brightness Gun," 2004.

[219] E. Esarey, J. Krall, A. Ting, and P. Sprangle, "Energy enhancement in a self-modulated laser wakefield accelerator," vol. 81, pp. 81–90, 2008, doi: 10.1063/1.46878.

[220] C. B. Schroeder *et al.*, "Thermal emittance from ionization-induced trapping in plasma accelerators," *Phys. Rev. Spec. Top. - Accel. Beams*, vol. 17, no. 10, p. 101301, Oct. 2014, doi: 10.1103/PhysRevSTAB.17.101301.

[221] K. Nakamura *et al.*, "GeV electron beams from a centimeter-scale channel guided laser wakefield acceleratora)," *Phys. Plasmas*, vol. 14, p. 056708, May 2007, doi: 10.1063/1.2718524.

[222] I. Blumenfeld *et al.*, "Energy doubling of 42 GeV electrons in a metre-scale plasma wakefield accelerator," *Nature*, vol. 445, no. 7129, pp. 741–744, 2007, doi: 10.1038/nature05538.

[223] S. P. D. Mangles *et al.*, "Monoenergetic beams of relativistic electrons from intense laser-plasma interactions," *Nature*, vol. 431, no. 7008, pp. 535–538, 2004, doi: 10.1038/nature02939.

[224] C. G. R. Geddes *et al.*, "High-quality electron beams from a laser wakefield accelerator using plasma-channel guiding," *Nature*, vol. 431, no. 7008, pp. 538–541, Sep. 2004, doi: 10.1038/nature02900.

[225] J. Faure *et al.*, "A laser-plasma accelerator producing monoenergetic electron beams," *Nature*, vol. 431, no. 7008, pp. 541–544, Sep. 2004, doi: 10.1038/nature02963.

[226] S. Y. Kalmykov *et al.*, "Electron self-injection into an evolving plasma bubble: Quasi-monoenergetic laser-plasma acceleration in the blowout regime," *Phys. Plasmas*, vol. 18, no. 5, p. 056704, May 2011, doi: 10.1063/1.3566062.

[227] S. Bulanov, N. Naumova, F. Pegoraro, and J. Sakai, "Particle injection into the wave acceleration phase due to nonlinear wake wave breaking," *Phys. Rev. E*, vol. 58, no. 5, pp. R5257–R5260, Nov. 1998, doi: 10.1103/PhysRevE.58.R5257.

[228] C. G. R. Geddes *et al.*, "Plasma-Density-Gradient Injection of Low Absolute-Momentum-Spread Electron Bunches," *Phys. Rev. Lett.*, vol. 100, no. 21, p. 215004, May 2008, doi: 10.1103/PhysRevLett.100.215004.

[229] K. Schmid *et al.*, "Density-transition based electron injector for laser driven wakefield accelerators," *Phys. Rev. Spec. Top. - Accel. Beams*, vol. 13, no. 9, p. 091301, Sep. 2010, doi: 10.1103/PhysRevSTAB.13.091301.

[230] A. J. Gonsalves *et al.*, "Tunable laser plasma accelerator based on longitudinal density tailoring," *Nat. Phys.*, vol. 7, no. 11, pp. 862–866, 2011, doi: 10.1038/nphys2071.

[231] E. Esarey, R. F. Hubbard, W. P. Leemans, A. Ting, and P. Sprangle, "Electron Injection into Plasma Wakefields by Colliding Laser Pulses," *Phys. Rev. Lett.*, vol. 79, no. 14, pp. 2682–2685, Oct. 1997, doi: 10.1103/PhysRevLett.79.2682.

[232] J. Faure, C. Rechatin, A. Norlin, A. Lifschitz, Y. Glinec, and V. Malka, "Controlled injection and acceleration of electrons in plasma wakefields by colliding laser pulses," *Nature*, vol. 444, no. 7120, pp. 737–739, Dec. 2006, doi: 10.1038/nature05393.

[233] C. McGuffey *et al.*, "Ionization Induced Trapping in a Laser Wakefield Accelerator," *Phys. Rev. Lett.*, vol. 104, no. 2, p. 025004, Jan. 2010, doi: 10.1103/PhysRevLett.104.025004.

[234] C. E. Clayton *et al.*, "Self-Guided Laser Wakefield Acceleration beyond 1 GeV Using Ionization-Induced Injection," *Phys. Rev. Lett.*, vol. 105, no. 10, p. 105003, Sep. 2010, doi: 10.1103/PhysRevLett.105.105003.

[235] B. B. Pollock *et al.*, "Demonstration of a Narrow Energy Spread, $\ensuremath{\sim}0.5\text{ }\text{ }\mathrm{GeV}$ Electron Beam from a Two-Stage Laser Wakefield Accelerator," *Phys. Rev. Lett.*, vol. 107, no. 4, p. 045001, Jul. 2011, doi: 10.1103/PhysRevLett.107.045001.

[236] J. S. Liu *et al.*, "All-Optical Cascaded Laser Wakefield Accelerator Using Ionization-Induced Injection," *Phys. Rev. Lett.*, vol. 107, no. 3, p. 035001, Jul. 2011, doi: 10.1103/PhysRevLett.107.035001.

[237] G. G. Manahan *et al.*, "Single-stage plasma-based correlated energy spread compensation for ultrahigh 6D brightness electron beams," *Nat. Commun.*, vol. 8, no. 1, p. 15705, Jun. 2017, doi: 10.1038/ncomms15705.

[238] K. Moon, S. Kumar, M. Hur, and M. Chung, "Longitudinal phase space dynamics of witness bunch during the Trojan Horse injection for plasma-based particle accelerators," *Phys. Plasmas*, vol. 26, no. 7, 2019, doi: 10.1063/1.5108928.

[239] J. B. Rosenzweig *et al.*, "Generation of ultra-short, high brightness electron beams for single-spike SASE FEL operation," *Nucl. Instrum. Methods Phys. Res. Sect. Accel. Spectrometers Detect. Assoc. Equip.*, vol. 593, no. 1, pp. 39–44, Aug. 2008, doi: 10.1016/j.nima.2008.04.083.

[240] F. H. O'Shea *et al.*, "Short period, high field cryogenic undulator for extreme performance x-ray free electron lasers," *Phys. Rev. Spec. Top. - Accel. Beams*, vol. 13, no. 7, p. 070702, Jul. 2010, doi: 10.1103/PhysRevSTAB.13.070702.

[241] X. Y. Wu, P. X. Wang, and S. Kawata, "Mechanism of electron acceleration by chirped laser pulse," *Appl. Phys. Lett.*, vol. 100, no. 22, p. 221109, May 2012, doi: 10.1063/1.4723847.

[242] X. Zhang *et al.*, "Effect of pulse profile and chirp on a laser wakefield generation," *Phys. Plasmas*, vol. 19, no. 5, p. 053103, May 2012, doi: 10.1063/1.4714610.

[243] Y. Cui *et al.*, "Beam quality improvement of ionization injected electrons by using chirped pulse in wakefield acceleration," *Plasma Phys. Control. Fusion*, vol. 61, no. 8, p. 085023, Jun. 2019, doi: 10.1088/1361-6587/ab249e.

[244] D. L. Bruhwiler, D. A. Dimitrov, J. R. Cary, E. Esarey, W. Leemans, and R. E. Giacone, "Particle-in-cell simulations of tunneling ionization effects in plasma-based accelerators," *Phys Plasmas*, vol. 10, pp. 2022–2030, 2003, doi: 10.1063/1.1566027.

[245] V. S. Popov, "Tunnel and multiphoton ionization of atoms and ions in a strong laser field (Keldysh theory)," *Phys.-Uspekhi*, vol. 47, no. 9, p. 855, Sep. 2004, doi: 10.1070/PU2004v047n09ABEH001812.

[246] J. B. Rosenzweig, "Nonlinear plasma dynamics in the plasma wake-field accelerator," *Phys. Rev. Lett.*, vol. 58, no. 6, pp. 555–558, Feb. 1987, doi: 10.1103/PhysRevLett.58.555.

[247] R. Lehe, M. Kirchen, I. A. Andriyash, B. B. Godfrey, and J.-L. Vay, "A spectral, quasi-cylindrical and dispersion-free Particle-In-Cell algorithm," *Comput. Phys. Commun.*, vol. 203, pp. 66–82, Jun. 2016, doi: 10.1016/j.cpc.2016.02.007.

[248] J. B. Murphy and C. Pellegrini, "Generation of high-intensity coherent radiation in the soft-x-ray and vacuum-ultraviolet region," *JOSA B*, vol. 2, no. 1, pp. 259–264, Jan. 1985, doi: 10.1364/JOSAB.2.000259.

[249] S. Kumar, H.-S. Kang, and D. E. Kim, "Generation of isolated single attosecond hard X-ray pulse in enhanced self-amplified spontaneous emission scheme," *Opt. Express*, vol. 19, no. 8, pp. 7537–7545, 2011.

[250] P. Sprangle, E. Esarey, J. Krall, and A. Ting, "Vacuum laser acceleration," *Opt. Commun.*, vol. 124, no. 1, pp. 69–73, Feb. 1996, doi: 10.1016/0030-4018(95)00618-4.

[251] X. Wang *et al.*, "Quasi-monoenergetic laser-plasma acceleration of electrons to 2 GeV," *Nat. Commun.*, vol. 4, p. 1988, Jun. 2013, doi: 10.1038/ncomms2988.

[252] V. Sharma, S. Kumar, N. Kant, and V. Thakur, "Excitation of the Laser wakefield by asymmetric chirped laser pulse in under dense plasma," *J. Opt.*, Aug. 2023, doi: 10.1007/s12596-023-01326-3.

[253] J. Singh, J. Rajput, N. Kant, and S. Kumar, "Simulation study of two color laser Wakefield acceleration," presented at the AIP Conference Proceedings, Aug. 2021, p. 050043. doi: 10.1063/5.0053366.

[254] C. Aniculaesei *et al.*, "Electron energy increase in a laser wakefield accelerator using up-ramp plasma density profiles," *Sci. Rep.*, vol. 9, no. 1, Art. no. 1, Aug. 2019, doi: 10.1038/s41598-019-47677-5.

[255] P. Sprangle *et al.*, "Wakefield generation and GeV acceleration in tapered plasma channels," *Phys. Rev. E Stat. Nonlin. Soft Matter Phys.*, vol. 63, no. 5 Pt 2, p. 056405, May 2001, doi: 10.1103/PhysRevE.63.056405.

[256] R. F. Hubbard *et al.*, "Simulation and design of stable channel-guided laser wakefield accelerators," *Phys. Rev. E Stat. Nonlin. Soft Matter Phys.*, vol. 63, no. 3 Pt 2, p. 036502, Mar. 2001, doi: 10.1103/PhysRevE.63.036502.

[257] R. Fallah and S. m. Khorashadizadeh, "Electron acceleration in a homogeneous plasma by Bessel-Gaussian and Gaussian pulses," *Contrib. Plasma Phys.*, vol. 58, no. 9, pp. 878–889, 2018, doi: 10.1002/ctpp.201700200.

[258] R. Fallah and S. Khorashadizadeh Mohammad, "Influence of Gaussian, Super-Gaussian, and Cosine-Gaussian Pulse Properties on the Electron Acceleration in a Homogeneous Plasma," *IEEE Trans. Plasma Sci.*, vol. 46, pp. 2085–2090, Jun. 2018, doi: 10.1109/TPS.2018.2834512.

[259] M. P. Tooley *et al.*, "Towards Attosecond High-Energy Electron Bunches: Controlling Self-Injection in Laser-Wakefield Accelerators Through Plasma-Density Modulation," *Phys. Rev. Lett.*, vol. 119, no. 4, p. 044801, Jul. 2017, doi: 10.1103/PhysRevLett.119.044801.

[260] F. Massimo, A. F. Lifschitz, C. Thaury, and V. Malka, "Numerical studies of density transition injection in laser wakefield acceleration," *Plasma Phys. Control. Fusion*, vol. 59, no. 8, p. 085004, Jun. 2017, doi: 10.1088/1361-6587/aa717d.

[261] D. N. Gupta, M. Yadav, A. Jain, and S. Kumar, "Electron bunch charge enhancement in laser wakefield acceleration using a flattened Gaussian laser pulse," *Phys. Lett. A*, vol. 414, p. 127631, Oct. 2021, doi: 10.1016/j.physleta.2021.127631.

[262] K. Gopal, D. N. Gupta, and H. Suk, "Pulse-length Effect on Laser Wakefield Acceleration of Electrons by Skewed Laser Pulses," *IEEE Trans. Plasma Sci.*, vol. 49, no. 3, pp. 1152–1158, Mar. 2021, doi: 10.1109/TPS.2021.3059643.

[263] X. Xia, G. Wei, K. Tian, J. Chen, and Q. Liang, "Electron acceleration by relativistic pondermotive force in the interaction of intense laser pulse with an axially inhomogeneous underdense plasma," *Mod. Phys. Lett. B*, vol. 36, p. 2230003, Sep. 2022, doi: 10.1142/S0217984922300034.

[264] H. Akou, "Excitation of upper-hybrid plasma wake wave by a low-frequency extraordinary electromagnetic wave," *Contrib. Plasma Phys.*, vol. 61, no. 1, p. e202000149, 2021, doi: 10.1002/ctpp.202000149.

[265] V. Sharma, S. Kumar, N. Kant, and V. Thakur, "Effect of Frequency Chirp and Pulse Length on Laser Wakefield Excitation in Under-Dense Plasma," *Braz. J. Phys.*, vol. 53, p. 157, Dec. 2023, doi: 10.1007/s13538-023-01370-1.

[266] M. Asri and H. Akou, "Influence of sense rotation of circularly polarized laser pulse on the wake-field acceleration in magnetized plasma," *Optik*, vol. 143, pp. 142–149, Aug. 2017, doi: 10.1016/j.ijleo.2017.06.058.

[267] M. A. and K. N. Rajput Jyoti, "Efficient electron energy by radial polarization of laser and obliquely incident magnetic field," *THINK INDIA J.*, vol. 22, no. 37, pp. 950–952, 2019.

[268] J. Singh, J. Rajput, N. Kant, and S. Kumar, "Simulation study of two color laser Wakefield acceleration," *AIP Conf. Proc.*, vol. 2352, pp. 1–4, 2021, doi: 10.1063/5.0053366.

[269] D. N. Gupta, K. Gopal, I. H. Nam, V. V. Kulagin, and H. Suk, "Laser wakefield acceleration of electrons from a density-modulated plasma," *Laser Part. Beams*, vol. 32, no. 3, pp. 449–454, 2014, doi: 10.1017/S0263034614000378.

[270] H. R. Askari and A. Shahidani, "Influence of properties of the Gaussian laser pulse and magnetic field on the electron acceleration in laser-plasma interactions," *Opt. Laser Technol.*, vol. 45, no. 1, pp. 613–619, 2013, doi: 10.1016/j.optlastec.2012.05.023.

[271] A. Pukhov and I. Kostyukov, "Control of laser-wakefield acceleration by the plasma-density profile," *Phys. Rev. E - Stat. Nonlinear Soft Matter Phys.*, vol. 77, no. 2, pp. 1–4, 2008, doi: 10.1103/PhysRevE.77.025401.

[272] L. Ke *et al.*, "Optimization of electron beams based on plasma-density modulation in a laser-driven wakefield accelerator," *Appl. Sci. Switz.*, vol. 11, no. 6, 2021, doi: 10.3390/app11062560.

[273] J. D. Sadler, C. Arran, H. Li, and K. A. Flippo, "Overcoming the dephasing limit in multiple-pulse laser wakefield acceleration," *Phys. Rev. Accel. Beams*,

vol. 23, no. 2, pp. 1–7, 2020, doi: 10.1103/PHYSREVACCELBEAMS.23.021303.

[274] H. Ding *et al.*, "Nonlinear plasma wavelength scalings in a laser wakefield accelerator," *Phys. Rev. E*, vol. 101, no. 2, pp. 1–9, 2020, doi: 10.1103/PhysRevE.101.023209.

[275] B. Miao *et al.*, "Multi-GeV Electron Bunches from an All-Optical Laser Wakefield Accelerator," *Phys. Rev. X*, vol. 12, no. 3, p. 31038, 2022, doi: 10.1103/PhysRevX.12.031038.

[276] V. Sharma and S. Kumar, "To study the effect of laser frequency-chirp on trapped electrons in laser wakefield acceleration," *J. Phys. Conf. Ser.*, vol. 2267, no. 1, 2022, doi: 10.1088/1742-6596/2267/1/012097.

[277] J. Rajput, N. Kant, and A. Singh, "Electron acceleration due to a circularly polarized laser pulse on a downward plasma density ramp in the presence of an azimuthal magnetic field," *AIP Conf. Proc.*, vol. 2006, pp. 0–10, 2018, doi: 10.1063/1.5051281.

[278] M. Kaur and D. N. Gupta, "Electron energy optimization by plasma density ramp in laser wakefield acceleration in bubble regime," *Laser Part. Beams*, vol. 36, no. 2, pp. 195–202, 2018, doi: 10.1017/S0263034618000162.

[279] S. Bulanov, N. Naumova, F. Pegoraro, and J. Sakai, "Particle injection into the wave acceleration phase due to nonlinear wake wave breaking," *Phys. Rev. E - Stat. Phys. Plasmas Fluids Relat. Interdiscip. Top.*, vol. 58, no. 5, pp. R5257–R5260, 1998, doi: 10.1103/PhysRevE.58.R5257.

[280] K. Dong *et al.*, "High-efficiency acceleration in the laser wakefield by a linearly increasing plasma density," *Phys. Plasmas*, vol. 21, no. 12, 2014, doi: 10.1063/1.4904403.

[281] R. Ariniello, C. E. Doss, K. Hunt-Stone, J. R. Cary, and M. D. Litos, "Transverse beam dynamics in a plasma density ramp," *Phys. Rev. Accel. Beams*, vol. 22, no. 4, p. 41304, 2019, doi: 10.1103/PhysRevAccelBeams.22.041304.

[282] G. Raj, A. K. Upadhyaya, R. K. Mishra, and P. Jha, "Electron acceleration by amplified wakefield generated by two copropagating laser pulses in plasma,"

Phys. Rev. Spec. Top. - Accel. Beams, vol. 11, no. 7, 2008, doi: 10.1103/PhysRevSTAB.11.071301.

[283]   S. Dalla and M. Lontano, "Large amplitude plasma wave excitation by means of sequences ofshort laser pulses," *Phys. Rev. E*, vol. 49, no. 3, pp. 1819–1822, 1994.

List of papers based on thesis

1. Simulation study of two-color laser wakefield laser acceleration *AIP Conf. Proc.* 2352, 050043 (2021) https://doi.org/10.1063/5.0053366

2. Comparative study of inverse free-electron laser interaction based on helical and planar wiggler" Optik, 260, June 2022, 169017

3. Electron acceleration in an inverse free electron laser with tapered wiggler magnetic field. *J. Phys.: Conf. Ser.* 2267 012068, DOI 10.1088/1742-6596/2267/1/012068

4. IFEL electron acceleration due to two laser pulses incident at an oblique angle. J Opt, https://doi.org/10.1007/s12596-024-01925-8(2024).

5. Synergistic Enhancement of Electron Acceleration by Chirp Laser Modulation and Wiggler Magnetic Field. J Opt, https://doi.org/10.1007/s12596-024-02079-3

Communications

1. Effect of Frequency-Chirped ionization laser on accelerated Electron Beam Characteristics in Plasma Wakefield Acceleration (The European physical journal plus)

2. Optimizing Laser Wakefield Acceleration through Plasma Density Profile Analysis (journal of Optics)

Conferences

Poster presentation at 5th National e-Conference on Advanced Materials and Radiation Physics (AMRP-2020), on study of Simulation study of two-color Laser Wakefield acceleration, Punjab.

Poster Presentation at Recent Advances in Fundamental and Applied Science, 2021 on Electron acceleration in an inverse free electron laser with a tapered wiggler field.

Poster Presentation at 1st "International Conference on Futuristic Materials" (ICFM-2022) on Analysis of electron's energy using chirped laser pulse.

Poster Presentation at Recent Advances in Fundamental and Applied Science, 2024 on Electron acceleration in an inverse free electron laser with a tapered wiggler field Enhanced Laser Wakefield Acceleration through Slanting Plasma Density Profile.

List of published work

RESEARCH ARTICLE | AUGUST 05 2021

Simulation study of two color laser Wakefield acceleration 🛒

Jagnishan Singh; Jyoti Rajput ✉; Niti Kant; Sandeep Kumar

➕ Author & Article Information

⌁ Share ∨   🔧 Tools ∨

Conventional accelerators used for particle acceleration are expensive due to their huge size. Moreover, the electrical breakdowns of the walls limit the maximum electric field gradient to 100 MVm^{-1}. On the other hand, plasma-based particle accelerators driven by laser or particle-beam show great potential owing to their large acceleration gradient that leads to compact structures. In this vein, two color laser Wakefield acceleration is studied using two dimensional particle in cell (2D-PIC) simulation. Our simulations show that more stable energy spectra can be produced via two-color laser Wakefield scheme compared to single color scheme. For given simulation parameters, 500 MeV energy gain is observed in 3.4 mm long plasma channel. The effect of relative time delays of the two color lasers and polarization effect of second laser on electron bunch acceleration is also presented. Such good quality electron-bunches are suitable candidate for future XFEL and Betatron sources.

Comparative study of inverse free-electron laser interaction based on helical and planar wiggler

Author links open overlay panel

Jagnishan Singh [a], Jyoti Rajput [a], Niti Kant [a], Sandeep Kumar [b]

Show more ∨

+ Add to Mendeley   Share   Cite

Abstract

In an inverse free-electron laser (IFEL) scheme, a comparative study of single electron acceleration is carried out using a tightly focused Gaussian laser beam along with helical and planar wiggler fields. The effect of laser and wiggler field parameters is analyzed on single-electron dynamics and its acceleration. For the laser field descriptions, up to fifth-order corrections are included in the diffraction angle to study the effect of a tight laser pulse on electron acceleration. The Lorentz equation is solved using the fourth-order Runge Kutta method. Our numerical results indicate that considerable electron energy is attained for the helical and planar wiggler both for the optimal laser and wiggler field parameters, respectively. The effect of the laser field, its waist -size, and the effect of the wiggler field and its tapering along undulator length is studied for both helical and planar wiggler. The total electron energy gain for the helical wiggler case is 1.3 GeV due to the long interaction length while for the planar wiggler case, the electron energy gain is limited to 300 MeV only due to its shorter interaction length. This comparative analysis will certainly help us to understand the electron dynamics in IFEL and show the importance of helical wiggler over planar wiggler.

Synergistic enhancement of electron acceleration by chirp laser modulation and wiggler magnetic field

Jagnishan Singh, Sandeep Kumar & Jyoti Rajput ✉

Abstract

A numerical analysis is done to examine electron acceleration caused by chirped laser pulses. A positive chirp is applied to determine the electron energy gain. In this work, the energy gain for an electron has been examined using the wakefield produced by a chirped laser pulse in the presence of a magnetic undulator. The maximum energy gain of 767 MeV has been investigated numerically for the different optimised values of laser frequency chirp, laser intensity, and external magnetic field. It is demonstrated that the chirp frequency and laser pulse amplitude have a significant impact on the total energy of the electron. The chirp parameter has an optimum value at which electron acceleration is accomplished. With optimum chirp and laser pulse amplitude, the energy gain rises. The importance of the chirp effect on the energy obtained by an electron from an electromagnetic wave is emphasized.

IFEL electron acceleration due to two laser pulses incident at an oblique angle

Jagnishan Singh, Sandeep Kumar, Kavish Middha & Jyoti Rajput ✉

Abstract

The vacuum laser acceleration scheme IFEL has been investigated. We have studied the best conditions for achieving higher energy gain using two laser pulses crossing at an angle in the presence of an undulator. A group of optimized variables for electrons and the laser pulse are employed to numerically investigate the phenomena of the crossing of two lasers using the inverse free electron acceleration (IFELA) mechanism. IFELA mechanism is used to produce a high quality, micro-bunched accelerated electron beam that is used to feed a Compton scattering interaction point, which produce x-rays of directional narrow bandwidth. The effect of linear frequency chirp has been investigated and shown that the final electron energy in the presence of an undulator is strongly dependent on different parameters like the laser's initial intensity, the crossing angle between the lasers, wiggler magnetic field strength, and the chirping of the laser pulse. It shows that the crossing of lasers plays a crucial role in the final energy gain as compared to the co-propagating lasers. The proportionality of the final energy gain on pre-accelerated electron's energy is also investigated. Hundreds of MeV energy gain has been obtained in the investigation. Currently these types of lasers are used in scientific research in the field of material science, Chemical engineering, medical science, biophysics, surface studies and solid state physics etc.

Electron acceleration in an inverse free electron laser with a tapered wiggler field

Save   Related Papers   Chat with paper

Jagnishan Singh[1], Jyoti Rajput[1], Niti Kant[1] and Sandeep Kumar[2]

Article PDF

References ▼

▼ Article and author information

Abstract

Numerical study of inverse free-electron laser acceleration (IFELA) in the presence of a tightly focused laser beam is investigated in vacuum. In this article, we investigate the dynamics of an electron in the inverse free-electron laser (IFEL) with a planer wiggler field geometry. The numerical study on particle acceleration is carried out for tightly focused laser parameters as well as the tapering along the wiggler field. It is observed that the effect of tapering point along the undulator is crucial to maintain the IFEL resonance condition and to maximize the energy gain. The role of normalized laser field and of tapering point of planar wiggler magnetic field is examined on the electron acceleration. The role of pre-energy modulation of real electron-bunch and its acceleration will be planned in our next simulation work.

CHAPTER-15

Inverse Free Electron Laser Acceleration Using Helical and Planar Wiggler Field

Jagnishan singh[1], Jyoti Rajput[1]

[1]Lovely Professional University, Phagwara, India

jyoti_physics@yahoo.co.in

Abstract. Laser accelerators have a great potential to become the predominant kind of particle accelerator, the inverse free electron laser accelerator is among the most efficient methods for transferring energy from an extremely powerful laser to electron beams. A magnetic undulator is used for transferring energy from laser to electron. In this chapter, a basic phenomenon of inverse free electron acceleration is studied using a tightly focused laser beam. Comparatively discussion of the influence of helical and planar wigglers shows that a helical wiggler is more useful instead of a planar one.

176

List of certificates

Certificate No. 329166

Certificate of Presentation

This is to certify that **Dr./Mr./Ms. Jagnishan Singh** of **Lovely Professional University, Phagwara** has given **Poster** presentation on **Enhanced Laser Wakefield Acceleration through Slanting Plasma Density Profile** in the **5th International Conference on Recent Advances in Fundamental and Applied Sciences (RAFAS-2024)** held from 19th to 20th April 2024, organized by School of Chemical Engineering and Physical Sciences, Lovely Faculty of Technology and Sciences, at Lovely Professional University, Punjab.

Date of Issue : 20-05-2024
Place : Phagwara (Punjab), India

Prepared by
(Administrative Officer-Records)

Organizing Secretary
(RAFAS-2024)

Head of Faculty
Lovely Professional University

178

Bio-data

Mr. JAGNISHAN SINGH

M.Sc.(Physics). B.Ed

jagnishankhalsa@gmail.com

9785486787

JAGNISHAN SINGH was born in RAJASTHAN, India in 1993. He has received B.Sc. Degree in Physics in 2016 from Maharaja Ganga Singh University, Rajasthan, India. He has also received the master's degree Physics from Maharaja Ganga Singh University, Rajasthan, India in 2018

In 2020, he joined Pulkit Angels model shikshan sansthan, Hanumangarh, Rajasthan, as a Physics lecturer and he is working till now. Presently, he has concentrated in theoretical research work in the field of "Laser driven electron acceleration in vacuum and plasma" under the guidance of Dr. Jyoti Rajput, Professor, LPU, Punjab, India.

Personal detail:

Date of Birth:	3rd March 1993
Parents :	Mr. Sadhu Singh
:	Smt. Sukjinder Kaur
Spouse :	Harmandeep Kaur
Language Known:	Punjabi, Hindi, English
Google Scholar:	Jagnishan singh (Author)
ORCID ids:	https://orcid.org/0009-0000-2954-4034
ResearchGate:	Jagnishan.41900654@lpu.in
Educational qualification:	B.Sc. in PHYSICS [2016],
	M.Sc. in PHYSICS [2018],
	B.Ed. [2020]